



Michigan Technological University
Create the Future Digital Commons @ Michigan Tech

Dissertations, Master's Theses and Master's
Reports - Open

Dissertations, Master's Theses and Master's
Reports

2008

Multiscale constitutive modeling of polymer materials

Pavan Kumar Valavala
Michigan Technological University

Follow this and additional works at: <https://digitalcommons.mtu.edu/etds>


 Part of the [Mechanical Engineering Commons](#)

Copyright 2008 Pavan Kumar Valavala

Recommended Citation

Valavala, Pavan Kumar, "Multiscale constitutive modeling of polymer materials", Dissertation, Michigan Technological University, 2008.
<https://doi.org/10.37099/mtu.dc.etds/417>

Follow this and additional works at: <https://digitalcommons.mtu.edu/etds>

 Part of the [Mechanical Engineering Commons](#)

MULTISCALE CONSTITUTIVE MODELING OF POLYMER MATERIALS

By

PAVAN KUMAR VALAVALA

A DISSERTATION

Submitted in partial fulfillment of the requirements

for the degree of

DOCTOR OF PHILOSOPHY

(Mechanical Engineering-Engineering Mechanics)

MICHIGAN TECHNOLOGICAL UNIVERSITY

2008

© 2008

Pavan Kumar Valavala

All Rights Reserved

This dissertation, "Multiscale Constitutive Modeling of Polymer Materials," is hereby approved in partial fulfillment of the requirements for the degree of DOCTOR OF PHILOSOPHY in the field of Mechanical Engineering-Engineering Mechanics.

DEPARTMENT:

Mechanical Engineering-Engineering Mechanics

Signatures:

Dissertation Advisor:

Prof. Gregory M. Odegard

Department Chair

Prof. William W. Predebon

Date

Acknowledgements

I would like to express a few heart felt words to the people who have been a part of this research in numerous ways, people who showed unrelenting support during my work at Michigan Technological University.

My sincere thanks to Prof. Gregory Odegard, for advising me on issues throughout the program; to Prof. Ranjit Pati, Prof. Spandan Maiti and Prof. Reza Yassar for their valuable guidance and for being on my dissertation committee. I am grateful to all my colleagues at Computational Mechanics and Materials Research Laboratory (CMMRL) and Prof. Pati's Laboratory for their support and assistance at various stages of this research. Most importantly, I will always be indebted to my family for their support and encouragement to pursue my dreams. Finally, I would like to express my appreciation for all the readers of this manuscript, who I hope will find it useful and carry on the work with same dedication and integrity I have valued in all the above mentioned people.

This research was jointly sponsored by National Aeronautics and Space Administration under grants NNL04AA85G and the National Science Foundation under grant DMI-0403876.

Abstract

Materials are inherently multi-scale in nature consisting of distinct characteristics at various length scales from atoms to bulk material. There are no widely accepted predictive multi-scale modeling techniques that span from atomic level to bulk relating the effects of the structure at the nanometer (10^{-9} meter) on macro-scale properties. Traditional engineering deals with treating matter as continuous with no internal structure. In contrast to engineers, physicists have dealt with matter in its discrete structure at small length scales to understand fundamental behavior of materials. Multiscale modeling is of great scientific and technical importance as it can aid in designing novel materials that will enable us to tailor properties specific to an application like multi-functional materials.

Polymer nanocomposite materials have the potential to provide significant increases in mechanical properties relative to current polymers used for structural applications. The nanoscale reinforcements have the potential to increase the effective interface between the reinforcement and the matrix by orders of magnitude for a given reinforcement volume fraction as relative to traditional micro- or macro-scale reinforcements. To facilitate the development of polymer nanocomposite materials, constitutive relationships must be established that predict the bulk mechanical properties of the materials as a function of the molecular structure. A computational hierarchical multiscale modeling technique is developed to study the bulk-level constitutive behavior of polymeric materials as a function of its molecular chemistry. Various parameters and modeling techniques from computational chemistry to continuum mechanics are utilized for the current modeling method. The cause and effect relationship of the parameters are studied to establish an efficient modeling framework. The proposed methodology is applied to three different polymers and validated using experimental data available in literature.

Table of Contents

<u>Acknowledgements.....</u>	<u>4</u>
<u>Abstract.....</u>	<u>5</u>
<u>Nomenclature.....</u>	<u>9</u>
<u>Chapter 1 - Introduction</u>	<u>11</u>
1.1 Motivation	12
1.2 Objective	13
1.3 Layout	14
<u>Chapter 2 – Literature Review.....</u>	<u>16</u>
2.1 Introduction	16
2.2 Modeling Methods Overview	18
2.3 Continuum Methods	23
2.4 Molecular Modeling	28
2.5 Simulated Results	36
2.6 Summary	37
<u>Chapter 3 – NonNonlinear Multiscale Modeling of Polymer Materials</u>	
<u>.....</u>	<u>39</u>
3.1 Introduction	39
3.2 Force Fields	42
3.3 Equivalent Continuum Modeling	43
3.4 Results and Discussions	56
3.5 Summary	67
<u>Chapter 4 – Multiscale Modeling of Polymer Materials Using a Statistics-</u>	
<u>Based Micromechanics Approach.....</u>	<u>70</u>
4.1 Introduction	70
4.2 Force Field	72
4.3 Molecular Model	74
4.4 Equivalent Continuum Modeling	76

4.5 Micromechanics	78
4.6 Results	83
4.7 Summary	89
 <u>Chapter 5 – Temperature Effects in Multiscale Modeling of Polymer</u>	
<u>Materials</u>	<u>91</u>
5.1 Introduction	91
5.2 Modeled Material System	93
5.3 Multiscale Modeling Procedure	94
5.4 Results and Discussions	99
 <u>Chapter 6– Influence of Representative Volume Element Size on</u>	
<u>Multiscale Modeling of Polymer Materials.....</u>	<u>106</u>
6.1 Introduction	106
6.2 Molecular Model.....	108
6.3 Equivalent Continuum Modeling	110
6.4 Effective Polymer Properties	112
6.5 Results.....	115
6.6 Summary	135
 <u>Chapter 7 – Effect of Water.....</u>	<u>137</u>
7.1 Introduction	137
7.2 Molecular Model.....	139
7.3 Equivalent Continuum Modeling	140
7.4 Results and Discussions	141
7.5 Summary	143
 <u>Chapter 8 – Summary and Conclusions</u>	<u>146</u>
8.1 Hyperelastic Continuum Modeling	147
8.2 Statistics-based Micromechanics Approach	150
8.3 Effects of Temperature	152
8.4 Influence of RVE size.....	154
8.5 Effects of Water	156
8.6 Concluding Remarks.....	156
 <u>Chapter 9 – Recommendations.....</u>	<u>158</u>
9.1 Higher-order and Non-local Continuum Theories	158
9.2 Improved Algorithms.....	159

9.3 Coarse-grained Models	159
9.4 Polymer Modeling	160
9.5 Temperature Effects.....	160
<u>References</u>	<u>161</u>
<u>APPENDIX A</u>	<u>180</u>
<u>APPENDIX B</u>	<u>184</u>
<u>APPENDIX C</u>	<u>186</u>

Nomenclature

$\bar{\sigma}_r$	Stress tensor of phase r and the overbar denotes a volume-averaged quantity
$\bar{\epsilon}_r$	Strain tensor of phase r and the overbar denotes a volume-averaged quantity
c_r	Volume fraction of phase r
\mathbf{C}_r	Stiffness tensor of phase r
\mathbf{A}_r	Concentration tensor of phase r
\mathbf{I}	Identity tensor
\mathbf{S}_r	Constituent Eshelby tensor
a_i^r	Reinforcement dimensions of the reinforcing phase r
A_r^{dil}	Dilute reinforcement approximation form of concentration tensor
\bar{C}	Composite modulus
\mathbf{F}_i	Force on atom i
\mathbf{m}_i	Mass of atom i in a system of N atoms
\mathbf{a}_i	Acceleration of atom i in a system of N atoms
\mathbf{r}_i	Position of atom i in a system of N atoms for a particular simulation step
r_{ij}	Distance between atom i and j
K	Kinetic energy of the molecular system
V	Potential energy of the molecular system
$V_R(r_{ij})$	Repulsive interaction between atom i and j
$V_A(r_{ij})$	Attractive interactions between atom i and j
B_{ij}	Many-body coupling between atoms i and j and the local environment of atom i .
K_r	Bond stretching force constant
r	Distance between atoms
r_{eq}	Equilibrium distance between atoms
K_θ	Bond-angle bending force constant
θ	Bond angle
θ_{eq}	Equilibrium bond angle

V_n	Torsion force constant
γ	Phase offset
n	Periodicity of the torsion
A_{IJ}, B_{IJ}	Van der Waals force constants between non-bonded atoms I and J
\mathbf{C}	Right Cauchy-Green deformation tensor
Ψ_c	Scalar strain-energy density function of the equivalent continuum
\mathbf{F}	Deformation gradient tensor
X_i, x_i	Vector components of material (undeformed) and the spatial (deformed) coordinates
t	Time
J	The ratio of the deformed to the undeformed volume is given by the Jacobian, which is defined as the determinate of the deformation gradient tensor \mathbf{F}
$\text{tr}(\mathbf{C}), \det(\mathbf{C})$	Trace and determinate of tensor \mathbf{C} , respectively.
$I_1, I_2, \text{ and } I_3$	Scalar invariant functions of \mathbf{C}
ψ_k	n convex scalar functions
$c_1, c_2, \text{ and } c_3$	Material constants and $c_1, c_2, c_3 \geq 0$
$\psi_{\text{vol}}, \psi_{\text{iso}}$	Strain energy densities associated with volumetric and isochoric deformations, respectively
$\Omega_1 \text{ and } \Omega_2$	Volumetric and isochoric deformation strain energy density terms, respectively
$\Lambda_{\text{total}}^0 \text{ and } \Lambda_{\text{total}}$	Potential energies of the molecular model before and after deformation, respectively
α_k	Scalar constant corresponding to the k^{th} deformation step
$\mathbf{x}^{(1)}, \mathbf{x}^{(2)}, \mathbf{x}^{(3)}, \text{ and } \mathbf{x}^{(4)}$	Spatial coordinates correspond to different strain levels

Chapter 1

Introduction

In 1959, Nobel laureate Richard P. Feynman delivered a talk at the American Physical Society at Caltech titled “There’s plenty of room at the bottom” [1]. This lecture was a solicitation to the innumerable opportunities in the uncharted area of nanoscience. Nanotechnology has opened doors to many fields of inter-disciplinary research spanning from engineering to biology.

“Materials Research to Meet 21st Century Defense Needs,” a publication by the National Research Council, reports that the Department of Defense has identified “materials design assisted by computation” as the top priority for research focus in the area of structural materials in 2003 [2]. Table 1.1 summarizes estimated savings with weight reductions from use of lightweight materials. Traditionally, the design process was subject to optimization for effective utilization of material properties. With the advancement in understanding of material behavior through computational studies one can achieve the dream of tailored materials designed specifically to suit the needs of an application.

Table 1.1 Estimated savings over lifetime with weight reductions for various applications [2]

Application	No. of Units Sold per Year	Pound of Weight Saved
Automobiles	30,000,000	\$2 per 100,000 miles
Commercial Aircraft	2,500	\$200 per 100,000 hours
Spacecraft	100	\$20000

1.1 MOTIVATION

Nanostructured composites are particularly conducive for material design because the properties can be carefully controlled through a top-down or bottom-up design approach by varying constituents and quantities of the constituents in a material. Aerospace applications can tremendously benefit from such material systems with a direct impact on weight savings resulting from efficient multifunctional materials performing more functions than being just structural members. In addition to savings in operational costs, weight reduction is of particular interest in unmanned air vehicles (UAV) and other defense applications where every pound of weight reduction has profound effects--resulting in improved flight time, maneuverability and survivability.

Polymer nanocomposites are expected to be widely used in the aerospace industry due to their unique strength-to-stiffness and weight-to-stiffness properties. The benefits of lightweight polymer composites can be enhanced with the incorporation of multifunctional capabilities. Multifunctional polymer materials have been shown to have wide range of motion under the influence of electric actuation. This property can be beneficial to aircraft structures, particularly in the case of UAV's by maximizing functionality of the structural members. A composite with desired properties can be synthesized through characterization of a large number of material systems by meticulous experimentation. However, this process involves exorbitant expense due to the costs and time involved in manufacture and the specialized equipment required for mechanical testing. Experimental methods also present great difficulty in the study of local interactions of constituent phases at nanoscale. The enormous cost and time demands can be offset through the use of virtual experimentation or computer simulations. Computer simulations facilitate ease of comprehensive parametric studies with much lower expenditure.

In recent decades, researchers have been actively involved in the development of comprehensive multiscale modeling techniques for metallic and ceramic materials. However, few modeling techniques for polymer composites have been explored due to the complex interactions that govern their physical behavior. Traditionally, continuum mechanics has been used for constitutive modeling of the mechanical behavior of composites. The scale of interactions of the constituent phases in nanocomposites is of the order of a few nanometers and the assumption of existence of continuum breaks down at the lengths involved. Recent studies have shown that a hierarchical multiscale modeling approach involving computational chemistry and continuum mechanics can help predict constitutive behavior of polymer nanocomposites without the need for assumption of continuum.

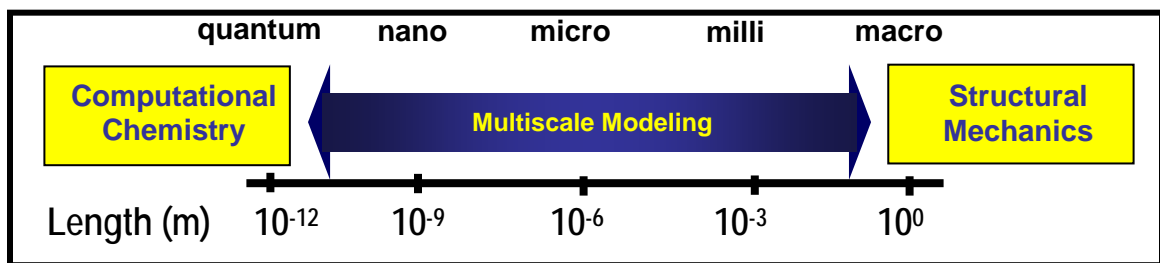


Figure 1.1 – Multiscale Modeling showing the modeling techniques involved at various length scales

1.2 OBJECTIVE

The objective of the proposed research is to develop a multiscale computational framework to predict mechanical constitutive behavior of polymeric materials from its molecular structure. The effects of the modeling parameters, such as force fields, molecular model size, and temperature will also be studied. A wide variety of parameters can be used with the computational chemistry tools that are used for molecular modeling in the multiscale modeling scheme. However, little has been

explored that would explain the cause and effect of the parameters and modeling procedure. A careful study of the predicted mechanical properties of a simple material system (pure polymer) as a function of their molecular structure can help develop an efficient modeling routine and provide understanding of material behavior from a fundamental standpoint. Pure polymeric materials models will be used in this study. This methodology will also be validated using experimental data available in the literature on the modeled materials.

1.3 LAYOUT

This dissertation is divided into nine chapters; each chapter is focussed on a specific topic. Chapter 1 serves as the introduction to the current work. In addition, it introduces the specific objectives of the current work presented in this manuscript and emphasizes the need for multiscale modeling. Chapter 2-7 are dedicated to various aspects of the multiscale modeling of the polymer materials.

Chapter 2 is a broader review of the various modeling techniques that can be employed for modeling of materials at various length scales. This chapter also reports some of the current state-of-the-art work in the area of multiscale modeling for polymers and polymer based materials. It introduces the widely used approaches that are used for predicting mechanical behavior based on molecular morphology. This chapter concludes with summarizing some of the recent finding reported by other research groups.

Chapter 3 presents the development of the equivalent continuum methodology that employs a hyperelastic continuum model to homogenize the molecular model to predict bulk-level properties. This methodology is applied to a polycarbonate and a polyimide and subsequently compared to experimental results available in literature.

At the molecular length scales, most polymers are highly inhomogenous and a single molecular model of the order of a few nanometers may not be able to capture the bulk-level behavior. In chapter 4, a methodology to incorporate multiple molecular models in conjunction with micromechanics is presented for better estimate of bulk-scale properties.

Bulk mechanical properties of polymer are almost constant but heterogeneities govern the behavior at smaller length scales. In chapter 5, the influence of model size on predicted mechanical properties are presented. Chapter 6 presents the results from the influence of temperature on the multiscale modeling methodology developed in the previous chapters. Chapter 7 reports the findings of the influence moisture on the predicted mechanical properties. Chapter 8 concludes the findings in the previous chapters and chapter 9 discusses possible extension of the multiscale modeling presented in the current manuscript.

Appendix A presents the functional form of the “force fields” that were used for the molecular dynamics. Appendix B presents some of the results of the influence of chain length on predicted mechanical properties.

Chapter 2

Literature Review

A review of modeling techniques for predicting the mechanical behavior of polymer nanocomposites is presented in this chapter. A detailed discussion of computational chemistry and computational mechanics modeling techniques is given. The specific molecular-based and continuum-based modeling approaches are described in terms of assumptions and theory. The approaches discussed are Ab initio simulations, Molecular dynamics, Monte Carlo, Analytical Micromechanics, Computational Micromechanics, Finite Element Methods, and Boundary Element Method. In addition to the discussion of the methods, specific results from recent studies are presented and compared. From these results, the general focus of current polymer nanocomposite modeling studies is summarized. It should be noted that the focus of the research presented in the current manuscript is to develop a multiscale modeling technique for prediction of mechanical properties of polymer materials, however, this chapter deals with the review of polymer nanocomposites in addition to pure polymers.

2.1 INTRODUCTION

In 1985, Smalley and co-workers at Rice University discovered cage-like carbon structures known as fullerenes; named after R. Buckminster Fuller [3]. These fullerenes are C₆₀ molecules with “buckyball” or “truncated icosahedron” structure consisting of 20 hexagons and 12 pentagons with a nearly spherical shape. In 1991, Iijma discovered carbon nanotubes [4], carbon nanotubes are closed graphene sheets with a cylindrical shape with end caps. They can be described as long and slender fullerenes. Research has shown that carbon nanotubes exhibit exceptional mechanical properties [5].

Although there has been some variation in the reported values for the carbon nanotube mechanical properties, the elastic modulus has been shown to be greater than 1 TPa and the tensile strength exceeds that of steel by over an order of magnitude. In view of the exceptional mechanical properties of carbon nanotubes, they have been considered as ideal reinforcements in composite structures. For nanotube composite materials, it has been shown that a carbon nanotube weight fraction of 1% results in the same increase in composite elastic modulus as a composite with a 10% weight fraction of carbon fibers, based on results from short-fiber composite theory [6]. This difference in elastic modulus is predicted even though the size scale of the two reinforcements differs by three orders of magnitude [7].

Nanoparticles with high aspect ratios have proven to be good reinforcing agents in polymeric materials [8]. Among all nanoparticle reinforced composites, the most widely investigated systems are based on silicates and clay particles. Ahn et.al. reported that the tensile modulus of composites reinforced with unmodified silica nanoparticles improved upon increasing the silica content, however, the elongation to failure decreased [9]. A research group at Toyota developed an economic industrial process for the manufacture of polymer/clay nanocomposites. This work led to the development of composites with twice the Young's modulus as that of the pure polymer. The increase in Young's modulus was also observed at elevated temperatures [10, 11].

The tremendous mechanical properties of carbon nanotubes and other nano-reinforcements can be realized only if efficient load transfer exists between the matrix and reinforcement [12-15]. It has been shown that in some cases the load transfer between nanotubes and the surrounding matrix can be increased by introducing non-bonded interfacial compounds or chemical cross-links between nanotubes and the matrix [16, 17, 18, Frankland, 2003 #94]. Despite these early efforts, more research is required to fully understand the effects of molecular structure of the nanotube/polymer interface on overall composite mechanical properties. Although experimental-based

research can ideally be used to determine structure-property relationships of nanostructured composites, experimental synthesis and characterization of nanostructured composites demands the use of sophisticated processing methods and testing equipment; which could result in exorbitant costs. To this end, computational modeling techniques for the determination of mechanical properties of nanocomposites have proven to be very effective [19-26]. Computational modeling of polymer nanocomposite mechanical properties renders the flexibility of efficient parametric study of nanocomposites to facilitate the design and development of nanocomposite structures for engineering applications.

This chapter will discuss the major modeling tools that are available for predicting the mechanical properties of nanostructured materials. Analytical and computational approaches to continuum-mechanics based modeling are discussed. Computational chemistry modeling approaches are also discussed briefly. Results found in the literature for the various modeling tools are tabulated and compared for six polymer nanocomposite systems. The comparison emphasizes the flexibility of the modeling approaches for different polymer nanocomposite geometries.

2.2 MODELING METHOD OVERVIEW

The importance of modeling in understanding of the behavior of matter is illustrated in Figure 2.1. The earliest attempt to understanding material behavior is through observation via experiments. Careful measurements of observed data are subsequently used for the development of models that predict the observed behavior under the corresponding conditions. The models are necessary to develop the theory. The theory is then used to compare predicted behavior to experiments via simulation. This comparison serves to either validate the theory, or to provide a feedback loop to improve the theory using modeling data. Therefore, the development of a realistic

theory of describing the structure and behavior of materials is highly dependent on accurate modeling and simulation techniques.

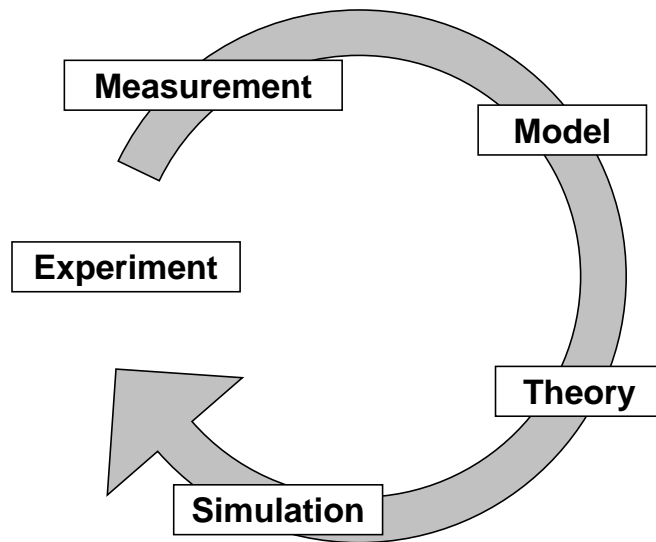


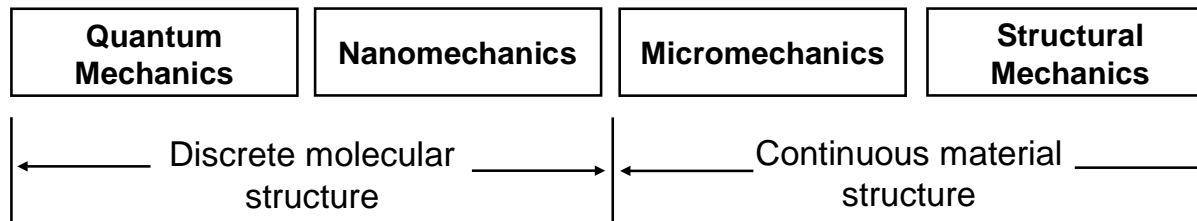
Figure 2.1. Schematic of the process of developing theory and the validation of experimental data (adapted from [25])

Mechanical properties of nanostructured materials can be determined by a select set of computational methods. These modeling methods span a wide range of length and time scales, as shown in Figure 2.2. For the smallest length and time scales, computational chemistry techniques are primarily used to predict atomic structure using first-principles theory and techniques based on it. For the macroscopic length and time scales, computational mechanics is used to predict the mechanical behavior of materials and engineering structures. Computational chemistry and computational mechanics modeling methods are based on thoroughly-established principles that have been developed in science and engineering. However, the intermediate length and time scales do not have general modeling methods that are as well-developed as those on the smallest and largest time and length scales. Therefore, multiscale modeling techniques are employed, which take advantage of computational chemistry and computational mechanics methods simultaneously for the prediction of the structure and properties of materials through bridging scales.

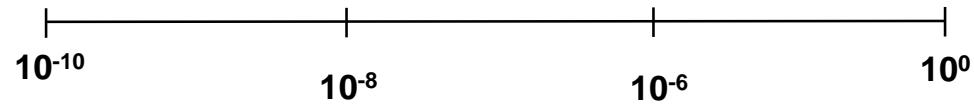
Modeling methods



Modeling tools



Length scale (m)



Time scale (sec)

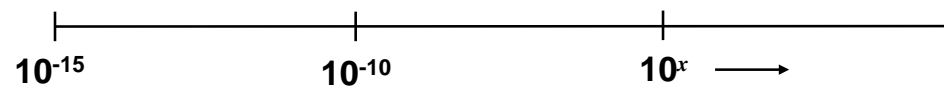


Figure 2.2. Various length and time scales used in determining mechanical properties of polymer nanocomposites

In Figure 2.2, each modeling method encompasses a broad class of relevant modeling tools. The quantum mechanical and nanomechanical modeling tools assume the presence of a discrete molecular structure of matter. Micromechanics and structural mechanics assume the presence of a continuum in the material structure. Figure 2.3 is a schematic that details the relationship of specific modeling techniques in computational mechanics and computational chemistry. The continuum-based methods primarily include techniques such as the Finite Element Method (FEM), the Boundary Element Method (BEM), and the micromechanics approach developed for composite materials. Specific micromechanical techniques include Eshelby approach, Mori-Tanaka method, Halpin-Tsai method [27-41]. The molecular modeling tools include molecular dynamics, Monte Carlo, and Ab-initio techniques. Each of this continuum and molecular-based modeling methods are described below.

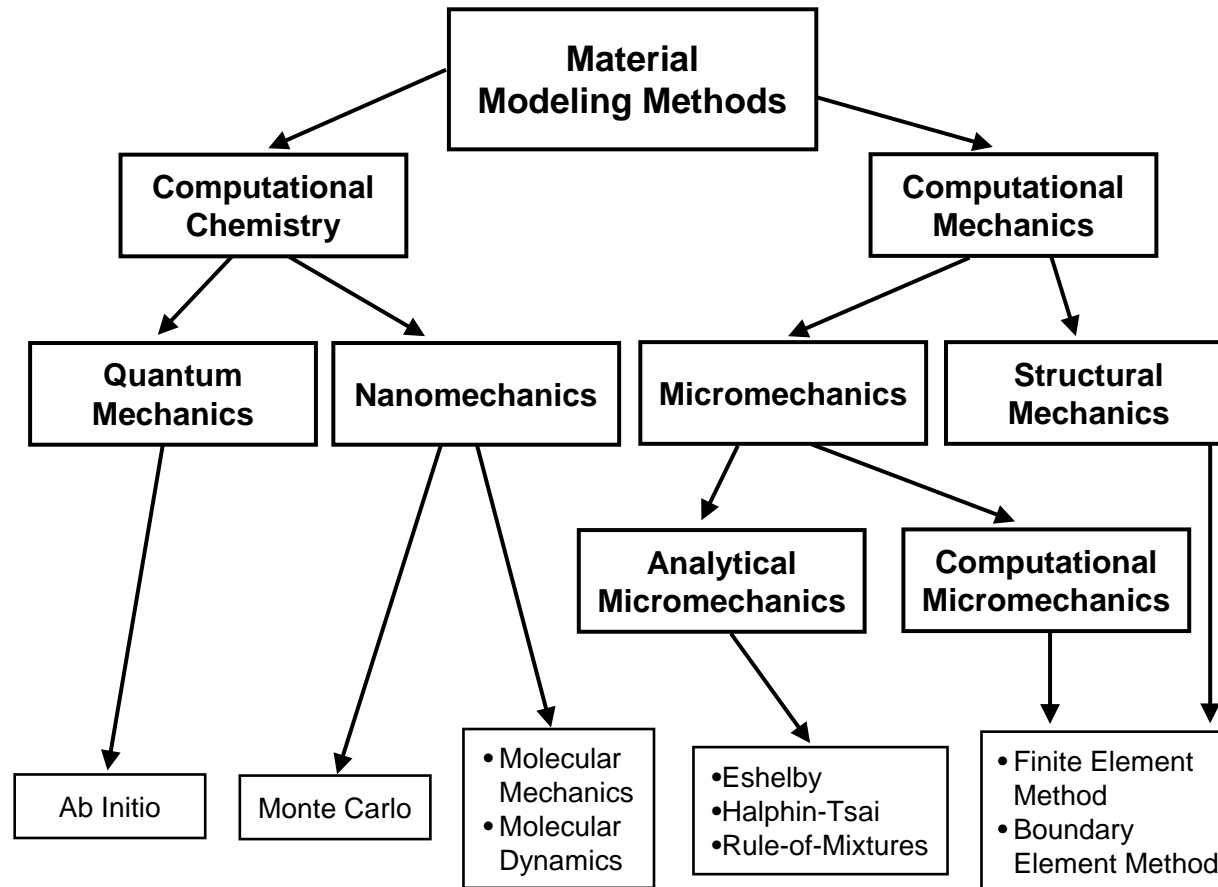


Figure 2.3. Diagram of material modeling techniques

2.3 CONTINUUM METHODS

These modeling methods assume the existence of continuum for all calculations and generally do not include the chemical interactions between the constituent phases of the composite. These methods can be classified as either analytical or computational.

A. Analytical Continuum Modeling

The overall properties of composites can be estimated by a volume average stress and strain fields of the individual constituents [36, 42]. The overall stress and strain of a composite with N distinct phases can be represented as follows

$$\bar{\boldsymbol{\sigma}} = \sum_{r=1}^N c_r \bar{\boldsymbol{\sigma}}_r \quad [2.1]$$

$$\bar{\boldsymbol{\varepsilon}} = \sum_{r=1}^N c_r \bar{\boldsymbol{\varepsilon}}_r \quad [2.2]$$

where $\boldsymbol{\sigma}_r$ is the stress tensor and $\boldsymbol{\varepsilon}_r$ is the strain tensor of phase r , c_r is the volume fraction of phase r , and the overbar denotes a volume-averaged quantity. The constitutive equation for each phase is given by

$$\boldsymbol{\sigma}_r = \mathbf{C}_r \boldsymbol{\varepsilon}_r \quad [2.3]$$

where \mathbf{C}_r is the stiffness tensor of phase r . The constitutive relationship between stress and strain for a composite material is given in terms of volume averaged stress and strain fields

$$\bar{\boldsymbol{\sigma}} = \mathbf{C} \bar{\boldsymbol{\varepsilon}} \quad [2.4]$$

The volume average strain of phase r is

$$\bar{\boldsymbol{\varepsilon}}_r = \mathbf{A}_r \bar{\boldsymbol{\varepsilon}} \quad [2.5]$$

where \mathbf{A}_r is the concentration tensor of phase r and

$$\sum_{r=1}^N c_r \mathbf{A}_r = \mathbf{I} \quad [2.6]$$

where \mathbf{I} is the identity tensor. Combining above equations results in the stiffness tensor in terms of the constituent stiffness tensors,

$$\mathbf{C} = \mathbf{C}_1 + \sum_{r=2}^N c_r (\mathbf{C}_r - \mathbf{C}_1) \mathbf{A}_r \quad [2.7]$$

Different methods exist for evaluation of the concentration tensor. When $\mathbf{A}_r = \mathbf{I}$; the above equation results in the rule-of-mixtures approach.

Neglecting the interaction between the reinforcing particles in the composite results leads to the dilute concentration approximation. The dilute concentration tensor is given by

$$\mathbf{A}_r^{dil} = \left[\mathbf{I} + \mathbf{S}_r \mathbf{C}_1^{-1} (\mathbf{C}_r - \mathbf{C}_1) \right]^{-1} \quad [2.8]$$

where \mathbf{S}_r is the constituent Eshelby tensor [37]. The Eshelby tensor can be evaluated as a function of reinforcement dimensions, a_i^r , of the reinforcing phase r and properties of the matrix,

$$S_r = f(C_1, a_1^r, a_2^r, a_3^r) \quad [2.9]$$

Various expressions for the Eshelby tensor can be found in literature [36]. For Mori-Tanaka approach, the concentration tensor is given by

$$A_s^{MT} = A_s^{dil} \left[c_1 I + \sum_{r=2}^N c_r A_r^{dil} \right]^{-1} \quad [2.10]$$

where A_r^{dil} is given by equation (VIII). Another form of concentration tensor used in the Self-consistent scheme is given by

$$A_r^{SC} = [I + S_r C^{-1} (C_r - C)]^{-1} \quad [2.11]$$

where C is the unknown composite modulus. The Self-consistent scheme utilizes an iterative technique to evaluate the modulus of the composite material.

Pipes et.al. used an anisotropic elasticity approach to study the behavior of a layered cylinder with layers of discontinuous CNT following a helical path in each layer [43-45]. Odegard et.al. used the Mori-Tanaka method to predict elastic properties of polyimide/CNT composites at various lengths, orientations, and volume fractions[46]. A similar micromechanics-based approach was used by Odegard et.al. to predict the properties of CNT/polyethelene composites. This study also examined the effects of CNT functionalization in CNT/polyethylene composites and showed that functionalization deteriorated the overall composite mechanical properties. In another

study, MWNT/polystyrene composite elastic properties were shown to be sensitive to nanotube diameter by an approach based on Halpin-Tsai micromechanical method [47]. Lagoudas et.al. predicted elastic properties of CNT/epoxy composites using a variety of analytical micromechanics approaches [48].

B. Computational Continuum Modeling

Some of the widely used continuum-based computational modeling techniques include FEM and BEM. While these approaches may not always supply exact solutions, they can provide very accurate estimates for a wide range of assumptions. These approaches are described in detail below.

i. Finite element method

FEM can be used for numerical computation of bulk properties based on the geometry, properties, and volume fraction of constituent phases [49-51]. FEM involves discretization of a material representative volume element (RVE) into elements for which the constitutive model based solutions lead to determination of stress and strain field. The coarseness of the discretization generally determines the accuracy of the solution. Nanoscale RVEs of different geometric shapes can be chosen for simulation of mechanical properties [19, 20]. However, high complexity of models, expensive software, and time-consuming simulations limit the utility of this method. In general, FEM models require an input of the constitutive model that describes the mechanical response of the material being modeled. So FEM models require benchmarking against molecular informed techniques.

FEM-based micromechanics have been used extensively for the prediction of mechanical properties of nanostructured composites. Li et.al. used an FEM-based approach to investigate the stress concentration at the end of carbon nanotubes and the

effects of nanotube aspect ratio on the load transfer between nanotubes and matrix [52]. Bradshaw et.al. used FEM to evaluate the strain concentration tensor in a composite consisting of wavy carbon nanotubes [53]. Fisher et.al. used FEM to determine the effect of waviness on effective moduli of CNT composites [54]. Chen et.al. used different shapes of RVEs to understand the dependence of predicted properties on the element shape [19].

ii. Boundary element method

BEM is a continuum mechanics approach which involves solving boundary integral equations for the evaluation of stress and strain fields [55]. This method uses elements only along the boundary, unlike FEM, which involves elements throughout the volume; thus making BEM less computationally exhaustive than FEM [55-58]. BEM can be applied from micro to macro scale modeling [56]. Like FEM in BEM, it is assumed that a material continuum exists, and therefore, the details of molecular structure and atomic interactions are ignored.

The rigid fiber model has been shown to be very effective in estimation of fiber composites [57]. Ingber et.al. have shown agreement in predicted modulus using BEM and analytical results for fiber composites [57]. Liu et.al. used a fast multipole method to model CNT composites [56]. They treated CNTs as rigid fibers and the properties were obtained in an analogous manner to a rigid inclusion problem. The estimated modulus was found to be very close to that predicted by MD simulations [56]. They concluded that BEM can be a very useful for first-order approximation of mechanical properties in large-scale modeling of CNT composites.

2.4 MOLECULAR MODELING

In recent years molecular modeling has emerged as an important tool in the prediction of physical material properties such as elastic response, atomic structure, vibrational frequencies, heat of reaction, thermal conductivity, electric permittivity, and binding energies. Molecular modeling assumes a non-continuous composition of the material, which makes it a powerful tool for a precise study of atomic interactions at the nanometer length scale. Due to the discrete nature of these techniques, they are often limited by the length and time scales that can be achieved in the simulations, and thus the techniques can be computationally exhaustive. Three widely used molecular modeling techniques for the prediction of mechanical properties of nanostructured materials are molecular dynamics (MD), monte carlo (MC), and ab initio simulation.

A. Molecular Dynamics

MD is the most widely used modeling technique for the simulation of nanostructured materials. MD allows accurate predictions of interactions between constituent phases at the atomic scale. It involves the determination of the time evolution of a set of interacting atoms, followed by integration of the corresponding equations of motion [59, 60]. The equations of motion of the atoms are given by Newton's second law:

$$F_i = m_i a_i \quad [2.12]$$

where \mathbf{F}_i is the force on atom i and \mathbf{m}_i and \mathbf{a}_i are the mass and acceleration, respectively, of atom i in a system of N atoms.

MD is a statistical mechanics method, a set of configurations are distributed according to a statistical ensemble or statistical distribution function. The trajectories of the motion of the atoms are calculated under the influence of interaction forces of the

atoms. The trajectory is calculated in a phase space with $6N$ dimensions; three position and three momenta components for each atom. Calculation of physical quantities by MD simulation is obtained by arithmetic averages of instantaneous energy values from individual simulation steps. MD simulations, if run for a sufficiently long time, theoretically can completely sample the phase space. However, in practice, simulation times are limited. Physical quantities are sampled after the molecular system reaches a thermodynamic equilibrium.

Interactions of different atom types are described by an atomic potential [60]. The total potential energy of the system can be evaluated as a function of the position of the atoms at a given time,

$$V = V(r_i, \dots, r_N) \quad [2.13]$$

where \mathbf{r}_i is the position of atom i in a system of N atoms for a particular simulation step. The positions of atoms are expressed relative to each other so that the atomic potential is invariant with respect to coordinate transformations. The force on an atom i is determined from the gradient of the potential V with respect to atomic displacements r_i ,

$$F_i = -\nabla V(r_1, \dots, r_N) \quad [2.14]$$

The total energy of the system is

$$E = K + V \quad [2.15]$$

where K is the kinetic energy and V is the potential energy of the system.

The potential describing the interaction of atoms in an organic material is given in many forms. For a system involving only carbon and hydrogen, Brenner's potential is widely

used for bonded interactions [61, 62]. Brenner's potential is based on the principle that the strength of the bond between two atoms is not constant, but depends on local conditions. It can be expressed as

$$V = \sum_i \sum_{j(>i)} [V_R(r_{ij}) - B_{ij} V_A(r_{ij})] \quad [2.16]$$

where the summation is performed over bonds of the system, r_{ij} is the distance between atoms i and j , $V_R(r_{ij})$ and $V_A(r_{ij})$ are repulsive and attractive interactions, respectively, and B_{ij} is the many-body coupling between atoms i and j and the local environment of atom i . Force fields provide a simple and effective approach for describing the atomic potential of interacting atoms consisting of many different atom types [60, 63-65]. The force field can be described by the sum of the individual energy contributions from each degree of freedom of the system of N atoms, as shown in Figure 2.4. The non-bonded interactions shown in Figure 2.4 represent van der Waals, hydrogen, and electrostatic bonding. The force field equation developed by Cornell et.al. for organic molecular systems is [63]

$$V = \sum_{bonds} K_r (r - r_{eq})^2 + \sum_{angles} K_\theta (\theta - \theta_{eq})^2 + \sum_{dihedrals} \frac{V_n}{2} [1 + \cos(n\phi - \gamma)] + \sum_{I < J} \left[\frac{A_{IJ}}{r_{IJ}^{12}} - \frac{B_{IJ}}{r_{IJ}^6} \right] \quad [2.17]$$

where K_r is the bond stretching force constant, r is the distance between atoms, r_{eq} is the equilibrium distance between atoms, K_θ is the bond-angle bending force constant, θ is the bond angle, θ_{eq} is the equilibrium bond angle, V_n is the torsion force constant, γ is the phase offset, n is the periodicity of the torsion, A_{IJ} and B_{IJ} are van der Waals force constants between non-bonded atoms I and J , and r_{IJ} is the non-bonded distance between atoms I and J . The van der Waals interaction term in Equation [2.17] is in the

form of the Lennard-Jones potential. Tables 2.1 and 2.2 list force constants for bond stretching and bond angles bending, respectively, for different atom types [63].

Table 2.1. Bond stretching force constants for aromatic carbon (CA) and aliphatic carbon (CT) [63]

Interacting Atom Types	Equilibrium Spacing r (Å)	Force Constant K_r (kcal/mol/ Å ²)
CA-CA	1.4	469
CT-CT	1.526	310
CA-CT	1.510	317

Table 2.2. Bond-angle bending force constants for aromatic carbon (CA), aliphatic carbon (CT), and hydrogen (HC) [63]

Interacting Atom Types	Equilibrium Angle θ (deg)	Force Constant K_θ (kcal/mol/rad ²)
CA-CA-CA	120	63
CA-CT-CT	114	63
CT-CT-HC	109.5	50

The Equivalent-Continuum Method (ECM) is used to determine the bulk-level mechanical properties of a material from the molecular model. ECM is a methodology for linking computational chemistry and solid mechanics. An equivalent continuum, identical to the MD model in geometry is developed and a constitutive law is used to describe the mechanical behavior of the continuum [26, 46, 66, 67]. Figure 2.5 shows a molecular model of a nanotube reinforced polymer composite and its equivalent continuum model. The energies of deformation of the molecular and equivalent-

continuum models are derived for identical loading conditions. The unknown mechanical properties of the equivalent continuum are determined by equating the energies of deformation of the two models under these loading conditions. The properties of a larger-scale material are then determined using the equivalent-continuum volume element properties.

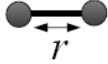
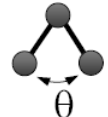

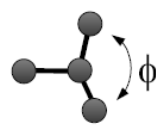
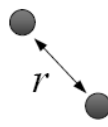
Bond stretching	
Bond Angle Bending	
Bond Torsion	
Improper Bond Torsion	
Non-Bonded Interactions	

Figure 2.4. Force field degrees of freedom

Odegard et.al. have used the ECM and MD to predict the properties of various CNT based composite systems [26, 46, 66, 68-70]. They predicted the elastic properties of PmPV CNT/polyimide composite for a wide range of nanotube lengths, orientations, and volume fractions. They also used a similar approach to predict behavior of functionalized and non-functionalized CNT/polyethylene composites[71]. Frankland et.al. used MD to study the influence of chemical functionalization on the CNT/polyethylene composites [16]. They also studied the critical nanotube length

required for effective load transfer. Frankland et.al. predicted stress-strain curves from MD and compared them to those obtained from micromechanical models for CNT/polyethylene composites[70]. Hu et.al [17, 18] used MD to understand the effect of chemical functionalization on toughness of CNT/polystyrene composites.

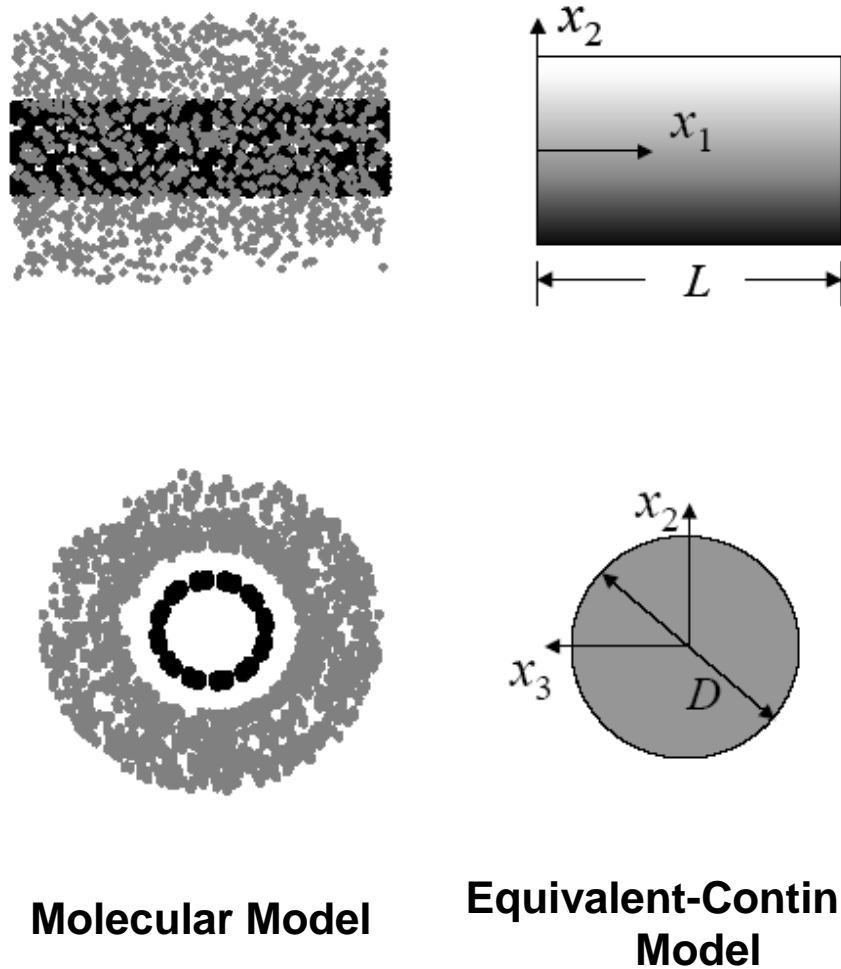


Figure 2.5. The Equivalent-continuum model of a PmPV-nanotube composite [46]
 (Reprinted from Composites Science and Technology, **63**(11), Odegard, G.M., *et al.*,
Constitutive Modeling of Nanotube-Reinforced Polymer Composites. p. 1671-1687, 2003,
 with permission from Elsevier, please refer to Appendix C)

MD has been used for simulation of other physical properties of nanocomposites. Wei et.al. showed that addition of CNTs to polyethylene resulted in an increase of thermal expansion, glass transition temperature, and diffusion coefficients of the polymer [72]. Lordi and Yao calculated sliding frictional stresses between CNT and various polymer substrates based on molecular mechanics simulations [73]. Liang et.al. showed the presence of an attractive interaction between SWNTs and epoxy polymer matrix [74]. Frankland et.al. characterized the interfacial friction model for the pull-out of SWNTs from a polyethylene matrix [75].

B. Monte Carlo

MC is a class of probabilistic mathematical models for the prediction of the behavior and outcome of a system [76]. The outcomes of MC are statistical in nature and subject to laws of probability. In most cases it involves a multidimensional integration over the sample space. Different MC techniques can be used for determination of material properties; classical MC, quantum MC, volumetric MC and kinetic MC. Classical MC involves drawing samples from a probability distribution, often the classical Boltzmann distribution, to obtain thermodynamic properties or minimum-energy structures. Quantum MC utilizes random walks to compute quantum-mechanical energies and wave functions to solve electronic structure problems, generally using Schrödinger's equation as starting point. Volumetric MC generates random numbers to determine molecular volumes per atom or to perform geometrical analysis. Kinetic MC simulates process by the use of scaling arguments to establish time scales. It also includes MD simulations which involves stochastic effects.

Based on the dependence of time, MC simulations can be classified as either metropolis MC or kinetic MC. Metropolis MC applies to systems under equilibrium, and thus is independent of time. This method generates configurations according to a statistical-mechanics distribution, whereas kinetic MC deals with systems under non-equilibrium.

The kinetic MC technique uses transition rates that depend on the energy barrier between the states, with time increments formulated so that they relate to the microscopic kinetics of the system.

Ford et.al. used MC techniques to study the mechanical and phase behavior of quartz, cristobalite, coesite, and zeolite structures [77]. The bulk modulus predicted from their model was found to be in good agreement with experimental values. They concluded that the model can be used to determine properties of silica nanostructures with atomistic detail. Chui et.al. used a MC-based modeling approach to study deformation, rate of deformation, and temperature dependence of large strain deformation in amorphous polymeric materials [78].

C. Ab-Initio

Unlike most materials simulation methods that are based on classical potentials, the main advantages of ab-initio methods, which is based on first-principles density functional theory (without any adjustable parameters), are the generality, reliability, and accuracy of these methods. They involve the solution of Schrödinger's equation for each electron, in the self-consistent potential created by the other electrons and the nuclei. Ab-initio methods can be applied to a wide range of systems and properties [79, 80]. However, these techniques are computationally exhaustive, making them difficult for simulations involving large numbers of atoms.

There are three widely-used procedures in ab-initio simulation. These procedures are single point calculations, geometry optimization, and frequency calculation. Single point calculations involve the determination of energy and wave functions for a given geometry. This is often used as a preliminary step in a more detailed simulation. Geometry calculations are used to determine energy and wave functions for an initial geometry, and subsequent geometries with lower energy. A number of procedures exist

for establishing geometries at each calculation step. Frequency calculations are used to predict infrared and Raman intensities of a molecular system. Frequency calculations can also be used to ascertain if a current structure corresponds to minimum energy. Ab-initio simulations are restricted to small numbers of atoms because of the intense computational resources that are required.

Ab-initio techniques have been used on a limited basis for the prediction of mechanical properties of polymer-based nanostructured composites. A study conducted by Mylvaganam et.al. demonstrated that nanotubes of smaller diameters have higher binding energies in a polyethylene matrix [81-83]. Bauschlicher studied the bonding of fluorine and hydrogen atoms to nanotubes [84]. He showed that fluorine atoms favored to bond to existing fluorine atoms.

2.5 SIMULATED RESULTS

As indicated in the previous sections, numerous attempts have been made to study the mechanical behavior of polymer nanocomposites using modeling techniques. A summary of some of these techniques as applied to six material systems is shown in Table 2.3. For each material system, one or more simulation methods have been applied to examine elastic modulus, constitutive behavior, interfacial bonding, or load transfer between the reinforcement and polymer matrix.

From the general results from these studies, several conclusions can be drawn. First, there is a strong effect of the interfacial conditions between the nano-reinforcement and matrix on the mechanical properties. The interfacial conditions can improve the load transfer via bonded (functionalization) or non-bonded means. Second, there is a measurable influence of the reinforcer length and diameter on the overall composite properties. Third, use of traditional micromechanical theories to predict overall composite properties without the aid of molecular modeling do not always result in

accurate predicted mechanical properties. Fourth, the study of CNT-based composites has been the focus these studies, with less attention given to nanoclays and nanoparticles. Fifth, the models have generally only examined elastic properties of composites. To date, little work has been performed on nonlinear mechanical behavior or failure of these materials.

2.6 SUMMARY

The modeling and simulation of polymer-based nanocomposites has become an important topic in recent times because of the need for the development of these materials for engineering applications. A review of the most widely used modeling techniques used for prediction of mechanical properties of polymer nanocomposites has been presented in this paper. In addition, results from recent modeling studies have been presented and discussed.

Because of the complex interactions between constituent phases at the atomic level, a combination of modeling techniques is often required to accurately simulate the bulk-level behavior of these composites. The computational chemistry techniques assume the presence of a discrete molecular structure, and are primarily used to predict the atomic structure of a material. Computational mechanics techniques assume that the matter is composed of one or more continuous constituents, and are used to predict the mechanical behavior of materials and structures. These two types of modeling techniques must be combined to an overall multiscale model that is capable of predicting the structure and properties of polymer nanocomposites based on fundamental and scientific principles.

Table 2.3. Material systems characterized by different modeling techniques

Material System	Simulation Method	Predicted Properties	Conclusions/Remarks
CNT/Polyethylene	MD, Mori-Tanaka	Elastic Modulus	The moduli of functionalized and non-functionalized systems were determined and compared [69]
	MD	Elastic Modulus	Effect of chemical crosslink density on load transfer was established [16]
	MD	Stress- Strain	Comparisons of composite modulus from MD and rule-of-mixtures techniques for three different cases of nanotubes was predicted [70, 85]
CNT/ Polyimide	MD, Mori-Tanaka	Elastic Modulus	Critical length for maximum load transfer was determined and the use of chemical interface between nanotube and matrix was explored [46]
Nanoclay/ Polyamide	MD, Halpin-Tsai	Elastic Modulus	The effects of interlayers, the structure of clay clusters, and platelet distributions on properties were determined and compared to Halpin-Tsai predictions [86, 87]
	MD, Halpin-Tsai, Mori-Tanaka, FEM	Elastic Properties	Multiscale modeling of nanoclay reinforced polymer composites was presented [22]
CNT/ Epoxy	MD	Interfacial Bonding	Effect of nanotube loading on mechanical properties was established [88]
CNT/ Polystyrene	MD, Halpin-Tsai	Load Transfer	The effects of nanotube diameter and cross-links between nanotubes and polymer on mechanical properties were studied [18, 47]
Nanoparticle/ Polyimide	MD, Eshelby	Elastic Modulus	Effect of the nanoparticle/polyimide interface on elastic properties was determined [89]

Chapter 3

(Reprinted from International Journal of Solids and Structures, **44**(3-4), Valavala, P.K. *et. al.*, *Nonlinear Multiscale Modeling of Polymer Materials*, p. 1161-1179, 2007, with permission from Elsevier, please refer to Appendix C)

Nonlinear Multiscale Modeling of Polymer Materials

In this chapter, a hyperelastic multiscale modeling technique is used to predict elastic properties of polycarbonate and polyimide polymer systems using a set of widely accepted atomistic force fields. The model incorporates molecular simulations and a nonlinear, continuum mechanics-based, constitutive formulation that incorporates the behavior of the polymer materials as predicted from molecular simulations. The predicted properties of the polymers using multiple force fields are compared to experimentally-measured values. Both static and dynamic molecular simulations are performed using Molecular Mechanics energy minimizations and Molecular Dynamics simulation techniques, respectively. The results of this study indicate that static molecular simulation is a useful tool to predict the bulk-level nonlinear mechanical behavior of polymers for finite deformations. It is found that the AMBER force field yields the most accurate predicted mechanical and physical properties of the modeled polymer systems compared to the other force fields used in this study. Please see Appendix C for copyright permission for this chapter.

3.1 INTRODUCTION

Polymers and polymer nanocomposites are important materials in the design of aerospace structures because of their large stiffness-to-weight and strength-to-weight ratios relative to metal- and ceramic-based materials. To facilitate the development of

these materials, multiscale modeling strategies must be developed that predict the bulk mechanical properties of the materials as a function of the molecular structure.

Molecular Mechanics (MM) and Molecular Dynamics (MD) simulation techniques can be used to predict the molecular structure of a material and the behavior of the molecular systems when subjected to applied mechanical deformations. Many studies have focused on modeling and simulation of polymers and polymer-based nanocomposites via MM and MD techniques [18, 70, 71, 73, 74, 85, 89-93]. These studies have demonstrated that molecular modeling techniques can be effectively used to predict both structure and elastic mechanical properties of polymer-based material systems. Three important factors required for the accurate prediction of properties of polymer material systems using a multiscale modeling approach are: (1) the assumed continuum mechanics-based constitutive relationship, (2) the selection of the molecular-level interatomic potential, and (3) the molecular modeling procedure.

To accurately describe the mechanical stress-strain response of polymer-based materials subjected to large deformations, it is necessary to formulate the constitutive law within a finite-deformation framework. While hyperelastic formulations have been developed and characterized for compressible and incompressible materials [94, 95], they have been scarcely used in the multiscale modeling of polymer-based materials. It is proposed that formulation of hyperelastic constitutive equations, in conjunction with molecular modeling, can be used for the development of reliable structure-property relationships in polymer material systems.

Several simplified atomic potentials, or force fields, for organic-based material systems have been developed in recent years that describe the interactions between bonded and non-bonded atoms [63, 64, 96-100]. Each of these force fields has been characterized via experimental techniques and quantum computations and is described by their own set of unique parameters and functional forms. Even though it is expected that these

different parameters and forms will affect the relationship between force field type and predicted mechanical properties, little is known about the specific cause-and-effect relationships as applied to polymeric materials.

The establishment of a molecular structure for a polymer material before and after deformation, for a given force field, can be achieved with either static or dynamic molecular simulation techniques using MM and MD, respectively. With the static approach, the potential energy of the molecular system, as defined by the force field, is minimized to reach the equilibrated state. While the static procedure converges onto the equilibrated structure quickly, the mapping of real time molecular motion onto the molecular structure is lost. With the dynamic approach, the motion of the individual atoms in real time is determined using Newton's laws of motion. While the dynamic approach preserves time as the independent variable with the corresponding molecular structure, convergence onto a minimized molecular energy can be computationally more time-intensive than with the static approach. It is unclear how these different approaches affect the accurate prediction of mechanical properties of polymer-based materials using a multiscale approach.

Therefore, the objective of the present paper is to develop a multiscale modeling technique based on molecular simulations and hyperelasticity to predict elastic constitutive properties of two different polymer systems. The predicted values of elastic properties, unique for each combination of force field and modeling technique, will be compared to experimentally-measured values. The polymers include a polycarbonate (Figure 3.1) and a polyimide from 3,3',4,4'-biphenyltetracarboxylic dianhydride (BPDA) and 1,3-bis(4-aminophenoxy)benzene (APB) monomers (Figure 3.2 and 3.3) [101, 102]. The three force fields used in this study are described in subsequent sections of the paper. Based on the comparison of prediction to experiment, the most appropriate force field and modeling technique for the prediction of mechanical properties of polymer-based nanocomposite systems is determined.

3.2 FORCE FIELDS

Three distinct force fields were used in this study to simulate the polymer deformations and provide inputs necessary to compute the mechanical properties; AMBER [63] (without electrostatic interactions), OPLS-AA [100, 103], and MM3 [64]. Each of the force fields has a unique functional form and set of force constants, which is summarized in the Appendix. These three force fields were chosen because of their frequent use in computational chemistry research and because they are capable of modeling virtually any organic structure. Other atomic potentials commonly used in computational chemistry research, such as the Brenner [61] and Tersoff [104, 105] models, are restricted to hydrocarbons and silicon systems. Tersoff potential is an empirical interatomic potential primarily developed for calculation of structural properties and energetics of silicon systems. However, it was later extended to accommodate for simulations involving graphite and amorphous carbon systems. Brenner potential is an empirical many-body potential which is a highly parameterized version of Tersoff's formalism that can account for intramolecular chemical bonding in hydrocarbons and diamond. Thus, the Brenner and Tersoff potentials could not be used for the systems considered in the present study.

Each of the force constants for these three force fields is unique for each force field and interacting atom types. For all three force fields, it was assumed that torsional force constants that were not defined in the respective literature references or by the simulation software [106] were zero-valued. For the AMBER force field, the specific force constants used were those specified by the AMBER99 parameter set in the simulation software.

3.3 EQUIVALENT CONTINUUM MODELING

The nonlinear-elastic (hyperelastic) properties of the two material systems were determined using the Equivalent-Continuum Modeling method [46, 68, 89, 107]. This modeling technique is ideally suited for large, amorphous atomic structures with a mixture of covalent and secondary chemical bonds, as the Cauchy-Born rule is ignored because of immense computational complexity that would result if it was incorporated under these conditions. It is important to note that the nonlinearity in the constitutive modeling refers only to the hyperelastic approach incorporated, not the presence of constitutive nonlinearities, such as plasticity. This approach consisted of three steps. First, representative volume elements (RVEs) of the molecular structures of both polymers for each force field were chosen that accurately described the bulk structures of the materials. Next, a constitutive law that described the behavior of the equivalent-continuum model was established. Finally, the energies of deformation of the two models were equated under identical sets of boundary conditions to determine each of the material parameters in the constitutive equation. Each of these steps is described in detail below.

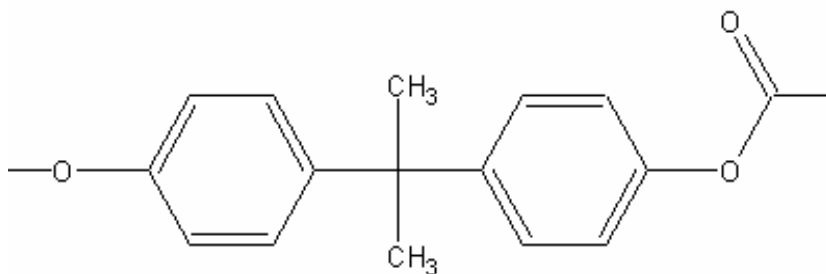


Figure 3.1. Schematic illustration of the polycarbonate monomer unit

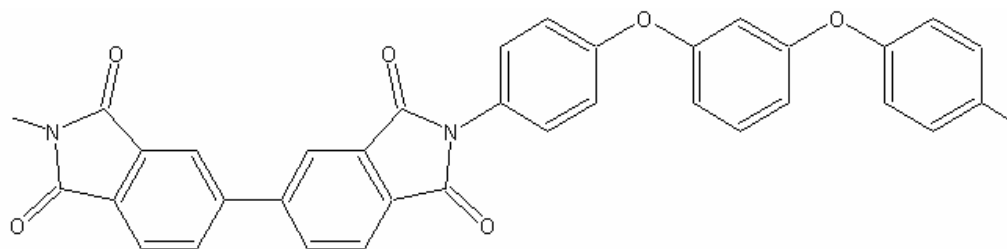


Figure 3.2. Schematic illustration of the BPDA (1,3,4) APB polyimide monomer unit

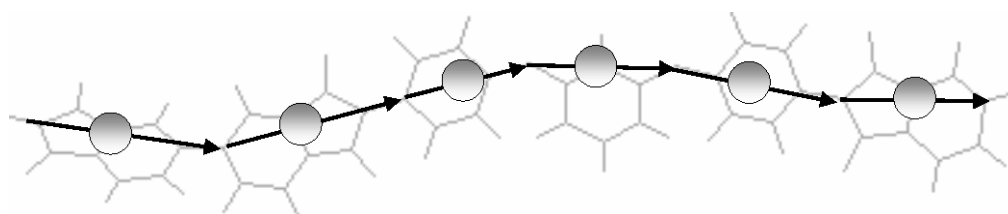


Figure 3.3. Depiction of the mapping of the atomistic polymer model to the coarse-grained linked vector model

A. Representative Volume Element

The RVEs of the molecular models were established from the equilibrium molecular structures of the polymers for each force field determined using MD simulations. The molecular structures of the polymers represent the room temperature condition. The RVE geometry of the molecular models selected was a cubic box and the specific configuration for the two polymer systems were established as described below.

The polycarbonate model was initially prepared in the gas phase. Six chains of 20 monomer units each (a total of 3972 atoms) were constructed and the system was condensed to a low density with an NPT (constant number of atoms, pressure, and

temperature) MD simulation at 300K and 1 atm for 50 ps. This process was followed by an NVT (constant number of atoms, volume, and temperature) simulation for 100 ps at 600K. The temperature was reduced in a stepwise fashion with a series of NPT MD simulations at 1 atm pressure to obtain the final equilibrated system. These equilibration simulations were performed with the CVFF force field [108].

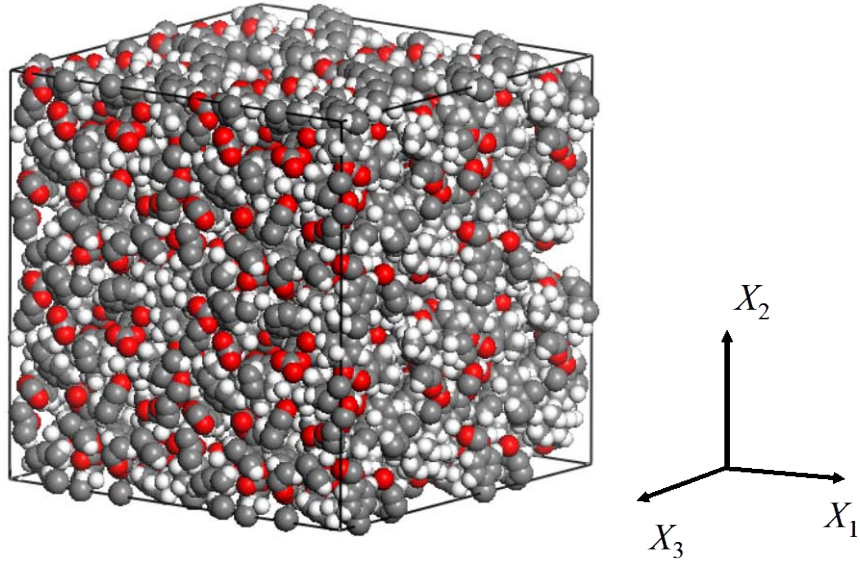


Figure 3.4. RVE of the polycarbonate material

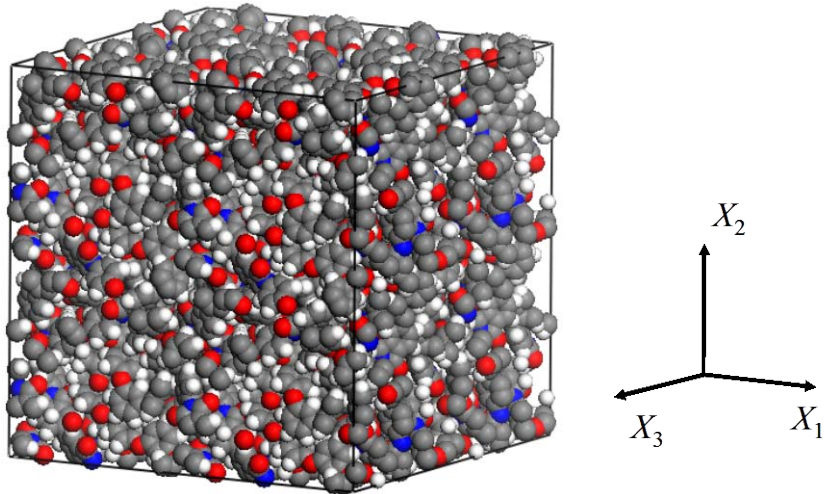


Figure 3.5. RVE of the polyimide material

The molecular model of the polyimide was prepared with the aid of a reverse-mapping procedure that utilizes a coarse-grained model [109]. In this process, each polyimide molecule, in the coarse-grained structure was a linked vector model used to represent the rigid rings that comprise the polyimide backbone (Figure 3.3). The linked vectors followed the contour of the molecule. The parameters used for this model consisted of angular distributions between consecutive vectors and long-range forces between beads placed along the midpoint of each vector. These parameters were estimated from MD simulation of the polyimide monomers with the CVFF force field [108]. The centroids of the beads placed at the midpoint of each vector were the centers for interaction forces between non-adjacent beads along the chain of the polymer and between beads on different chains. The coarse-grained polymers were initially placed as random walk chains inside a simulation box such that the density was close to the bulk value. The bulk polymer model consisted of seven chains of polymers each composed of ten of the repeat units shown in Figure 3.1. The choice of seven chains was made to create a moderately large simulation box with 4214 atoms. In this initial placement, only the angular distributions between adjacent vectors along the chain were considered in the equilibration. Monte Carlo simulation was used to equilibrate the chains from their initial starting configuration. The simulation ran at 650K until relaxation of an autocorrelation function [110] of the end vectors was achieved and the average centers of mass were displaced a distance greater than the square of the average radii of gyration. After sufficient equilibration with the coarse-grained Monte Carlo model, the chains were reverse-mapped to the fully atomistic configuration by replacing the deleted atoms back into position along the vectors of the coarse-grained model.

The resulting equilibrated atomistic structures for both polymers were subsequently subjected to NPT MD simulations for 200 ps at 300 K and 1 atm using the AMBER, OPLS-AA, and MM3 force fields respectively. These constant-pressure MD

simulations allowed the atomistic structures to relax to the equilibrium density and thus any residual stresses averaged over the RVE were minimized. It was assumed that this step also eliminated any spurious effects of using different techniques to create the two polymer structures. The employed algorithm preserved the cubic structure of the simulation box while allowing the size of the simulation box to change. The final periodic boundary box sizes varied from 37.7 Å to 47.2 Å on a side depending on the force field used. After the NPT MD simulations, the densities of the polycarbonate were 1.2, 0.4, and 1.1 g/cm³ for the AMBER, OPLS-AA, and MM3 force fields, respectively, and the densities of the polyimide were 1.0, 0.6, and 1.2 g/cm³ for the AMBER, OPLS-AA, and MM3 force fields, respectively. The densities for the two polymers predicted with the AMBER and MM3 force fields are within the range of reasonable values of 1.2 - 1.4 g/cm³ [111]. However, the densities of the polymers predicted with the OPLS-AA force field are much lower than the expected values. Examples of RVEs of the polycarbonate and polyimide are shown in Figures 3.3 and 3.4, respectively.

B. Constitutive Equation

For the computational simulation of a hyperelastic polymer material subjected to finite deformation, it is assumed that the strain-energy function is associated with stress and deformation tensors that are thermodynamic work conjugates in the balance of mechanical energy and satisfies the Clausius-Duhem inequality and the requirement of observer-frame indifference (known as the hyperelastic approach) [112]. Although many authors choose to model the deformation of polymers using a strain-energy function based on a free energy associated with changes in entropy (known as the statistical approach) [113], it has been shown that the hyperelastic approach yields more accurate results than the statistical approach [94]. Furthermore, the statistical approach neglects all molecular interactions except the straightening of the polymer chains, while

the hyperelastic approach can consider a wide range of polymer degrees of freedom, such as those specified in Equations (A.1) - (A.18).

The second Piola-Kirchhoff stress tensor is

$$\mathbf{S} = 2 \frac{\partial \Psi_c(\mathbf{C})}{\partial \mathbf{C}} \quad [3.1]$$

where \mathbf{C} is the right Cauchy-Green deformation tensor and Ψ_c is the scalar strain-energy density function of the equivalent continuum. The second Piola-Kirchhoff stress tensor and the right Cauchy-Green deformation tensor are henceforth referred to as the stress tensor and deformation tensors, respectively. The deformation tensor is defined as

$$\mathbf{C} = \mathbf{F}^T \mathbf{F} \quad [3.2]$$

where \mathbf{F} is the deformation gradient tensor whose components are given by

$$F_{ij} = \frac{\partial x_i}{\partial X_j} \quad [3.3]$$

In Equation [3.3], the vector components X_i and x_i are the material (undeformed) and the spatial (deformed) coordinates, respectively, which are related by the deformation equations [94]

$$\mathbf{x} = \chi(\mathbf{X}, t) \quad [3.4]$$

where t is time. The ratio of the deformed to the undeformed volume is given by the Jacobian, J , which is defined as the determinate of the deformation gradient tensor.

All polymers, in general, are viscoelastic and experience time-dependent behavior. However, because of the time-scale limitations in the atomistic modeling of polymers, it is assumed in this study that the polymers exhibit a hyperelastic, time-independent response. This assumption does not preclude the use of time-dependent models for the mechanical behavior of polymers [95, 114]. Therefore, Equation [3.4] reduces to

$$\mathbf{x} = \chi(\mathbf{X}) \quad [3.5]$$

The functional form of the strain-energy density is restricted by considering the invariance properties of the material such that the strain-energy density remains invariant with respect to the coordinate transformations expressed by the material symmetry. For an isotropic material, the reducible invariants of the deformation tensor \mathbf{C} are

$$\begin{aligned} I_1 &= \text{tr}(\mathbf{C}) \\ I_2 &= \frac{1}{2} \left\{ [\text{tr}(\mathbf{C})]^2 - \text{tr}(\mathbf{C}^2) \right\} \\ I_3 &= \det(\mathbf{C}) \end{aligned} \quad [3.6]$$

where $\text{tr}(\mathbf{C})$ and $\det(\mathbf{C})$ are the trace and determinate of tensor \mathbf{C} , respectively. In addition to the symmetry requirement, the functional form of the strain-energy density function must also satisfy the global existence requirement of polyconvexity [115]. While the physical meaning of polyconvexity is not well-understood, the extensive mathematical details of polyconvex strain-energy density function formulation can be found elsewhere [115-117]. It is clear that the strain-energy density function can be expressed as a linear combination of scalar invariant functions of I_1 , I_2 , and I_3 ; each of which satisfies convexity. Therefore, a strain-energy density function that satisfies this requirement has the form

$$\Psi_c = \sum_{k=1}^n \psi_k(I_1, I_2, I_3) \quad [3.7]$$

where ψ_k are n convex scalar functions. Using the chain rule of calculus, Equation [3.1] becomes

$$\mathbf{S} = 2 \sum_{k=1}^n \frac{\partial \psi_k(I_1, I_2, I_3)}{\partial \mathbf{C}} = 2 \sum_{k=1}^n \left(\frac{\partial \psi_k}{\partial I_1} \frac{\partial I_1}{\partial \mathbf{C}} + \frac{\partial \psi_k}{\partial I_2} \frac{\partial I_2}{\partial \mathbf{C}} + \frac{\partial \psi_k}{\partial I_3} \frac{\partial I_3}{\partial \mathbf{C}} \right) \quad [3.8]$$

It can be shown that

$$\begin{aligned} \frac{\partial I_1}{\partial \mathbf{C}} &= \mathbf{I} \\ \frac{\partial I_2}{\partial \mathbf{C}} &= I_1 \mathbf{I} - \mathbf{C} \\ \frac{\partial I_3}{\partial \mathbf{C}} &= I_3 \mathbf{C}^{-1} \end{aligned} \quad [3.9]$$

A set of convex functions for ψ_k are [118]

$$\psi_1 = c_1 (I_3 - 1)^2 \quad [3.10]$$

$$\psi_2 = c_2 \left(\frac{I_1}{I_3^{1/3}} - 3 \right) \quad [3.11]$$

$$\psi_3 = c_3 \left(\frac{I_2^3}{I_3^2} - 27 \right) \quad [3.12]$$

where c_1 , c_2 , and c_3 are material constants and $c_1, c_2, c_3 \geq 0$. It has been shown [118] that Equation [3.10] corresponds to the purely volumetric portion of the total material deformation, while Equations [3.11] and [3.12] correspond to the isochoric, or volume

preserving, portion of the total deformation. Because Equations [3.11] and [3.12] both correspond to isochoric deformation, these terms can be combined such that $c_2 = c_3$, and the total strain-energy density from Equations [3.10] and [3.11]-[3.12] is

$$\Psi_c = \psi_1 + \psi_2 + \psi_3 = \psi_{\text{vol}} + \psi_{\text{iso}} = c_1 (I_3 - 1)^2 + c_2 \left(\frac{I_1}{I_3^{1/3}} + \frac{I_2^3}{I_3^2} - 30 \right) \quad [3.13]$$

where ψ_{vol} and ψ_{iso} are the strain energy densities associated with volumetric and isochoric deformations, respectively. Equation [3.7] can be rewritten as

$$\Psi_c = c_1 \Omega_1 + c_2 \Omega_2 \quad [3.14]$$

where

$$\begin{aligned} \Omega_1 &= (I_3 - 1)^2 \\ \Omega_2 &= \left(\frac{I_1}{I_3^{1/3}} + \frac{I_2^3}{I_3^2} - 30 \right) \end{aligned} \quad [3.15]$$

The quantities Ω_1 and Ω_2 are introduced to denote the volumetric and isochoric deformation terms, respectively, independent of the material parameters c_1 and c_2 . Substitution of Equation [3.13] into [3.8] yields

$$\mathbf{S} = \frac{2}{3} \left[6c_1 I_3 (I_3 - 1) - c_2 \left(\frac{I_1}{I_3^{1/3}} + 6 \frac{I_2^3}{I_3^2} \right) \right] \mathbf{C}^{-1} + 2c_2 \left(\frac{1}{I_3^{1/3}} + 3 \frac{I_1 I_2^2}{I_3^2} \right) \mathbf{I} - 6c_2 \frac{I_2^2}{I_3^2} \mathbf{C} \quad [3.16]$$

Equation [3.14] satisfies the normalization condition, that is, it vanishes in the undeformed configuration

$$\Psi_c(I_1 = 3, I_2 = 3, I_3 = 1) = 0 \quad [3.17]$$

Equation [3.14] also satisfies the required growth conditions. Specifically, as the Jacobian approaches zero (vanishing volume), and as the Jacobian approaches infinity (infinite deformation), the strain-energy density approaches infinity,

$$\lim_{\det \mathbf{F} \rightarrow 0} \Psi_c = \infty \quad [3.18]$$

$$\lim_{\det \mathbf{F} \rightarrow \infty} \Psi_c = \infty \quad [3.19]$$

Equation [3.16] describes the mechanical behavior of the equivalent-continuum model. At this point, however, the materials constants c_1 and c_2 are unknown, and must be determined using the molecular structure of the polymer. This is accomplished in the subsequent modeling step.

C. Energy Equivalence

The energies of deformation of the equivalent-continuum, Ψ_c , and molecular models, Ψ_m , were equated for identical sets of boundary conditions to determine the bulk mechanical properties of the polyimide for each of the force fields. The molecular strain-energy density (potential energy) is

$$\Psi_m = \frac{1}{V_0} (\Lambda_{total} - \Lambda_{total}^0) = \frac{\Delta \Lambda}{V_0} \quad [3.20]$$

where Λ_{total}^0 and Λ_{total} are the potential energies of the molecular model from either Equations (A.1), (A.6), or (A.11) before and after deformation, respectively, and V_0 is

the initial volume of the RVE. For finite deformations, the deformation of the boundary of the RVE is generalized by Equation. [3.5]

Because the strain-energy density of the equivalent continuum, Ψ_c , is the sum of the volumetric and isochoric deformation components, as shown in Equations [3.14] -[3.15], volumetric and isochoric modes of deformation were applied to the molecular models to determine the material parameters c_1 and c_2 . For each deformation, the strain-energy densities in Equations [3.13] and [3.20] were equated by adjusting these two material parameters. To relate these deformations to those typically applied to a specimen during laboratory testing, the deformation levels are expressed in terms of the Lagrangian strain tensor (henceforth referred to as the strain tensor)

$$\mathbf{E} = \frac{1}{2}(\mathbf{C} - \mathbf{I}) \quad [3.21]$$

For the volumetric deformations, the deformation equations are

$$\mathbf{x}^{(k)} = \alpha_k \mathbf{x}^{(k-1)} \quad [3.22]$$

where the deformation step $k = 1, 2, 3, 4$; $\mathbf{x}^{(0)} = \mathbf{X}$; and α_k is the scalar constant corresponding to the k^{th} deformation step. The spatial coordinates $\mathbf{x}^{(1)}$, $\mathbf{x}^{(2)}$, $\mathbf{x}^{(3)}$, and $\mathbf{x}^{(4)}$ correspond to volumetric strains ($E_{11} = E_{22} = E_{33}$) of 0.25%, 0.50%, 0.75%, and 1.0%, respectively. The relative deformation gradient tensor components, which relate the deformation at a given strain level to those of the previous strain level are

$$F'_{ij}(\mathbf{x}^{(k)}) = \frac{\partial x_i^{(k)}}{\partial x_j^{(k-1)}} \quad [3.23]$$

where $\mathbf{F}'(x^{(1)}) = \mathbf{F}(x^{(1)})$. Therefore, the deformation gradient tensor components that relate the coordinate for each strain level to those of the material coordinate system are

$$F_{ij}(\mathbf{x}^{(k)}) = \frac{\partial x_i^{(k)}}{\partial X_j} = F'_{im}(\mathbf{x}^{(k)}) F_{mj}(\mathbf{x}^{(k-1)}) \quad [3.24]$$

where $\mathbf{F}(\mathbf{x}^{(0)}) = \mathbf{I}$. Using Equations [3.22] -[3.24], the constants α_1 , α_2 , α_3 , and α_4 where adjusted to achieve the exact desired volumetric strain levels in Equation[3.21]. These values are listed in Table 3.1.

The deformation equations for the isochoric deformations are

$$\begin{aligned} x_1^{(1)} &= \beta_1 (X_2 + X_3) + X_1 \\ x_2^{(1)} &= \beta_1 (X_1 + X_3) + X_2 \\ x_3^{(1)} &= \beta_1 (X_1 + X_2) + X_3 \\ x_1^{(k)} &= \beta_k (x_2^{(k-1)} + x_3^{(k-1)}) + x_1^{(k-1)} \\ x_2^{(k)} &= \beta_k (x_1^{(k-1)} + x_3^{(k-1)}) + x_2^{(k-1)} \\ x_3^{(k)} &= \beta_k (x_1^{(k-1)} + x_2^{(k-1)}) + x_3^{(k-1)} \end{aligned} \quad [3.25]$$

where β_1 , β_2 , β_3 , and β_4 are scalar constants and the superscripts 1, 2, 3, and 4 ($k = 2, 3$, and 4) correspond to 3-dimensional shear strain levels of $\gamma_{23} = \gamma_{13} = \gamma_{12} = 0.25\%$, 0.50% , 0.75% , and 1.0% , respectively ($\gamma_{ij} = 2E_{ij}$ when $i \neq j$). Similar to the case of the volumetric deformation, the constants β_1 , β_2 , β_3 , and β_4 were adjusted such that these shear strains were achieved by using Equations [3.21] and [3.23] -[3.25]. The values of the β constants are listed in Table 3.1.

The change in the potential energies of the molecular models, $\Delta\Lambda$ in Equation[3.20], were determined using static (MM) and dynamic (MD) molecular simulations. Both volumetric and isochoric deformations were applied to the equilibrium molecular structures for each force field by deforming the RVE and all of the atoms in the models according to the applied deformation field. In the static simulations, an energy minimization technique was subsequently performed using a quasi-Newton L-BFGS method [119] as implemented with the MINIMIZE program in the TINKER modeling package [106]. The minimizations were executed for RMS gradient values of 0.1 kcal/mole/Å. During the energy minimization, the RVE volume was kept constant as the atoms were shifted to minimize the potential energy. In the dynamical simulations, an NVT simulation with periodic boundary conditions was subsequently used for each deformation to allow the RVE dimensions to remain fixed while the atoms were allowed to move into new equilibrium positions. The dynamic molecular simulations were run up to 40 ps with 1.0 fs time steps at 298 K, and were performed using the TINKER modeling package [106]. The potential energies of deformation of the molecular models were averaged over the final 10 ps of each simulation, as for the first 30 ps showed significant changes in the potential energy as the molecular structure relaxed into the deformed configuration. The temperatures of the simulations were monitored with the Groningen method of coupling to an external bath [120]. The temperature of the system is achieved through modification of the equation of motion by the use of stochastic and friction terms yielding in a Langevin equation. As a result of this modification in the equation of motion the velocities are scaled to achieve the desired temperature of the system. The simulations were repeated for all necessary deformation modes of each polymer. Therefore, a total of nine (including the undeformed configuration) strain-energy densities of the molecular model, Ψ_m , were determined for the complete range of deformations. For the static simulations, the repeated values of Ψ_m were identical to the original set.

For the static and dynamic simulations, periodic boundary conditions were applied such that atoms were free to cross the boundary of the deformed and undeformed simulation cells. Atoms that crossed the boundary entered the simulation cells on the opposite side, as described in detail elsewhere [110]. Therefore, none of the atoms in the molecular simulations were kinematically over-constrained, as can occur in simulations of RVEs of heterogeneous material systems with kinematic boundary conditions [121, 122].

3.4 RESULTS AND DISCUSSIONS

Because Equation [3.14] is linear in Ω_1 and Ω_2 , the strain-energy density of the molecular models is plotted with respect to Ω_1 and Ω_2 in Figures 3.6 and 3.7, respectively, for the static molecular simulations. From Figures 3.6 and 3.7 it is evident there is a slight nonlinearity in the data. Ideally, for materials under large elastic deformations, the slope of the curves in Figures 3.6 and 3.7 would be expected to be linear, as indicated by Equation [3.14]. Therefore, for larger deformations in the static simulations, a small amount strain-energy density is lost, most likely because of viscoelastic relaxation of the polymer chains or because of an evolution of damage on the molecular level (e.g. void nucleation). Because of the difficulty in quantifying the simulated time in static molecular simulations, viscoelastic relaxation can be neither verified nor characterized for this data.

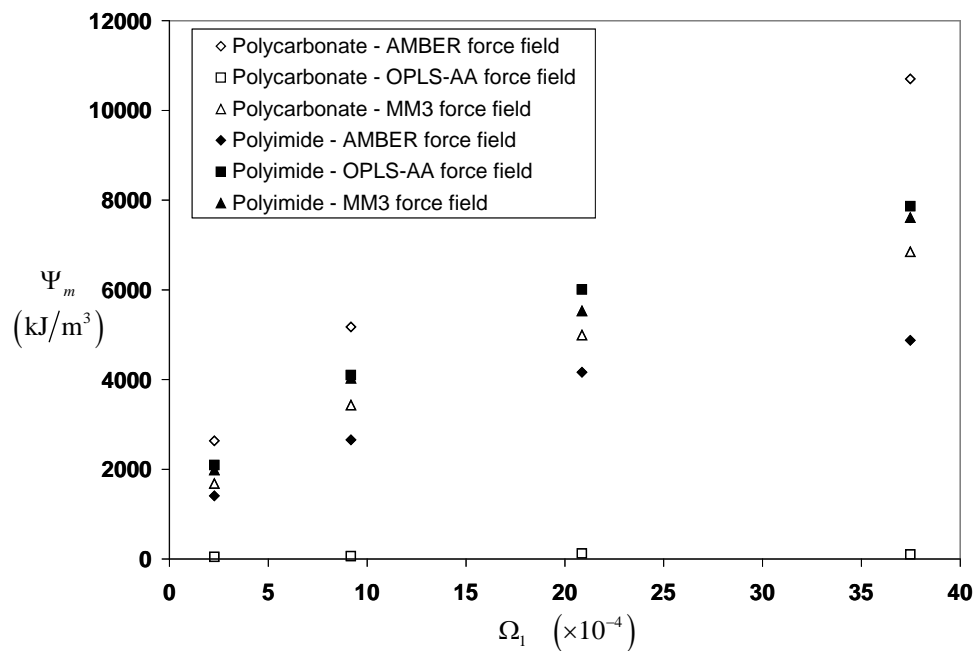


Figure 3.6. Simulated molecular strain-energy density for volumetric deformation with static molecular simulations

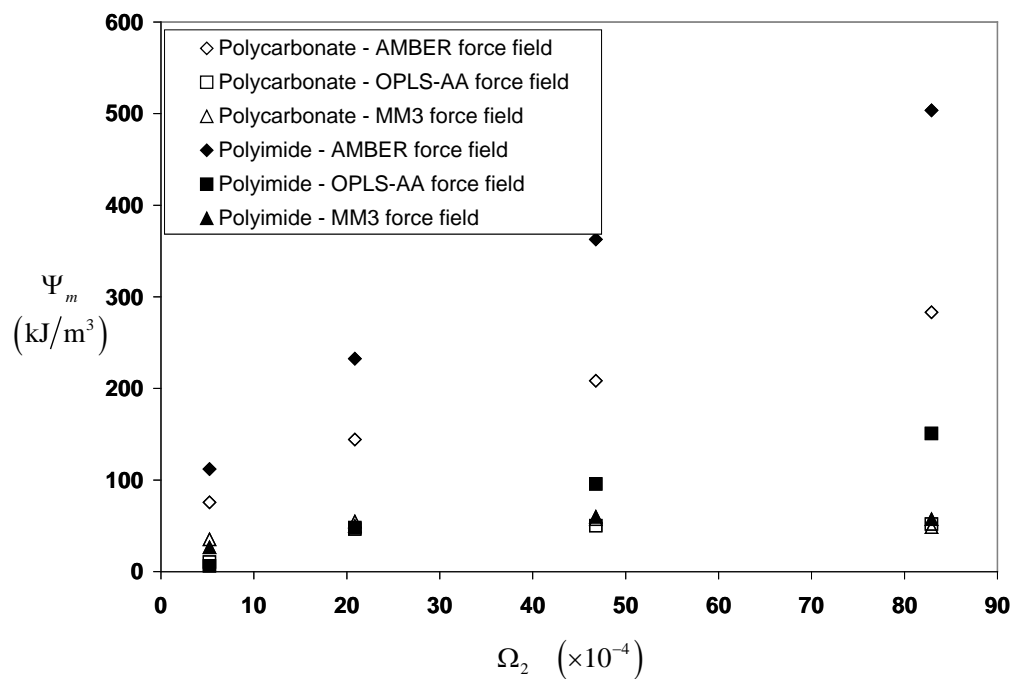


Figure 3.7. Simulated molecular strain-energy density for isochoric deformation with static molecular simulations

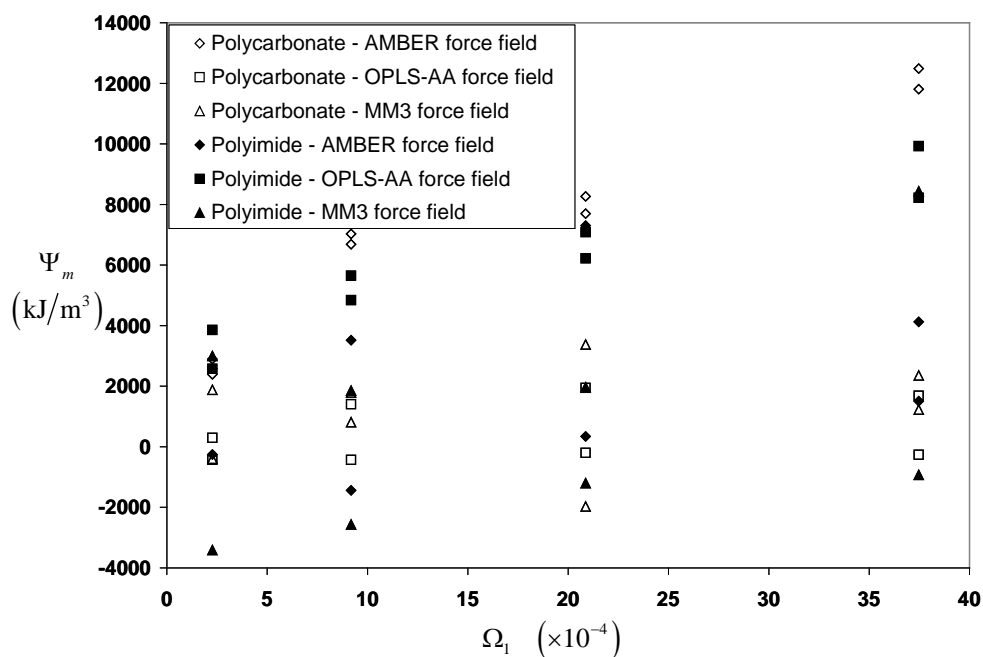


Figure 3.8. Simulated molecular strain-energy density for volumetric deformation with dynamic molecular simulations

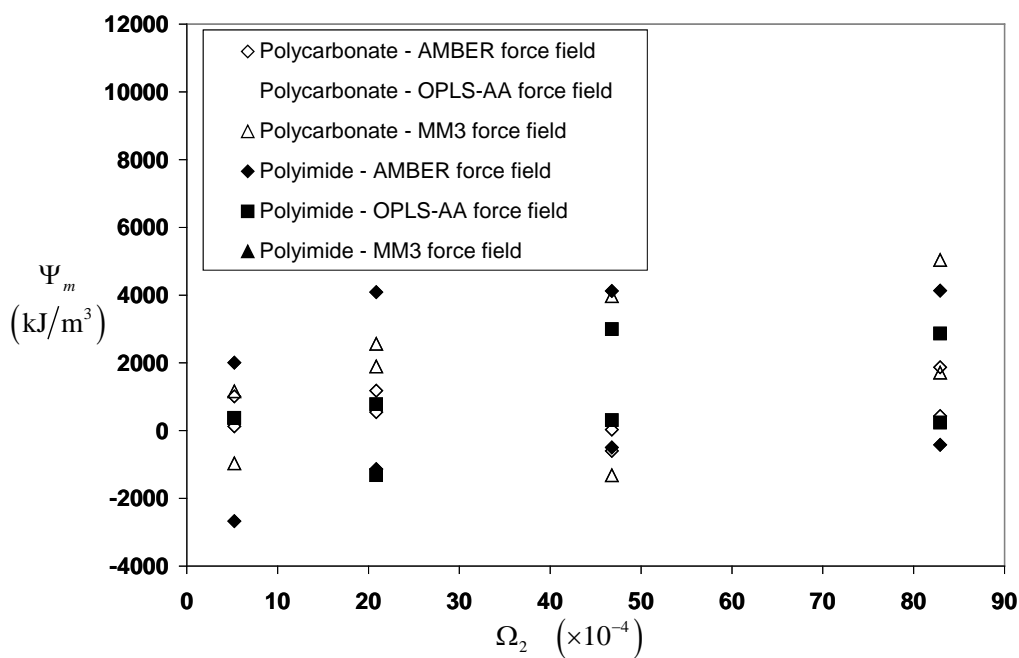


Figure 3.9. Simulated molecular strain-energy density for isochoric deformation with dynamic molecular simulations

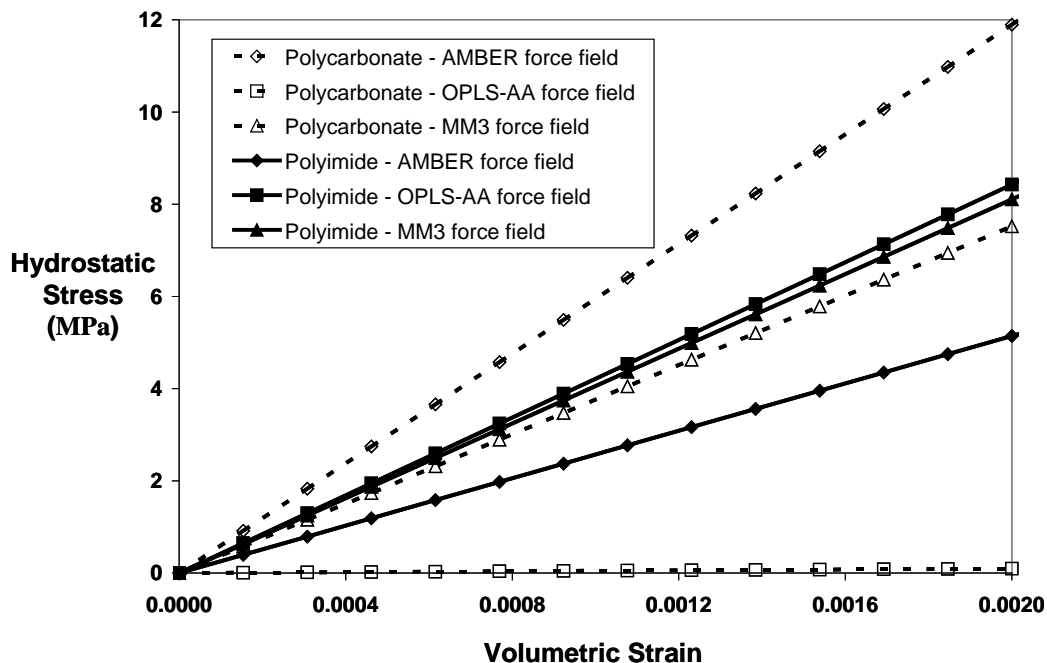


Figure 3.10. Predicted hydrostatic stress versus volumetric strain behavior for the material parameters determined with the static molecular simulations

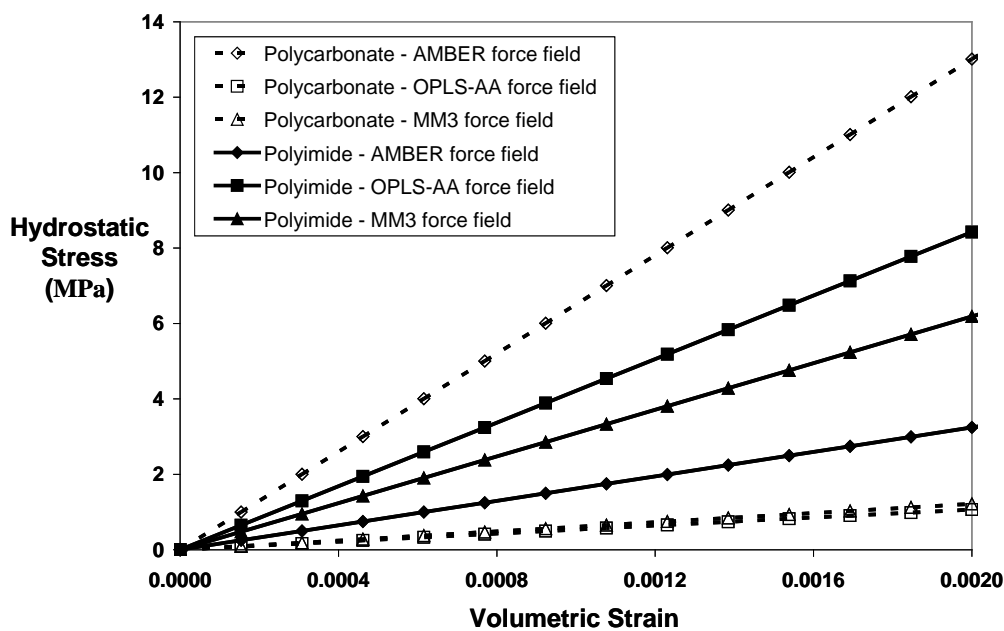


Figure 3.11. Predicted hydrostatic stress versus volumetric strain behavior for the material parameters determined with the dynamic molecular simulations

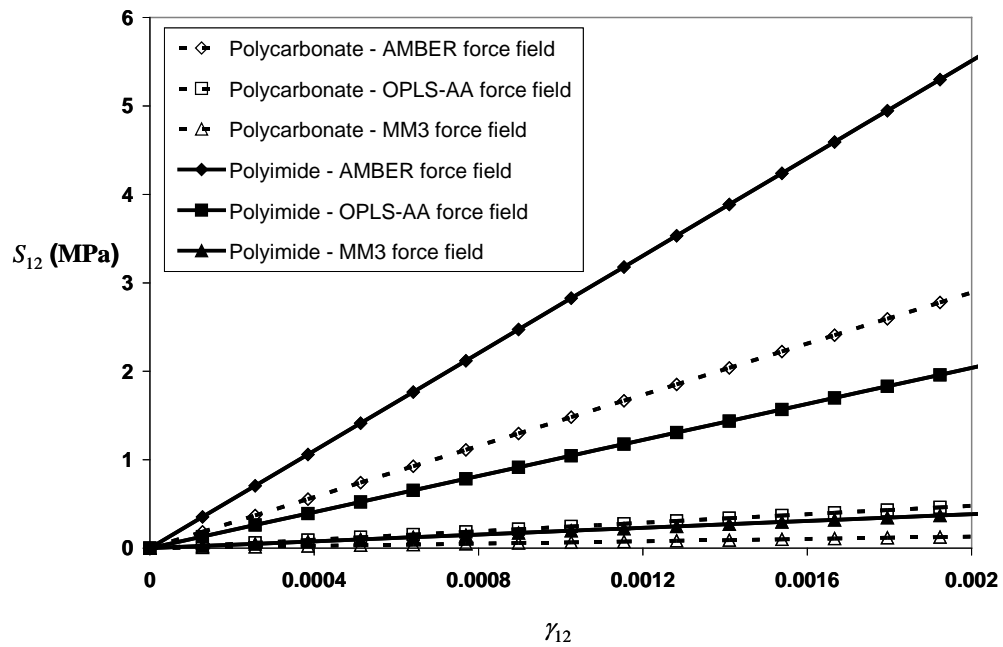


Figure 3.12. Predicted shear stress versus shear strain behavior for the material parameters determined with the static molecular simulations

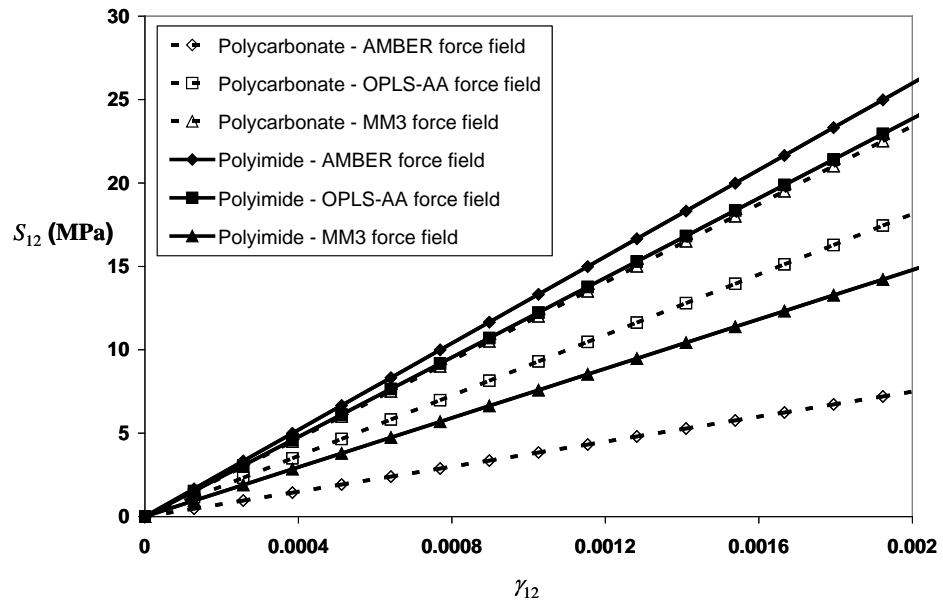


Figure 3.13. Predicted shear stress versus shear strain behavior for the material parameters determined with the dynamic molecular simulations

Similarly, the molecular strain-energy densities for the volumetric and isochoric deformations are shown in Figures 3.8 and 3.9, respectively, from the dynamic simulations. Specific trends in the plotted data are difficult to discern due to the scatter for each loading level, force field, and polymer. This scatter is mostly a result of the motions (velocities) of the atoms and the resulting fluctuations in atomic coordinates and pressure for each simulation time step [110]. It is expected that as the number of atoms in the simulation RVEs increase, this scatter will decrease. That is, as the number of vibrating atoms in the simulation cell increases, each with its own velocity components at a give time step, the overall fluctuation of the energy will decrease. Of course, at the bulk level, such arbitrary fluctuations in energy are not witnessed because of the large number of total atoms that are being observed in an element of material. Because of the existence of the data scatter in Figures 3.8 and 3.9, the nonlinear behavior observed in the static simulations is not observed in the dynamic simulations.

From Figures 3.6 – 3.9, it is evident that the slopes of each set of data do not necessarily approach a molecular potential energy value of zero as Ω_1 and Ω_2 approach zero. In the establishment of material RVEs using finite-sized molecular systems, as described section 3.1, it is very difficult to obtain a completely stress-free system in the reference configuration using an NPT simulation. This is because of the unavoidable, small fluctuations of the pressure in NPT simulations (even though the pressure changes are minimized) [110]. Therefore, the RVEs for each material and force field are not completely free of residual stresses.

For both static and dynamic simulations, linear least-squares regressions were performed for the Ψ_m vs. Ω_1 and Ω_2 data sets shown in Figures 3.6 – 3.9 for each loading condition, polymer, and force field. Because Equation [3.14] is linear in Ω_1 and Ω_2 , the slopes of the regression curves in Figures 3.6 and 3.8 are the material parameter c_1 , and the slopes of the regression curves in Figures 3.7 and 3.9 are the material parameter c_2 . Because of the aforementioned residual stress in the molecular modeling

data, the linear regressions were performed over the deformation increments without forcing the regression to approach a zero-valued molecular potential energy as Ω_1 and Ω_2 approached zero. Therefore, the slopes of the regressions accurately reflect the values of c_1 and c_2 in a bulk-level material without the existence of any residual stresses. The values of the material parameters c_1 and c_2 are listed in Tables 3.2 and 3.3 for the static and dynamic simulations, respectively.

The constitutive relationship in Equation [3.16] and the material parameters in Tables 3.2 and 3.3 were used to predict the stress-strain responses of the two polymer systems. Figures 3.10 and 3.11 depict the hydrostatic stress-volumetric strain curves using the parameters from the static and dynamic simulations, respectively. For this loading condition, it was assumed that $C_{11} = C_{22} = C_{33}$ with all other C_{ij} equal to zero. The volumetric strain was

$$\frac{\Delta V}{V} = 3E_{11} = 3E_{22} = 3E_{33} \quad [3.26]$$

Table 3.1. Values of deformation parameters

Deformation parameters	Value (unitless)	Finite-valued strain components
α_1	1.002497	$E_{11} = E_{22} = E_{33} = 0.25\%$
α_2	1.002485	$E_{11} = E_{22} = E_{33} = 0.50\%$
α_3	1.002472	$E_{11} = E_{22} = E_{33} = 0.75\%$
α_4	1.002460	$E_{11} = E_{22} = E_{33} = 1.00\%$
β_1	0.001249	$\gamma_{23} = \gamma_{13} = \gamma_{12} = 0.25\%$
β_2	0.001246	$\gamma_{23} = \gamma_{13} = \gamma_{12} = 0.50\%$
β_3	0.001243	$\gamma_{23} = \gamma_{13} = \gamma_{12} = 0.75\%$
β_4	0.001240	$\gamma_{23} = \gamma_{13} = \gamma_{12} = 1.00\%$

Table 3.2. Predicted material parameters of the polymers from static molecular simulations (all parameters have units of Pa).

Material	c_1	c_2
Polycarbonate (AMBER force field)	2.23×10^9	2.58×10^7
Polycarbonate (OPLS-AA force field)	1.81×10^7	4.29×10^6
Polycarbonate (MM3 force field)	1.41×10^9	1.17×10^6
Polyimide (AMBER force field)	9.64×10^8	4.92×10^7
Polyimide (OPLS-AA force field)	1.58×10^9	1.82×10^7
Polyimide (MM3 force field)	1.52×10^9	3.43×10^6

The corresponding hydrostatic stress was given by Equation [3.16] where $S_{11} = S_{22} = S_{33}$ with all other S_{ij} equal to zero. In Figures 3.10 and 3.11, the mechanical responses of both polymers are linear, as expected, and their slopes are the bulk moduli as predicted by the constitutive law and the material parameters. Figures 3.12 and 3.13 illustrate the shear stress-shear strain (S_{12} versus γ_{12}) response of the two polymers from Equation [3.16] using the static and dynamic simulations parameters, respectively, in Tables 3.2 and 3.3. For this loading condition, it was assumed that $C_{11} = C_{22} = C_{33} = 1$, $C_{23} = C_{13} = 0$, and $C_{12} \neq 0$. The resulting stress state was $S_{12} \neq 0$ with all other $S_{ij} = 0$. Because the responses of the two polymer systems in both figures are linear over the given range of shear strains, the slope of the curves is the predicted shear modulus. The Young's and shear moduli of the two polymer systems for the three force fields and two simulation types, listed in Tables IV and V, were determined from the data shown in Figures 3.10-3.13 and from the standard relations for elastic properties of isotropic materials [123].

Experimentally-determined values of the Young's and shear moduli for the polycarbonate [124] and the polyimide, with an assumed Poisson's ratio of 0.4 [101], are also listed in Tables IV and V, respectively. The data in Figures 3.10 – 3.13 were plotted for relatively small deformations because the data for larger deformations shows the same trends and the modeling procedure does not model larger deformation effects such as plastic yielding or craze formation.

Table 3.3. Predicted material parameters of the polymers from dynamic molecular simulations (all parameters have units of Pa).

Material	c_1	c_2
Polycarbonate (AMBER force field)	2.44×10^9	6.69×10^7
Polycarbonate (OPLS-AA force field)	2.00×10^8	1.62×10^8
Polycarbonate (MM3 force field)	2.28×10^8	2.09×10^8
Polyimide (AMBER force field)	6.08×10^8	2.32×10^8
Polyimide (OPLS-AA force field)	1.58×10^9	2.13×10^8
Polyimide (MM3 force field)	1.16×10^9	1.32×10^8

Table 3.4. Predicted and Experimental Elastic Properties of Polycarbonate.

Method	Young's Modulus (GPa)	Shear Modulus (GPa)
Experiment	2.2	0.8
AMBER force field (static simulation)	4.0	1.4
OPLS-AA force field (static simulation)	0.3	0.2
MM3 force field (static simulation)	0.2	0.1
AMBER force field (dynamic simulation)	9.4	3.7
OPLS-AA force field (dynamic simulation)	4.1	9.1
MM3 force field (dynamic simulation)	4.7	11.7

Table 3.5. Predicted and Experimental Elastic Properties of Polyimide.

Method	Young's Modulus (GPa)	Shear Modulus (GPa)
Experiment	3.6	1.3
AMBER force field (static simulation)	6.1	2.8
OPLS-AA force field (static simulation)	2.8	1.0
MM3 force field (static simulation)	0.6	0.2
AMBER force field (dynamic simulation)	10.6	13.0
OPLS-AA force field (dynamic simulation)	18.4	11.9
MM3 force field (dynamic simulation)	12.3	7.4

From the data in Tables 3.4 and 3.5, the static simulations predicted mechanical properties that are lower than those predicted by the dynamic simulations for both polymer materials. Comparison of the properties from static and dynamic simulations also reveals that the properties predicted with the static simulations are closer to the experimentally-obtained values. For the properties predicted from static simulations, the OPLS-AA and MM3 force fields predicted mechanical properties that are lower than those predicted with the AMBER force field. Also, the static simulations predict Young's and shear moduli that are higher than those from experiment with the AMBER force field, while the same predicted properties are lower than the experiment with the OPLS-AA and MM3 force fields. There are no distinct trends between predicted moduli and polymer type or force field for the dynamic simulations.

3.5 SUMMARY

In this study, a combined atomistic-hyperelastic multiscale modeling technique, based on the Equivalent-Continuum Model, was developed and used to predict elastic properties of polycarbonate and polyimide polymer systems using the AMBER, OPLS-AA, and MM3 molecular force fields. The hyperelastic model was formulated with a strain-energy potential function that had a functional form based on molecular simulation predictions. Both static and dynamic molecular simulations were performed using Molecular Mechanics and Molecular Dynamics simulation techniques, respectively. The predicted bulk properties of the polymers using the three force fields were compared to experimentally-measured values.

A. Static versus Dynamic Simulation

Examination of the predicted values of Young's and shear moduli for the two polymers indicates that the static simulations predicted mechanical properties that are lower than those predicted by the dynamic simulations, with the properties from static simulations closer to the experimental properties than the properties from the dynamic simulations. These results can be attributed to two possible factors, data scatter and mechanical relaxation.

The results indicate that the scatter in the data from the dynamic simulations is much greater than that from the static simulations and therefore there is a greater chance of the dynamic simulations yielding predicted mechanical properties that are less accurate than those from the static simulations (when comparing to the experiment). It is expected that with dynamic simulations of larger molecular systems, the scatter would generally decrease.

The mechanical relaxation of the polymer chains that occurs in the experiments and in the static simulations is not expected to be accurately accounted for in the dynamic simulations. Polymers generally behave in a viscoelastic manner when subjected to applied deformations because of the time-dependent response of polymer-chain sliding and chain-torsional motions. Therefore, in the experiments, it is speculated that the strain rates were small enough that mechanical relaxation occurred as the specimens were deformed, thus reducing the resultant stress on the specimen. In the static simulations, energy minimizations are performed that mimic the relaxation mechanisms of a deformed polymer; conversely, in the dynamic simulations, the time scale is on the order of picoseconds, which is not long enough to allow for significant mechanical relaxation. Therefore, the strain-energy density is much higher for a given deformation in the dynamic simulations relative to the static simulations, and the corresponding constitutive equations will predict higher stresses for a given applied deformation. As a result, the predicted elastic material properties from the dynamic simulations are greater than those from the static simulations and the experiments.

B. Force Field Comparisons

The predicted moduli from the static simulations are larger than those from experiment for the AMBER force field, and are smaller than the experimental values for the OPLS-AA and MM3 force fields. The relatively low predicted elastic properties from the OPLS-AA force field are likely a direct result of the lower simulated polymer densities because it is expected that higher elastic constants would result from simulations of denser materials. The functional forms of the AMBER and OPLS-AA force fields, from Equations (A.1) to (A.6), are nearly identical. The differences in the two force fields (as used in this study) are the presence of electrostatic interactions in the OPLS-AA force field and the differences in the force constant parameters, particularly for the torsions. These differences result in the significantly different predicted densities for both polymer systems. The lower predicted properties of the MM3 static simulations

cannot be attributed to the same effect because the simulated material densities were close to the expected values. The functional form of the MM3 force field from Equations (A.11) - (A.18) attempts to account for a wider range of behavior than those of the AMBER and OPLS-AA force fields. However, because the predicted properties using the MM3 force field in static simulations are farther from the experimental properties than those predicted with the AMBER and OPLS-AA force fields, the more complex functional form does not predict properties as accurately as the more simple functional forms of AMBER and OPLS-AA for the polymer systems used in this study.

The relatively high predicted mechanical properties from the static simulations with the AMBER force field follow a trend that has been observed in the literature. Previous studies [92, 125] have pointed out that the predicted mechanical properties from molecular simulations are expected to be 50 - 100% larger than those obtained from experiments. In the current study, the predicted properties from the AMBER force field were 70 - 115% higher than experiment. Most likely, this difference can be attributed to the fact that the RVEs in molecular modeling simulations represent a nearly perfect molecular structure, whereas, in the actual experimental test specimens, the material contains low volume fractions of air pockets, inclusions, and unreacted monomers. Therefore, it is expected that simulated mechanical properties should be larger than experimentally-obtained properties if the polymer system imperfections are not included in the molecular modeling. It is also expected that the computational modeling of these imperfections in these polymer systems would yield predicted properties that are closer to the experiment than those predicted in the current study. From this perspective, for the polymer systems investigated in this study, the AMBER force field appears to be more accurate than the OPLS-AA and MM3 force fields for predicting elastic properties.

.

Chapter 4

Multiscale Modeling of Polymer Materials Using a Statistics-Based Micromechanics Approach

In this chapter, we present a methodology to account for a multiple polymer chain conformations that are probable for a given volume of an amorphous polymer. The prediction of elastic properties of a polymer must therefore consider more than a single combination of chain conformations. A multiscale modeling approach is proposed to predict the bulk elastic properties of polymer materials using a series of molecular models of individual polymer microstates and a statistics-based micromechanical modeling method. The method is applied to polyimide and polycarbonate systems. It is shown that individual microstates can yield a wide range of predicted elastic properties, whereas the consideration of multiple microstates yield predicted properties that more-closely agree with experimentally-determined values of Young's modulus. Additionally, the upper and lower limits of possible elastic constants are also established based on the consideration of multiple microstates.

4.1 INTRODUCTION

Unlike crystalline materials, amorphous polymer materials contain an elaborate network of molecular chains with highly-complex and irregular conformations that dictate the bulk mechanical properties. Many combinations of the conformations of multiple polymer chains are possible for a particular representative volume element (RVE in an equilibrated or non-equilibrated state because of the finite entropy of the material for

any temperature above 0 K owing to the dynamics of the constituent chains[126-130]. As a result, the molecular structure, and thus density, of a polymer material varies substantially on the nanometer length-scale [130-138]. The large number of possible conformations for a specific volume of a polymer material constitutes a conformation space. Each combination of chain conformations in a RVE has an associated potential energy which can be interpreted as an energy landscape that depends on the conformational state of the polymer network. The conformational space does not necessarily have a one-to-one correspondence to the energy landscape. Therefore, the energy landscape generally consists of multiple local minima. As a result, for a RVE consisting of a finite number of polymer chains, there can exist multiple locally-equilibrated states.

A majority of high performance polymer-based materials operate at temperatures much below their glass transition temperatures. An amorphous polymeric material in a glassy state can be envisioned as a super-cooled liquid that is “frozen” in a local potential energy equilibrium state, which is not necessarily a globally-minimized potential energy state. The different microstates that are not at the global-minimum energy state are essentially “metastable” states with exceptionally long relaxation times as the energy barriers to cross over to the global minimum energy state in are generally very high. Therefore, the bulk material behavior can be imagined to be an average response from all the available conformational microstates. In order to accurately predict the bulk-level behavior of polymer-based systems based on molecular structure, a range of conformational microstates of a polymeric network must be included in multiscale constitutive modeling approaches. In this study, a multiscale modeling technique is used to predict the bulk elastic moduli of a polyimide and a polycarbonate material system using multiple conformational states. and establish statistical bounds of the predicted moduli are subsequently established. Physically-motivated statistically weighting of properties obtained from individual microstates for each polymer was incorporated into the modeling approach. It was found that the established bounds included

experimentally-measured values of moduli for these materials. The framework of modeling presented here is very adaptable and can be extended to include any bulk physical property for an amorphous polymer material.

4.2 FORCE FIELD

Force fields are generally used in MD and Molecular Mechanics (MM) based atomistic simulations to describe the interactions between individual atoms and to relate the specific molecular configuration to the potential energy of a RVE of a material system. Force fields are generally semi-empirical and assume specific degrees of freedom for the constituent atomic structures. The total energy of the RVE of a molecular system is obtained as the summation of energies associated with individual degrees of freedom. One of the most widely-used force fields, AMBER, implemented as AMBER99 in the Tinker software package[106] was utilized for this study. The AMBER force field has a relatively simple functional form compared to other well-known force fields[139]. The simulations used in the current study did not include electrostatic interactions based on the dipole moment of the atoms. The AMBER force field was chosen over other available force fields of rather complex functional form for efficiency and accuracy [67].

The total potential energy of a simulated molecular system computed with the AMBER force field is based on the summation of the bond-stretching, bond-bending, bond-torsion, and nonbonded energies given by

$$\Lambda = \Lambda_{\text{stretch}} + \Lambda_{\text{bend}} + \Lambda_{\text{torsion}} + \Lambda_{\text{nb}} \quad [4.1]$$

where

$$\Lambda_{\text{stretch}} = \sum_{\text{stretch}} K_r (r - r_{eq})^2 \quad [4.2]$$

$$\Lambda_{\text{bend}} = \sum_{\text{bend}} K_{\theta} (\theta - \theta_{eq})^2 \quad [4.3]$$

$$\Lambda_{\text{torsion}} = \sum_{\text{torsion}} \left\{ \begin{aligned} &\frac{V_1}{2} [1 + \cos(\phi + \zeta)] \\ &+ \frac{V_2}{2} [1 - \cos(2\phi + \zeta)] \\ &+ \frac{V_3}{2} [1 + \cos(3\phi + \zeta)] \end{aligned} \right\} \quad [4.4]$$

$$\Lambda_{\text{nb}} = \sum_{I < J} 4\epsilon_{IJ} \left[\frac{(\sigma_{IJ})^{12}}{r_{IJ}^{12}} - \frac{(\sigma_{IJ})^6}{r_{IJ}^6} \right] \quad [4.5]$$

In Equations [4.1] -[4.5], the summations are taken over all of the corresponding interactions in the molecular model (RVE); K_r and K_{θ} are the bond-stretching and bond-angle bending force constants, respectively; r and r_{eq} are the bond length and equilibrium bond lengths, respectively; θ and θ_{eq} are the bond angle and equilibrium bond angles, respectively; $V_n/2$, ζ , and ϕ are the torsion magnitude ($n=1,2,3$), phase offset, and the torsion angle, respectively; and ϵ_{IJ} , r_{IJ} , and σ_{IJ} are van der Waals well depth, non-bonded distance between atoms I and J , and the equilibrium distance between atoms I and J , respectively. Figure 4.1 shows the repeat unit and molecular model for the two polymer materials used in the current study.

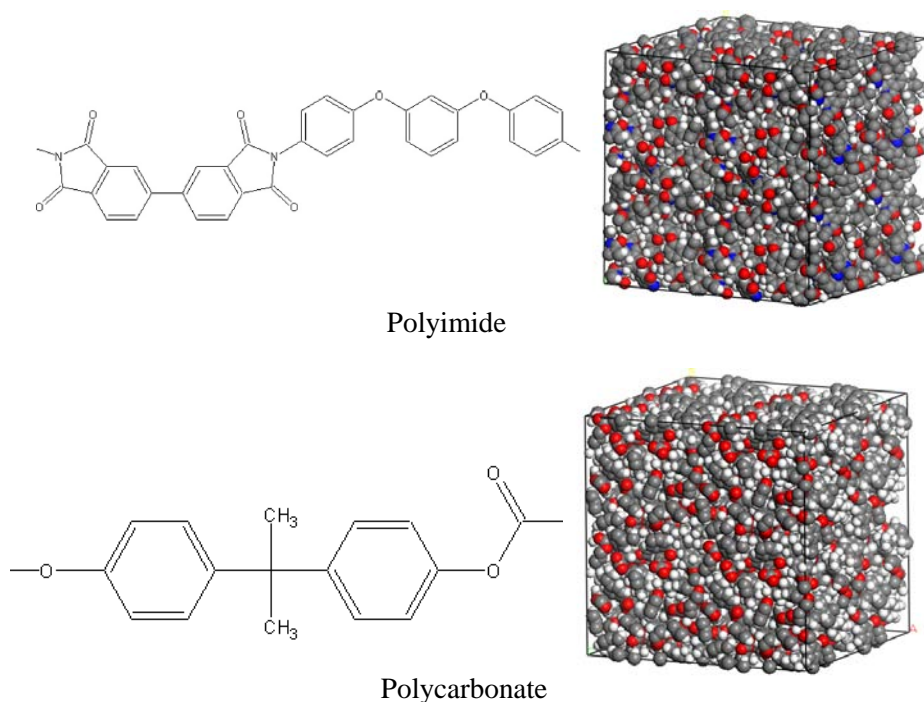


Figure 4.1. Schematic of the repeat unit for polymeric chains and the corresponding representative molecular model of the polymeric network

4.3 MOLECULAR MODELING

The simulations were carried out on both a polyimide and a polycarbonate system. These two polymers have been previously synthesized, tested, and modeled [67, 101, 109, 140]. Figure 4.1 shows the chemical repeat structures of both polymers. Multiple RVEs representing samples from the conformational space were obtained for the two polymer materials. Nine thermally-equilibrated structures were obtained for polycarbonate, each consisting of 5958 atoms with 9 polymer chains and each chain comprised of 20 repeat units. Each of the nine resulting equilibrated structures represented a microstate for the polycarbonate system. For the polyimide system, seven locally equilibrated molecular structures of 6,622 atoms each were established with 11

chains and 10 repeat units per chain. Each of these seven polyimide structures represented a single microstate.

All RVE structures were initially prepared in a gas-like phase with extremely low densities. For each RVE sample, the polymer chains were placed in a simulation box with random conformations and orientations. Energy minimization simulations with periodic boundary conditions were conducted at gradually-increasing densities. The MINIMIZE [119] and NEWTON [141] subroutines of the TINKER [106, 142] modeling package were used for the energy minimization, which correspond to a quasi-Newton L-BFGS method and a truncated Newton energy minimization methods, respectively. The minimizations were performed to RMS gradients of 1×10^{-2} and 1×10^{-5} kcal/mole/Å, respectively.

Once the RVEs were established with the approximately correct solid bulk density, a series of MD simulations were used to establish thermally-equilibrated solid structures in the following order at 300 K: (1) a 50 ps simulation with the NVT (constant number of atoms, volume, and temperature) ensemble to prepare the structure for further equilibration, (2) a 100 ps simulation with the NPT (constant number of atoms, pressure, and temperature) ensemble at 100 atm to evolve the system to higher densities as the structure was prepared from a low density structure, (3) a 100 ps NPT simulation at 1atm to reduce the effects of high-pressure simulations and to let the system evolve to a state of minimal residual stresses, and (4) a 100 ps NVT simulation to allow the system to equilibrate at the simulated temperature and density for a specific microstate. The DYANAMIC subroutine of the TINKER modeling package was used for the MD simulations with periodic boundary conditions. Periodic boundary conditions were employed. Examples of the molecular models that were established in a manner described above are shown in Figure 4.2.

4.4 EQUIVALENT-CONTINUUM PROPERTIES

To relate the molecular structure of the microstates of the polymer systems to their corresponding bulk mechanical properties, an equivalent-continuum modeling approach was used as described in Chapter 3 that effectively represented the mechanical behavior of the molecular RVEs. Because the molecular structures of the polymers were completely amorphous, it was assumed that the equivalent-continuum constitutive equation for the microstates exhibited isotropic symmetry. Based on this material symmetry for the equivalent continuum, a hyperelastic continuum constitutive relation [67] was used to model the deformation characteristics of the discrete molecular models. For generality, it was desired that the constitutive relationship of the equivalent continuum satisfy the following requirements: (1) formulated in a finite-deformation framework, (2) established using a thermodynamic potential, (3) incorporating isotropic material symmetry, and (4) expressed in terms of volumetric (shape preserving) and isochoric (shape changing) contributions. The assumed form of the equivalent-continuum strain energy is

$$\Psi_c = \psi_{vol} + \psi_{iso} \quad [4.6]$$

where

$$\begin{aligned} \psi_{vol} &= c_1 \Omega_1 \\ \psi_{iso} &= c_2 \Omega_2 \end{aligned} \quad [4.7]$$

and

$$\begin{aligned} \Omega_1 &= (I_3 - 1)^2 \\ \Omega_2 &= \left(\frac{I_1}{I_3^{1/3}} + \frac{I_2^3}{I_3^2} - 30 \right) \end{aligned} \quad [4.8]$$

The parameters Ω_1 and Ω_2 in Equation [4.8] represent the volumetric and isochoric components of the strain-energy density; c_1 and c_2 are constants which represent material properties; and I_1 , I_2 , and I_3 are the scalar invariants of the right Cauchy-Green deformation tensor, \mathbf{C} . The second Piola-Kirchhoff stress tensor is therefore [67]

$$\mathbf{S} = \frac{2}{3} \left[6c_1 I_3 (I_3 - 1) - c_2 \left(\frac{I_1}{I_3^{1/3}} + 6 \frac{I_2^3}{I_3^2} \right) \right] \mathbf{C}^{-1} + 2c_2 \left(\frac{1}{I_3^{1/3}} + 3 \frac{I_1 I_2^2}{I_3^2} \right) \mathbf{I} - 6c_2 \frac{I_2^2}{I_3^2} \mathbf{C} \quad [4.9]$$

where \mathbf{I} is the identity tensor.

Equation [4.9] contains material parameters c_1 and c_2 which were evaluated for each microstate by equating the equivalent-continuum strain energy and the molecular potential energy for a set of identical deformation fields applied to the equivalent continuum and the molecular models, as has been performed in previous studies of other nanostructured materials [21, 67, 68, 70, 90]. For the molecular models, the strain energy densities were computed from the force fields using

$$\Psi_m = \frac{1}{V_0} (\Lambda_m - \Lambda_m^0) \quad [4.10]$$

where, Λ_m^0 and Λ_m are the molecular potential energies before and after application of the deformations, which are directly computed from the force field, and V_0 is the volume of the simulation box in the undeformed state.

The models of the polymer systems were subjected to two different deformation fields, a pure volumetric deformation and an isochoric deformation. Finite deformations were applied to the molecular and equivalent-continuum models in incremental steps. For the volumetric deformation, volumetric strains ($E_{11} = E_{22} = E_{33}$ where \mathbf{E} is the Green strain

tensor) of 0.1%, 0.2%, 0.3%, 0.4% and 0.5% were applied. For the isochoric deformations, three-dimensional shear strain levels of $\gamma_{23} = \gamma_{13} = \gamma_{12} = 0.1\%$, 0.2%, 0.3%, 0.4% and 0.5% ($\gamma_{ij} = 2E_{ij}$ when $i \neq j$) were applied. The volumetric and isochoric deformations were used to determine the bulk moduli K and shear moduli μ , respectively, for each microstate of the two polymer systems [67]. The components of the stiffness tensor \mathbf{L} were determined for each microstate using

$$L_{ijkl} = K\delta_{ij}\delta_{kl} + \mu\left(\delta_{ik}\delta_{jl} + \delta_{il}\delta_{jk} - \frac{2}{3}\delta_{ij}\delta_{kl}\right) \quad [4.11]$$

Further details on these deformations and modulus calculations can be found elsewhere [67]. Elastic constants, such as Young's modulus, can be directly determined from the stiffness tensor of a material using Equation [4.11] and the relationships between elastic constants of isotropic materials[123].

4.5 MICROMECHANICS

Because a given RVE has a unique combination of chain conformations, it is expected that the above-discussed approach to predicting the elastic properties of a polymer system will generally yield different predicted properties for different nanometer-scale RVEs. It is also expected that the bulk material response will be dependent on the mechanical response of all such microstates .that are possible for a given polymer system. Because of the computational difficulty of establishing every possible microstate for a polymer system, the modeling procedure described herein is restricted to the finite number of microstate RVEs obtained as described above.

Micromechanics-based techniques[36] were used to determine the equivalent bulk-level response of the two polymer systems based on the mechanical response of the microstates. This section describes the use of these techniques to establish the bulk

properties and the upper and lower bounds of possible bulk properties for the two polymer systems.

A. Equivalent Bulk Property Bounds

Upper and lower bounds of elastic constants of composite materials are often established to set the boundaries of possible predicted properties predicted with micromechanical approaches. If it is assumed that the strains of all of the phases of a composite material are the same for a given bulk-level deformation, the resulting Voigt model predicts the upper bound of possible bulk composites elastic properties[36]. If it is assumed that the phases of a composite material have the same stress components for a given bulk-level deformation, the resulting Reuss model serves as a lower bound of possible bulk composite properties. The Voigt and Reuss models are given by, respectively,

$$\mathbf{L}^V = \sum_{r=0}^N c_r \mathbf{L}_r \quad [4.12]$$

$$\mathbf{L}^R = \left[\sum_{r=0}^N c_r \mathbf{M}_r \right]^{-1} \quad [4.13]$$

where \mathbf{L}^V and \mathbf{L}^R are the effective stiffness tensor representing Voigt and Reuss bounds, respectively; \mathbf{L}_r and \mathbf{M}_r are the stiffness and compliance tensor components of phase r , respectively; N is the total number of microstates considered; and c_r is the volume fraction of phase r where

$$\sum_{r=0}^N c_r = 1 \quad [4.14]$$

Although tighter bounds have been established for composite materials[27], these bounds assume specific geometries of the phases, such as fibrous or spherical reinforcements. Because the phases considered herein do not necessarily have a defined geometric shape, Equations [4.12]-[4.13] are assumed to be the bounds for the bulk mechanical properties of the two polymer systems.

B. Equivalent bulk elastic properties

While the above-discussed upper and lower bounds of stiffness tensor components provide the limits of the overall bulk properties, it is useful for engineering and material design purposes to use micromechanical techniques to predict an accurate estimate of bulk-level properties. The vast majority of micromechanical techniques focus on predicting properties of composite materials with well-defined reinforcement geometry[36]. However, the geometry of simulated microstates within the polymer material is unknown. Therefore, it was assumed that the bulk polymer stiffness tensor \mathbf{L} is determined using the following simple rule-of-mixtures equation

$$\mathbf{L} = \sum_{r=0}^N c_r \mathbf{L}_r \quad [4.15]$$

It is important to note that the form of Equation [4.15] is the same as that of Voigt model, Equation [4.12]. The form of Equation [4.15] was chosen because of its simplicity. Therefore, the simplest estimates of the bulk mechanical properties will coincide with the upper bound of possible predicted properties of the bulk polymer.

C. Energy-based Statistics

Both the Voigt-Reuss bounds and predicted bulk properties are dependent on the volume fractions of the constituent microstates, as indicated by Equations [4.13] and [4.15]. However, because the distribution of microstates in a polymer material is not always known, simple approaches for selecting the relative volume fractions of the

phases must be established. If it is assumed that the volume fraction of a particular microstate is equal to the probability of the existence of that same microstate, then c_r in Equations [4.13] and [4.15] can be replaced by the probability p_r . Because there are no well-established distribution functions that describe p_r for a polymer material, three assumed forms of the function are considered herein.

The first approach is to assume that all the microstates of the polymer are statistically equally likely, which leads to same volume fractions for each microstate. Therefore, the resulting probability of a microstate r existing in a sample of a polymer material is

$$p_r^{(1)} = \frac{1}{N} \quad [4.16]$$

where N is the total number of different microstates considered, and the superscript 1 indicates the probability associated with this first assumption. The definition in Equation [4.16] satisfies the requirement that

$$\sum_{r=1}^N p_r^{(1)} = 1 \quad [4.17]$$

Although this approach is very simple, a second approach to determining p_r is to use a physically-intuitive probability distribution that is dependent on the energy of a particular microstate. Boltzmann statistics are widely-used to determine the probability of a particular microstate[143]. The service temperature of most engineering polymers is much below the glass transition temperature, and thus many polymers are in a glassy state. Due to the statistical nature of the growth of polymer networks during the synthesis of addition polymers[144], the networks do not crystallize and the chain dynamics are significantly hindered due to the formation of elaborate entanglements.

The entanglements resist the free movement of the polymer chains and therefore hinder the network evolution to a globally-minimized potential energy state. Therefore, it is expected that the lowest-energy microstates are more common, with a finite number of higher-energy microstates that are in metastable states. Motivated by the second law of thermodynamics, a second probability distribution function is assumed that favors lower-energy microstates over the higher-energy microstates which results in an energy-biased distribution

$$p_r^{(2)} = \frac{\Lambda_r^{-1}}{\sum_{s=1}^N (\Lambda_s)^{-1}} \quad [4.18]$$

where Λ_r is the potential energy of microstate r calculated using Equations [4.1]-[4.5].

In a similar manner, a third probability distribution function is assumed to be

$$p_r^{(3)} = \frac{\Lambda_r^{-2}}{\sum_{s=1}^N (\Lambda_s)^{-2}} \quad [4.19]$$

The probability distributions described by Equations [4.18] and [4.19] obey the normalization condition of Equation [4.17]. The functional forms of Equations [4.18] and [4.19] clearly assign higher probabilities to microstates with lower energies.

4.6 RESULTS

Table 4.1 – Polyimide microstate properties

Microstate	Λ_r (kcal/mole)	Simulation box size (Å)	Density (g/cc)	Young's modulus (GPa)	Shear modulus (GPa)	$p_r^{(1)}$	$p_r^{(2)}$	$p_r^{(3)}$
1	42,788.42	44.31	1.16	0.02	0.01	0.143	0.233	0.345
2	52,780.01	44.29	1.16	0.24	0.08	0.143	0.189	0.227
3	79,859.22	44.46	1.14	4.71	1.64	0.143	0.125	0.099
4	84,264.01	44.76	1.12	11.10	4.14	0.143	0.118	0.089
5	84,682.77	44.94	1.11	3.82	1.31	0.143	0.118	0.088
6	85,469.25	44.87	1.11	10.20	3.66	0.143	0.116	0.086
7	97,465.05	44.55	1.14	16.70	6.44	0.143	0.102	0.066

Table 4.2 – Polycarbonate microstate properties

Microstate	Λ_r (kcal/mole)	Simulation box size (Å)	Density (g/cc)	Young's modulus (GPa)	Shear modulus (GPa)	$p_r^{(1)}$	$p_r^{(2)}$	$p_r^{(3)}$
1	13,706.69	41.21	1.09	2.29	0.78	0.111	0.175	0.232
2	13,722.27	40.77	1.12	5.14	1.77	0.111	0.175	0.231
3	15,905.73	41.38	1.07	2.01	0.68	0.111	0.151	0.172
4	18,093.05	40.90	1.11	12.00	4.21	0.111	0.133	0.133
5	21,674.48	40.49	1.15	20.90	7.65	0.111	0.111	0.093
6	23,372.80	40.91	1.11	0.09	0.03	0.111	0.103	0.080
7	38,850.61	40.86	1.12	5.69	1.95	0.111	0.062	0.029
8	50,629.76	41.18	1.09	7.08	2.44	0.111	0.047	0.017
9	55,728.69	41.94	1.03	1.65	0.56	0.111	0.043	0.014

Tables 4.1 and 4.2 show the results obtained from the MD simulations of microstate of the polyimide and polycarbonate materials, respectively. The results are arranged in the increasing order of the equilibrium energies. From these tables, it is clear that the equilibrium energies of the microstates varied greatly for both polymers. The variation in microstate energies confirms the assumption that the conformational space accessible to the polymeric chain network is extensive and the current modeling techniques sample a very small subset of the metastable potential energy states that exist in local equilibrium. The densities of the polyimide ranged from 1.11 g/cc to 1.16 g/cc with a mean of 1.13 g/cc. The densities of the polycarbonate ranged from 1.03 g/cc to 1.15 g/cc with an average of 1.10 g/cc. Therefore, the densities obtained from these simulations were very consistent among the different microstate of both polymers. Similarly, the equilibrium RVE cubic side dimensions varied little between the microstates of the polymer systems.

Tables 4.1 and 4.2 also list the Young's and shear moduli determined for each microstate using the above-described method. The calculated Young's moduli for polyimide varied from 0.02 – 16.70 GPa, with an average of 6.68 GPa and a standard deviation of 6.19 GPa. In case of polycarbonate the Young's modulus varied from 0.09 to 20.90 GPa with an average of 6.32 GPa and a standard deviation of 6.54 GPa. For both the polymer materials the standard deviations are on the order of the averages of the Young's moduli. A similar trend exists for the predicted shear moduli of the two polymer systems, as shown in Tables 4.1 and 4.2. The large standard deviations in the predicted elastic properties are a consequence of the limited number of samples used in the study and the limited size of the RVE. Because of computational costs, the number and size of RVEs was limited in this study and significant standard deviations in the predicted properties were expected. A much more useful approach to establishing the effective properties of the polymer is to use the proposed micromechanical methods, which is described below. Tables 4.1 and 4.2 also list the resulting values of $p_r^{(1)}$, $p_r^{(2)}$, and $p_r^{(3)}$ for each microstate of both polymers. Clearly the probability distribution is

more skewed toward lower energy values for $p_r^{(2)}$ and $p_r^{(3)}$ for both polymers. Furthermore, $p_r^{(3)}$ has the highest probabilities at the lowest energies, and the lowest probabilities at the highest energies relative to $p_r^{(1)}$ and $p_r^{(2)}$ for both polymers.

Table 4.3 shows the predicted bulk Young's modulus values for both polymer systems for each of the three microstate probability distribution functions. In addition, experimentally-obtained Young's modulus values from the literature[101, 124] have also been listed in Table 4.3. For the polyimide, the predicted value of Young's modulus for the $p_r^{(3)}$ probability distribution is the lowest of the three distribution functions. The predicted Young's modulus from the $p_r^{(1)}$ distribution were the highest relative to the other distribution functions and showed the least agreement with the experimentally-obtained Young's modulus. The same trend is observed for the predicted moduli of the polycarbonate. However, the predicted polyimide Young's modulus from the $p_r^{(3)}$ distribution matched the experimental value very closely while the polycarbonate Young's modulus from the same distribution function is significantly higher than the experimental value.

Table 4.3 –Young’s modulus values of polymer systems

Material	Young’s modulus from experiment (GPa)	Young’s modulus from $p_r^{(1)}$ distribution (GPa)	Young’s modulus from $p_r^{(2)}$ distribution (GPa)	Young’s modulus from $p_r^{(3)}$ distribution (GPa)
Polyimide	3.90	6.86	5.42	3.93
Polycarbonate	2.20	6.41	6.38	6.02

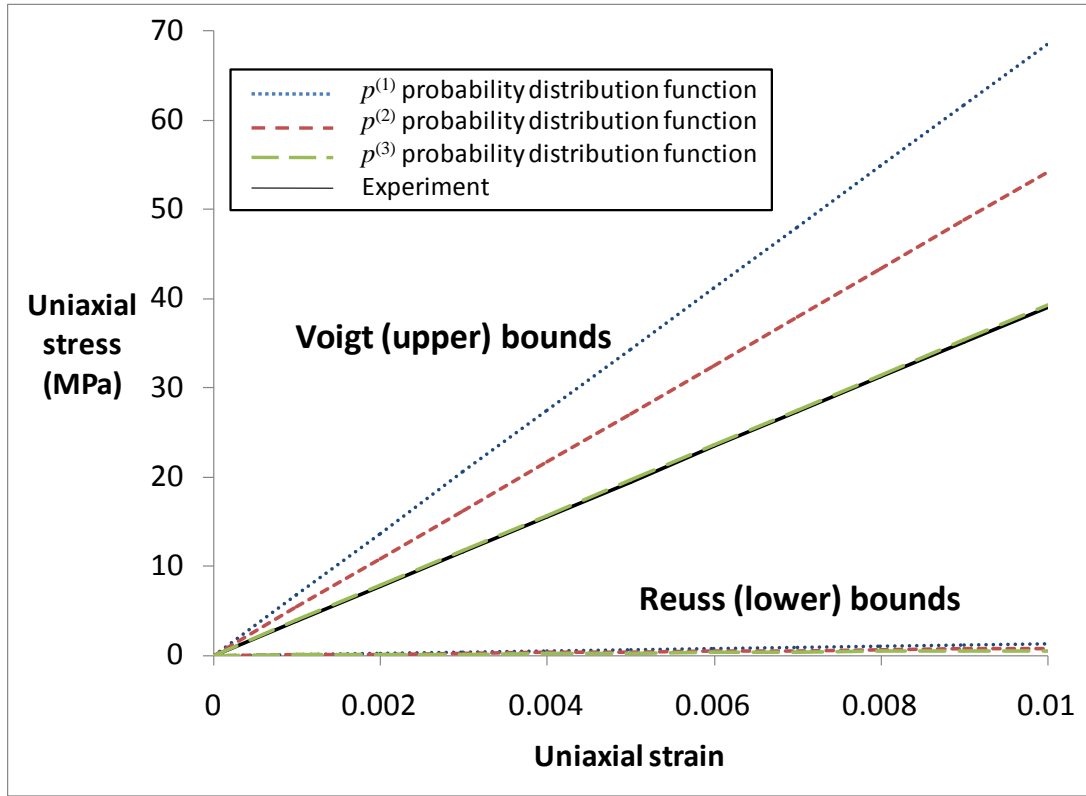


Figure 4.2. Bounds for Young's modulus of polyimide

Because the micromechanical model that was used to predict the elastic response of the polymers Equation[4.15] is a simple approximation, the Voigt-Reuss bounds provide a set of limits that the bulk Young's modulus is physically constrained to based entirely on mechanical interactions between the microstates. Figures 4.2 and 4.3 are linear-elastic uniaxial stress-strain curves for the polyimide and polycarbonate systems, respectively. On both graphs appear the Voigt-Reuss bounds determined with Equation [4.12]-[4.13] for each of the three probability distribution functions $p_r^{(1)}$, $p_r^{(2)}$, and $p_r^{(3)}$. Also shown in Figures 4.3 and 4.4 are the response as determined from experimentally-obtain values of Young's modulus[101, 124]. For the polyimide, the experimental data fall in between the upper and lower bounds, and matches the upper bound of the

response determined with $p_r^{(3)}$. For the polycarbonate system, the experimental curve appears to be nearly half-way between the Voigt and Reuss bounds.

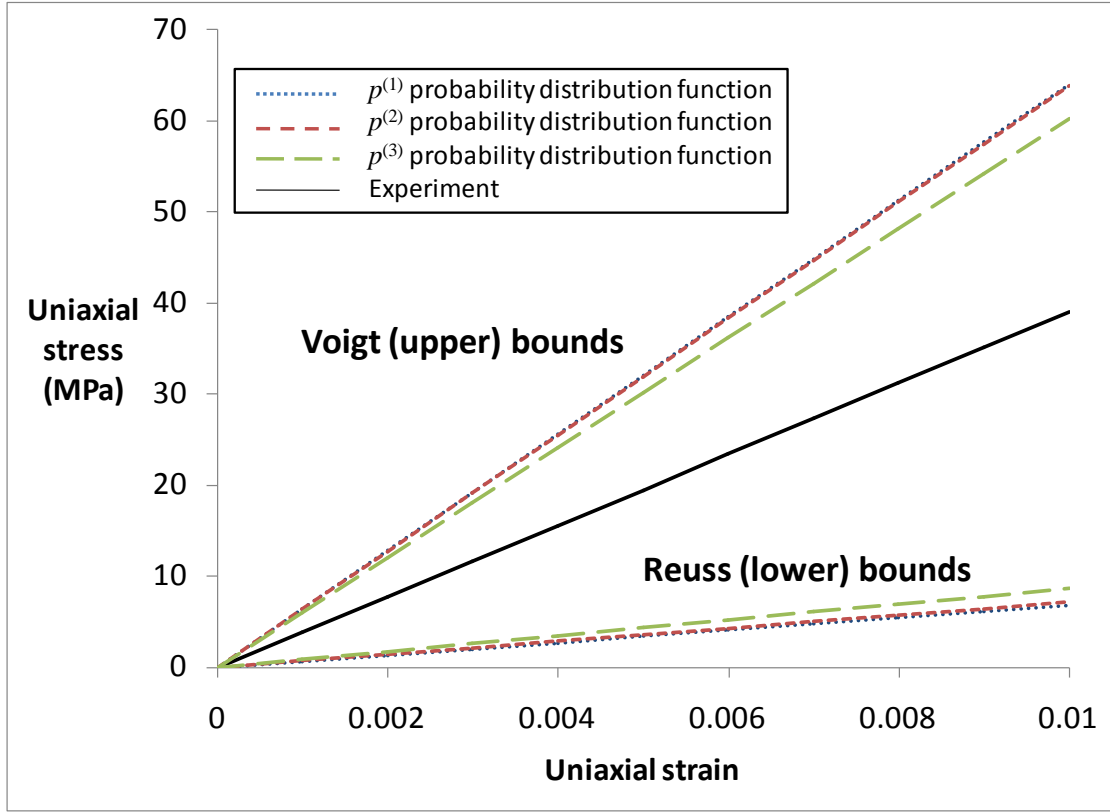


Figure 4.3. Bounds of Young's modulus of polycarbonate

4.7 SUMMARY

The bulk elastic properties of a polyimide system and a polycarbonate polymer have been predicted based on the molecular structure of several microstate representative volume elements whose cubic side dimensions are on the order of a few nanometers. A micromechanical approach has been used to predict the bulk properties based on the predicted mechanical response of each microstate for both polymer systems. The theoretical bounds of possible predicted properties have also been established. The results indicate that individual microstates can have a wide range of Young's moduli,

differing by as much as 16.7 GPa for the polyimide and 21.8 GPa for the polycarbonate. These differences are a factor of 4 and 10, respectively, higher than the experimentally-obtained values of Young's modulus from the literature. On the other hand, using the proposed statistics-based modeling approach has yield predicted bulk Young's modulus values that are higher than the experimental values by a factor of 1 to 3, depending on the assumed probability distribution function. Therefore, the consideration of multiple microstates for a polymer is necessary for the multiscale prediction of elastic properties based on molecular structure.

Although the predicted Young's moduli of both polymers systems are higher than the experimental values for all three distribution functions proposed, an over-prediction of elastic properties is expected for two reasons. First, the molecular systems modeled in the current study represent polymer structures without any chain length distribution and unreacted monomer, both of which are expected to reduce the overall elastic properties of a polymer. Therefore, the predicted properties from these models are expected to be higher than those experimentally-observed in the laboratory. Second, the proposed micromechanics model functional form is a simple rule-of-mixtures formulation. The form of the model is identical with the upper-bound of possible elastic properties. Therefore, a more realistic, and possibly more complex, micromechanics model will likely predict bulk Young's modulus values that are closer to experiment than those presented herein.

Chapter 5

Temperature Effects in Multiscale Modeling of Polymer Materials

The effects of temperature on the predicted mechanical properties of an amorphous polyimide (LaRC-CP2) have been investigated. A multiscale constitutive modeling approach was used to evaluate the equivalent-continuum properties of the modeled polyimide over a series of temperatures ranging from 73K to experimentally measured glass transition temperature. The resulting mechanical properties have been compared to experimentally-obtained properties. The predicted moduli did not show the expected temperature dependence and the sudden change at the glass transition temperature. The lack of expected trends in the results is discussed in the context of the mechanism proposed by three widely accepted theories of glass transition phenomenon.

5.1 INTRODUCTION

The interactions at the nanoscale in materials can be understood with the use of molecular modeling techniques. Molecular Dynamics (MD) and Molecular Mechanics (MM) have been used in numerous studies for prediction of the structure and mechanical properties of polymer-based material systems.[145] MM is a procedure through which the potential energy of a molecular structure can be determined under static conditions for a given molecular geometry.[110] MD can be interpreted as a kinetic MM technique, which involves determination of the time evolution of a set of interacting particles under the influence of forces from interaction with neighboring atoms at a finite temperature. The interaction forces are obtained from a MM potential

known as a *force field*. [63, 139, 146, 147] MD simulations can be used to obtain locally-equilibrated molecular structure for a prescribed temperature for a polymer material and to predict the behavior of the system when subjected to prescribed deformations. Although a limited number of studies have used MD and MM techniques to predict mechanical properties of polymer-based materials at fixed temperatures, [148, 149] little is known about the effects of simulated temperature on predicted properties.

It is well-known that materials generally expand when subjected to increase in temperature and the opposite is true for the decrease in temperature irrespective of their molecular make-up. The effect of the temperature at the molecular level manifests itself into a change in properties at the macroscale. At certain temperatures, the molecular building blocks of a material can undergo significant modification in their structural arrangement leading to a phenomenon which can be broadly classified as a phase transition. Phase transitions typically are associated with marked changes in other physical properties such as specific heat, thermal expansion coefficient, elastic modulus, and mechanical damping. One of the defining characteristics of most amorphous polymers is the glass transition temperature (T_g), which is widely accepted as a second-order phase transition marked by a sudden and significant change in many physical properties. The intended application of a polymer dictates the necessary T_g for optimal performance. For instance, a polymer used as a sealant or a gasket needs to exhibit rubbery behavior, a defining feature of a polymer exposed to temperatures above its T_g . A polymer intended for use in a structural member is usually required to operate at temperatures much below its T_g for increased load-bearing capabilities.

Most computational studies that predict the effects of temperature on physical properties of polymers are generally focused on the density-temperature relationship. These studies are focused on the relevance of density, density correlation functions, and radial distribution functions for various simulated temperatures. [150-152] Also, most studies have generally utilize predictions from a single molecular model. [148] For

instance, mode coupling theory has been used to study the correlation of density in time as a system is evolved.[151, 153] Some studies utilize single-chain representative volume elements (RVEs) and the frequency of trans-gauche transformation as a measure of temperature influence.[154] Real polymers exhibit an extensive entangled network of chains. Therefore, improved modeling methods are needed to predict the influence of temperature on mechanical performance of polymer-based materials.

The objective of this study is to understand the influence of simulated temperature on the predicted mechanical behavior of a polymer system (LaRC-CP2) using a multiscale simulation technique. The predicted mechanical properties of the polymer are compared to those obtained from experiments for a wide range of temperatures. Multiple RVE models at each temperature for a statistical sampling of predicted properties. The proposed framework provides the next step in establishing accurate and efficient multiscale modeling approaches for polymer materials under a wide range of conditions.

5.2 MODELED MATERIAL SYSTEM

To provide a comparative basis for the effectiveness of the current simulation procedure employing MM and MD, a polymeric system with known mechanical properties is studied. LaRC-CP2 is an amorphous, thermoplastic, colorless polyimide originally developed at NASA Langley Research Center. This polyimide can potentially be used for inflatable solar concentrators and antennas due to its superior UV radiation resistance when compared to other polymeric materials. Solar concentrators are envisioned to be widely-used in *Gossamer* (large ultra-light weight) spacecraft in the future, which offer tremendous cost advantage compared to on-orbit constructions.[155, 156] The advantage of using inflatable structures for space application is low weight, and minimal stowage volume during launch.[157] The chemical structure of the LaRC-CP2 repeat unit is shown in Figure 5.1. LaRC-CP2 is synthesized from 1,3-bis(3-

aminophenoxy) benzene (APB) and 2,2-bis(3,4-anhydrodicarboxyphenyl) hexafluoropropane (6FDA).[158]

5.3 MULTISCALE MODELING PROCEDURE

The nonlinear-elastic (hyperelastic) properties of the LaRC-CP2 material system were determined using the Equivalent-Continuum Modeling method.[46, 66, 68, 71, 89, 159-161] This modeling technique was developed for amorphous materials that consist of a mixture of covalent and secondary chemical bonds. This procedure can be divided into three steps. First, a representative volume element (RVE) of the polymer is established that describes the molecular structure in local thermodynamic equilibrium. The second step involves establishing a constitutive equation that can accurately describe the bulk mechanical behavior of the equivalent continuum. Finally, the energies of deformation were obtained for both molecular and equivalent-continuum models under identical states of deformation. The energy for the molecular model was obtained from the MM force field and the energy for the continuum model calculated from the assumed constitutive equation.

A. Molecular RVE

For polymeric materials that are close to or above their glass transition temperature, the simulation time restricts the number of microstates sampled during the MD simulation. It can be imagined that the system would sample all the available microstates provided the simulation is run for extremely large times and that the system has enough kinetic energy to overcome the barrier separating various minimum on the energy landscape. This limitation on time scale can be overcome by the use of multiple samples of the modeled materials.[162] Regardless of the system being glassy or near the glass transition, the bulk material behavior can be imagined to be an average response from all the available conformational microstates.

A series of molecular RVEs of the LaRC-CP2 polymer were constructed using the repeat unit shown in Figure 5.1. The amorphous RVEs of the polymer material were initially constructed in a very low-density gas phase with 7,742 atoms. The molecular models had seven polymer chains each with sixteen repeat units per chain. The gas-phase molecular models so prepared were subjected to an iterative series of energy minimizations coupled with reductions in the size of the RVEs. The minimizations were performed using a quasi-Newton L-BFGS method[119] as implemented with the MINIMIZE program in the TINKER modeling package,[106, 142] and were minimized to reach RMS gradients of convergence of 0.01 kcal/mole/Å. The resulting RVEs of the polymer were subsequently subjected to a series of MD simulations to a local thermally-equilibrated structure. Periodic boundary conditions were used for all of the simulations to minimize the effects of finite size. An example of the resulting RVEs of the polymer is shown in Figure 5.2. The RVEs from this procedure were used to generate three molecular models at five different temperatures: 73K, 173K, 296K, 373K and 473K.

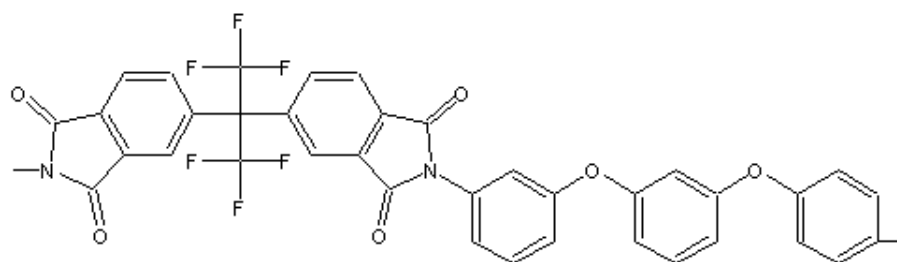


Figure 5.1. Schematic illustration of chemical structure of LaRC-CP2 monomer

Molecular models rely on force fields for characterizing the interactions between the constituent atomic species. Most force fields are semi-empirical and assume specific degrees of freedom for a given molecular structure. The total energy of the molecular model is the summation of energies from these individual degrees of freedom. One of the most widely-used force fields, AMBER, was utilized for this study. The simulations in the current study did not include the electrostatic interactions which are based on the

dipole moments of the atoms. The AMBER force field was chosen over other available force fields of rather complex functional form for efficiency and accuracy.[67]

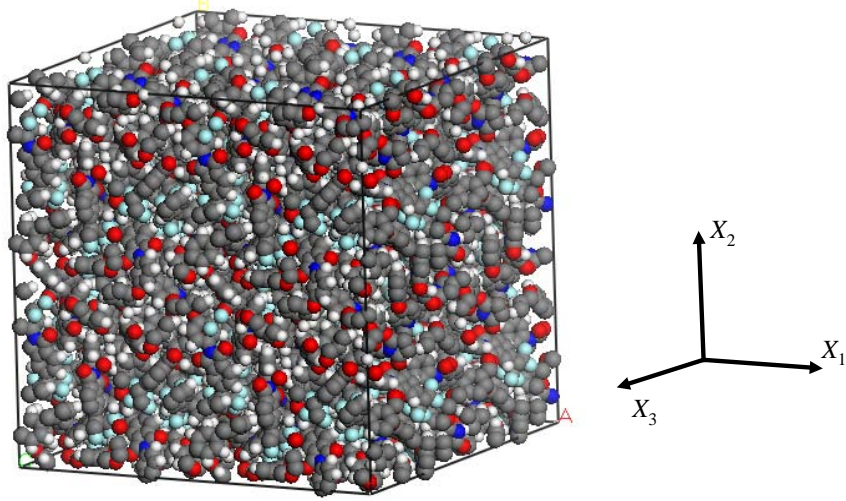


Figure 5.2. Representative volume element of LaRC-CP2

The total potential energy of a simulated molecular system computed with the AMBER force field is based on the summation of the bond stretching, bending, torsion and nonbonded energies given by

$$\Lambda_m = \Lambda_{\text{stretch}} + \Lambda_{\text{bend}} + \Lambda_{\text{torsion}} + \Lambda_{\text{nb}} \quad [5.1]$$

where

$$\Lambda_{\text{stretch}} = \sum_{\text{stretch}} K_r (r - r_{eq})^2 \quad [5.2]$$

$$\Lambda_{\text{bend}} = \sum_{\text{bend}} K_\theta (\theta - \theta_{eq})^2 \quad [5.3]$$

$$\Lambda_{\text{torsion}} = \sum_{\text{torsion}} \left\{ \begin{aligned} &\frac{V_1}{2} [1 + \cos(\phi + \zeta)] \\ &+ \frac{V_2}{2} [1 - \cos(2\phi + \zeta)] \\ &+ \frac{V_3}{2} [1 + \cos(3\phi + \zeta)] \end{aligned} \right\} \quad [5.4]$$

$$\Lambda_{\text{nb}} = \sum_{I < J} 4\varepsilon_{IJ} \left[\frac{(\sigma_{IJ})^{12}}{r_{IJ}^{12}} - \frac{(\sigma_{IJ})^6}{r_{IJ}^6} \right] \quad [5.5]$$

where the summations are taken over all of the corresponding interactions in the molecular model; K_r and K_θ are the bond-stretching and bond-angle bending force constants, respectively; r and r_{eq} are the bond length and equilibrium bond lengths, respectively; θ and θ_{eq} are the bond angle and equilibrium bond angles, respectively; $V_n/2$, ϕ , and ζ are the torsion magnitude ($n=1,2,3$), phase offset, and the torsion angle, respectively; and ε_{IJ} , r_{IJ} , and σ_{IJ} are van der Waals well depth, non-bonded distance between atoms I and J , and the equilibrium distance between atoms I and J , respectively.

B. Continuum Model

A hyperelastic approach was used for the constitutive modeling of the equivalent-continuum polymer material subjected to finite deformations. It was assumed that the strain energy function is associated with stress and strain tensors that are thermodynamic work conjugates in the balance of mechanical energy.

It can be shown[161] that the equivalent-continuum strain energy density can be decomposed into volumetric (shape preserving) and isochoric (shape changing) components, ψ_{vol} and ψ_{iso} , respectively,

$$\Psi_c = \psi_{\text{vol}} + \psi_{\text{iso}} \quad [5.6]$$

where

$$\begin{aligned}\psi_{vol} &= c_1 \Omega_1 \\ \psi_{iso} &= c_2 \Omega_2\end{aligned}\tag{5.7}$$

and

$$\begin{aligned}\Omega_1 &= (I_3 - 1)^2 \\ \Omega_2 &= \left(\frac{I_1}{I_3^{1/3}} + \frac{I_2^3}{I_3^2} - 30 \right)\end{aligned}\tag{5.8}$$

In Equation [5.7] the constants c_1 and c_2 are material parameters and I_1 , I_2 and I_3 are the strain invariants. The hyperelastic strain energy function in equation [5.6] is constructed with two material parameters as the bulk LaRC-CP2 is known to exhibit isotropic material symmetry. The material parameters c_1 , c_2 are unknown and will be calculated by equating the potential energy of the molecular model and the strain energy of the equivalent-continuum under identical deformation fields. The deformed energy for the molecular model is calculated using the *force-field*. For the continuum model, the hyperelastic strain energy function in equation [5.6] is used. Since equation [5.6] involves two independent material parameters, we subject both continuum and molecular models to two independent deformation fields giving rise to a set of equations in c_1 and c_2 . The solution of these equations results in determination of materials parameters. Once the material parameters are evaluated, substitution of equations [5.7] and [5.8] into equation [5.6] and using Coleman-Noll[112] approach yields the continuum constitutive relationship :[67]

$$\mathbf{S} = \frac{2}{3} \left[6c_1 I_3 (I_3 - 1) - c_2 \left(\frac{I_1}{I_3^{1/3}} + 6 \frac{I_2^3}{I_3^2} \right) \right] \mathbf{C}^{-1} + 2c_2 \left(\frac{1}{I_3^{1/3}} + 3 \frac{I_1 I_2^2}{I_3^2} \right) \mathbf{I} - 6c_2 \frac{I_2^2}{I_3^2} \mathbf{C} \tag{5.9}$$

It can be shown that this constitutive equation satisfies the required growth conditions for a hyperelastic material. A more detailed discussion of the derivation of the constitutive relationship in equation [5.9] can be found elsewhere. [67]

5.4 RESULTS AND DISCUSSIONS

Table 5.1 shows the results obtained from the molecular simulations and the multiscale analysis to extract the effective-continuum properties. Three molecular RVEs were generated for each simulated temperature. The third column of Table 5.1 is the simulated length of the cubic RVE box size for the corresponding temperature. All the molecular models contain the same mass so a trend in the volume or the length of the RVE side exhibits a corresponding trend in the density. The increase in temperature would be expected to result in thermal expansion. From Table 5.1, it can be seen that the average length of the RVE side does not exhibit a monotonic dependence with increasing temperature. A characteristic of a glass is limited molecular motion leading to large standard deviations in physical properties [153]. It can be seen that from 73K to 296K there is a steady decrease in the standard deviation in the RVE box length. The lack of the trend in density for higher temperatures could be a consequence of the limited number of microstates or the fluctuation due to finite size effects. In addition, the length scales accessible to MD simulations is orders of magnitude less than the typical time scales involved in laboratory testing. Sufficiently long simulation times can relax the structure to realize a better trend in simulation box size. Figure 5.3 shows the trend in the volume of RVE for the five different temperatures with the standard deviation indicated by the markers. It can be seen that the large standard deviation at every temperature makes it difficult to discern a definite trend in density with temperature. LaRC-CP2 is expected to exhibit glass transition around 476K based on experimental measurements [163].

Table 5.2 presents the experimentally measured storage modulus using Dynamic Mechanical Analysis (DMA) with a tensile sample at a frequency of 1Hz.[163] The results for shear modulus are presented in the fourth column of Table 5.1. From 173K to 373K we observe a decrease in the shear modulus, along with a corresponding decrease in the standard deviation based on three samples for each temperature. From Table 5.2, the experimental value at 173K to 373K decreases from 3.18 (\pm 0.54) GPa to 2.57 (\pm 0.19) GPa, while the simulated moduli vary from 11.3 (\pm 8.99) GPa to 2.36 (\pm 2.93) GPa respectively. The experimentally measured values for modulus from 173K to 373K lie within one standard deviation of the simulated results as shown in Figure 5.4. There is a decrease in the simulated modulus and the standard deviation as expected with increase of temperature over 173K-373K. However, the large standard deviation at 73K and 473K make it difficult to make a quantitative assessment of the overall trend. It is not expected that the simulated results will quantitatively match the experimental values as the molecular models are perfect materials without any defects which generally results in overestimation of properties. In conclusion, the simulated results do not capture the qualitative trend expected from experiments.

Now we turn our discussion to the lack of definite trends in predicted properties of LaRC-CP2 when compared to the experimental values of mechanical properties. The temperature dependence of physical properties can be explained using different theories.[164] Although most of these theories were initially proposed for explaining the glass transition phenomenon in polymers, they are also well-suited to explain the trends in other physical properties. These theories can be broadly classified into free volume theories, kinetic theories, and thermodynamic theories. Free volume theory assumes that a small fraction of the polymer is empty (not occupied by polymer molecules) which plays a large role in the temperature-dependent behavior of polymers. The glassy state of a polymer is governed by very limited molecular mobility a consequence of an iso-free volume state. This can be tied into the empirical Doolittle viscosity and the William-Landel-Ferry equations.[164] The kinetic theories propose

that the temperature-dependent behavior is entirely governed by the polymer chain kinetics and its response time when compared to the experimental time scales.

Thermodynamic theories have been established to explain the Kauzmann paradox. The Kauzmann paradox states that for a supercooled liquid below a critical temperature, the liquid has lower entropy than the corresponding solid at the same temperature. This gives rise to the Gibbs-DiMarzio theory which states that there is a phase transition that occurs above that critical temperature at which the configurational entropy of a polymer network goes to zero leading to a glassy phase. From these three different theories, it is clear that there is no general agreement on the physical basis of the glass transition behavior of polymers. Furthermore, the applicability of these theories to molecular modeling has not been fully explored.[149] Thermodynamic theories are not easily usable with molecular simulations as they require some knowledge of entropy of the system, which involved extensive sampling of the energy landscape making it computationally cumbersome. The kinetic theory mechanism in the context of classical MD relies on the time scale of the simulation which poses a severe restriction on its application with the current methodology. Therefore, there is currently no definite physics-based approach to modeling the glass transition effects of polymer materials using molecular simulations. However, what is clear from these theories is that as the temperature of a polymer increases, the mobility of the molecular chains also increases, which results in a rapid change in the properties at the glass transition temperature. These effects are not properly accounted for in currently-used force fields (e.g. AMBER). Thus, a definite trend between properties and temperatures is not expected, and not observed, in Table 5.1.

Table 5.1. Results of the molecular simulations

Temperature	Sample	Box Size (in Å)	Energy (Kcal/Mol)	G (GPa)
73	S1	46.8386	96879.5684	3.792
	S2	47.4810	141053.7630	1.509
	S3	47.3481	86773.3854	5.823
Average		47.2226	108235.5723	3.708
Std. Dev.		0.3391	28867.0914	2.158
173	S1	46.9170	96308.6788	7.651
	S2	47.1948	107195.3880	1.069
	S3	46.9049	145303.0020	3.797
Average		47.0055	116269.0229	4.173
Std. Dev.		0.1640	25726.6217	3.307
296	S1	47.3056	120162.2097	1.305
	S2	47.4055	99264.5785	1.106
	S3	47.1345	146279.9791	4.859
Average		47.2819	121902.2558	2.423
Std. Dev.		0.1370	23555.9503	2.112
373	S1	47.2465	65211.3838	1.980
	S2	46.9368	110989.5430	0.1996
	S3	47.5418	101005.4485	0.2478
Average		47.2417	92402.1251	0.8092
Std. Dev.		0.3025	24071.2036	1.014
473	S1	47.5455	92199.5107	3.831
	S2	47.4407	126475.4820	3.189
	S3	47.2549	96337.4581	1.118
Average		47.4137	105004.1503	2.713
Std. Dev.		0.1472	18709.4686	1.418

Table 5.2 Experimental values for storage modulus of LaRC-CP2 at different temperatures³¹

Temperature (in K)	Modulus (GPa)	Standard Deviation (GPa)
173	3.18	0.54
296	3.00	0.21
373	2.57	0.19
423	2.24	0.15

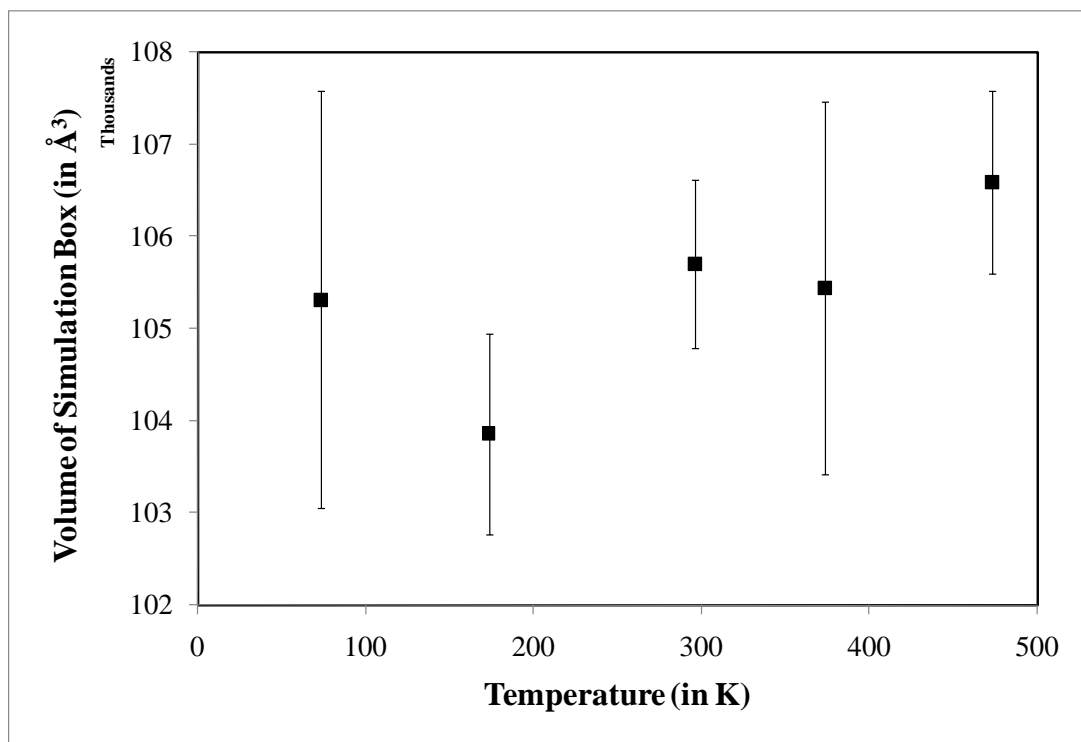


Figure 5.3 Volume of RVE as a function of the simulated temperature

An efficient and accurate approach to modeling the effect of temperature on the mechanical response of a molecular RVE using molecular simulations is needed. This approach must account for the increased mobility of polymer molecules near the glass transition temperature. The increase in polymer chain mobility, or the increase in the RVE size as a function of temperature, is not accounted for in simple state-of-the-art force fields that are used to predict the properties of large polymer systems. This shortcoming may be alleviated through introduction of physically-motivated temperature dependence in the force field parameters.

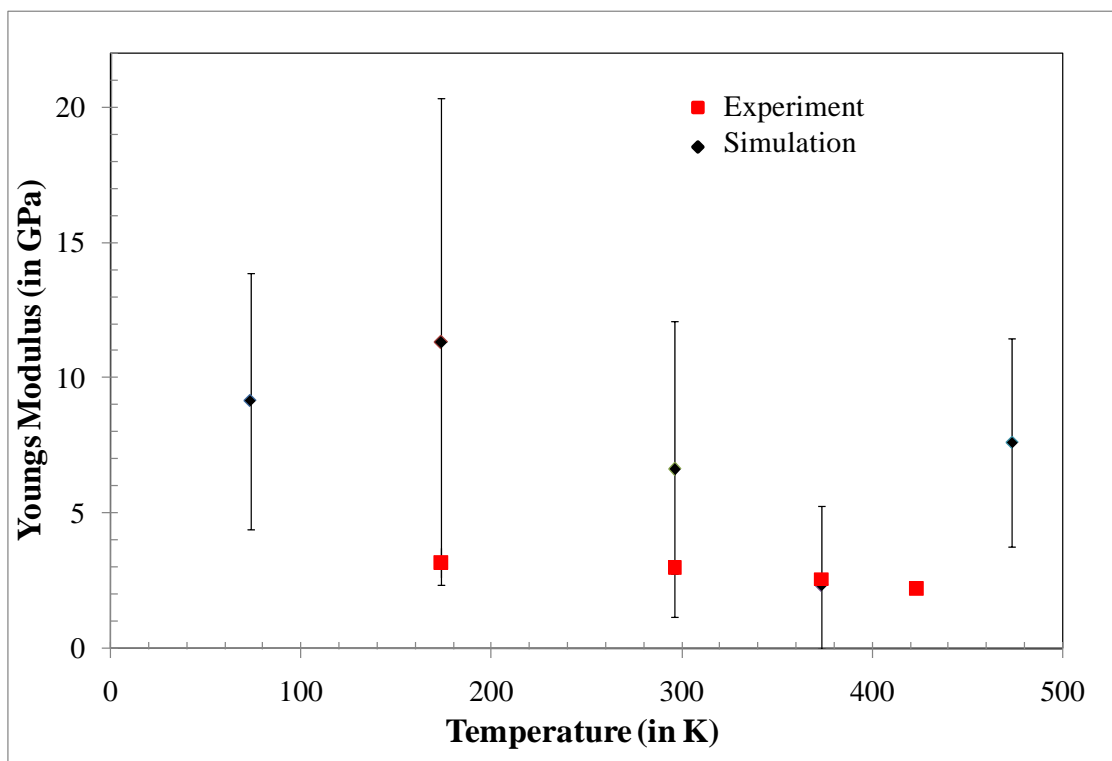


Figure 5.4 Modulus of LaRC-CP2 as a function of temperature

Chapter 6

Influence of Representative Volume Element Size on Multiscale Modeling of Polymer Materials

Molecular dynamics (MD) simulations and micromechanical modeling are used to predict the bulk-level Young's modulus of polycarbonate and polyimide polymer systems as a function of representative volume element (RVE) size and force field type. The bulk-level moduli are determined using the predicted moduli of individual finite-sized RVEs (microstates) using a simple averaging scheme and an energy-biased micromechanics approach. The predictions are compared to experimental results. The results indicate that larger RVE sizes result in predicted bulk-level properties that are in greater agreement with experiment than the smaller RVE sizes. Also, the energy-biased micromechanics approach predicts values of bulk-level moduli that are in better agreement with experiment than those predicted with simple microstate averages. Finally, the results indicate that negatively-valued microstate Young's moduli are expected, as observed previously in the literature, and should be included in the overall determination of bulk-level elastic properties for improved accuracy.

6.1 INTRODUCTION

The efficient development of these materials requires simple and accurate structure-property relationships that are capable of predicting the bulk mechanical properties of as a function of the molecular structure and interactions. Modeling techniques spanning over multiple length scales must be used to establish these structure-property

relationships. At the atomistic length scale, molecular dynamics (MD) has shown to be a powerful technique for predicting the equilibrated molecular structures of polymer-based materials for a given thermodynamic state [16, 66, 67, 70, 128, 159, 165-168]. The mechanical behavior of such material systems can be studied with the aid of a representative volume element (RVE) that is capable of quantitatively depicting the macro-scale characteristics.

RVEs have been extensively used in the constitutive modeling of both crystalline and amorphous materials [121, 169-174]. However, central to this methodology is the choice of the RVE that can accurately capture the material's bulk-scale mechanical behavior. The optimal choice of an RVE for an amorphous nanostructured material remains a challenge. Although traditional methodologies have been applied to continuous materials [169], selection of nanometer-sized RVEs for discrete polymer structures has not been rigorously addressed [162, 175]. Ostoja-Starzewski has established a statistical volume element (SVE) that approaches an RVE under certain limiting conditions [173, 174]. A multiscale modeling approach has been recently developed to account for a range of conformational microstates of a polymeric network must be accounted for [162, 176]. Physically-motivated statistical weighting of properties obtained from individual microstates for each polymer were utilized to establish bounds of the predicted moduli and are subsequently compared to experimentally-measured values of moduli for these materials.

The mechanical response of polymers is a consequence of the entanglement of the constituent molecular chains. The entangled network of a finite number of chains can only sample a small portion of the conformational space of the bulk polymer. As a result, the physical properties of a polymer can vary substantially on the nanometer length-scale [130-138, 177]. Similarly, the RVE size can influence the predicted mechanical properties of a polymer [178] using multiscale modeling techniques. Increasing the RVE size of a modeled polymer establishes predicted physical properties

over a larger conformational space. The effect of the molecular RVE size on predicted polymer properties in multiscale models of polymers needs to be rigorously investigated.

In this study, a multiscale modeling technique has been used to predict the bulk elastic moduli of polyimide and polycarbonate material systems using different RVE sizes. Multiple microstates for each RVE size were considered. The calculated weighted average for the microstates of each RVE size was found to be in good agreement with the experimentally measured properties. Also, it was found that increasing the RVE size provided evidence for a convergence to limiting values, as expected from data from bulk-scale experimentals.

6.2 MOLECULAR MODELING

Figure 6.1 shows the polymer repeat units for the two polymer materials used in the current study. MD simulations were carried out on two polymer materials, a polyimide and a polycarbonate. These polymers have been synthesized in the laboratory, tested, and also modeled by various research groups [67, 101, 109, 140]. Three different RVE sizes were modeled for the two polymer materials. Nine thermally-equilibrated structures were obtained for each polycarbonate RVE size. For polycarbonate, the smallest RVE consisted of 3,972 atoms with 6 polymer chains; the medium-sized RVE had 5,958 atoms with 9 polymer chains and the largest RVE had 7,944 atoms with 12 polymer chains. All polycarbonate chains for the different RVE sizes had 20 repeat units per chain. Each of the nine structures for each RVE size represents a microstate for the polycarbonate system. For the polyimide system, the smallest RVE consisted of 4,244 atoms with 7 polymer chains; the medium sized RVE consisted of 6,622 atoms with 11 polymer chains, and the largest RVE consisted of 8,248 atoms with 14 polymer chains. Each polyimide chain consisted of 10 repeat units per chain. A total of nine RVEs were established for the small and the large models of polyimide and seven for

the medium-sized RVE. Similar to polycarbonate, each polyimide model represented a single microstate for the corresponding RVE size.

All RVE structures were initially prepared in a gas-like phase with extremely low densities. For each RVE sample, the polymer chains were placed in a simulation box with random conformations and orientations. Energy minimization simulations were conducted initially without periodic boundary condition to relax individual chains. Afterwards, the periodic boundary conditions were applied and a series of minimizations were carried out at gradually-increasing densities. The MINIMIZE [119] and NEWTON [141] subroutines of the TINKER [106, 142] modeling package were used for these minimizations, which correspond to a quasi-Newton L-BFGS method and a truncated Newton energy minimization methods, respectively. The minimizations were performed to RMS gradients of 1×10^{-2} and 1×10^{-5} kcal/mole/Å, respectively.

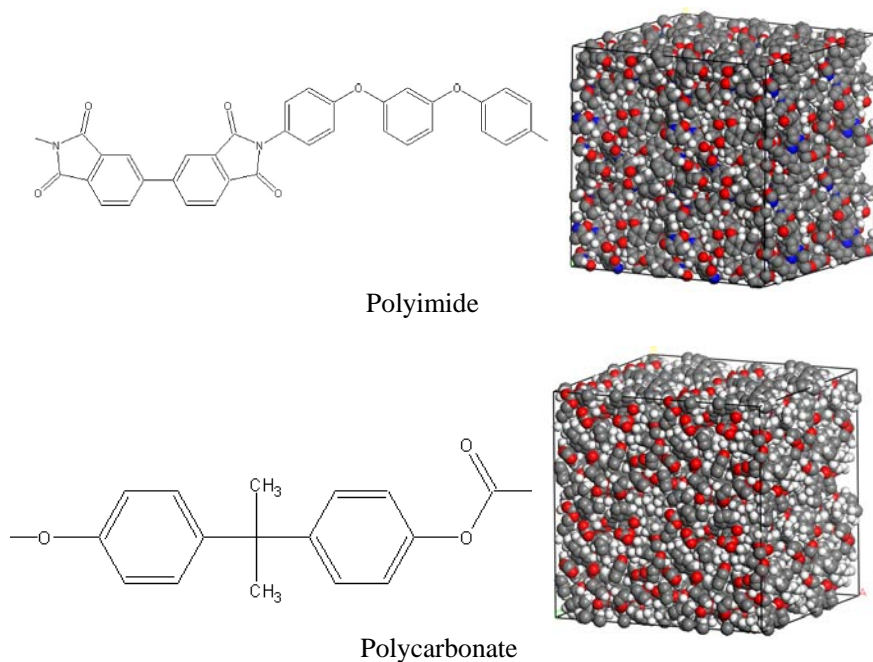


Figure 6.1. Schematics of the polymeric chain repeat units and the corresponding representative volume elements for polyimide and polycarbonate

Once each of the RVEs were established with the approximate solid bulk density, a series of MD simulations were used to establish thermally-equilibrated solid structures in the following order at 300 K: (1) a 50 ps simulation with the NVT (constant number of atoms, volume, and temperature) ensemble to prepare the structure for further equilibration, (2) a 100 ps simulation with the NPT (constant number of atoms, pressure, and temperature) ensemble at 100 atm to evolve the system to higher densities as the structure was prepared from a low density structure, (3) a 100 ps NPT simulation at 1atm to reduce the effects of high-pressure simulations and to let the system evolve to a state of minimal residual stresses, and (4) a 100 ps NVT simulation to allow the system to equilibrate at the simulated temperature and density for a specific microstate. The DYNAMIC subroutine of the TINKER modeling package was used for the MD simulations with periodic boundary conditions. Examples of the molecular models that were established in a manner described above are shown in Figure 6.1. The above-described procedure was identically used for with two widely used force fields, namely, AMBER as implemented as AMBER99 in TINKER and an all-atom version of OPLS, namely OPLS-AA. The functional forms of these force fields are described in greater detail in the Chapter 3. The final specific weight of each RVE was approximately between 1.1 and 1.2. A total of 115 RVEs were modeled for the current study.

6.3 EQUIVALENT CONTINUUM MODELING

An equivalent-continuum modeling approach was used to determine the equivalent-continuum mechanical properties of each RVE (microstate). A hyperelastic-continuum constitutive relation [67] was used to model the elastic behavior of the equivalent-continuum material models. The constitutive relationships of these models had the following characteristics: (1) isotropic material symmetry due to the amorphous molecular structures, (2) finite-deformation framework, (3) expressed in terms of

volumetric (shape preserving) and isochoric (shape changing) contributions, and (4) established using a thermodynamic potential. The assumed form of the equivalent-continuum strain energy is

$$\Psi_c = \psi_{vol} + \psi_{iso} \quad [6.1]$$

where

$$\begin{aligned} \psi_{vol} &= c_1 \Omega_1 \\ \psi_{iso} &= c_2 \Omega_2 \end{aligned} \quad [6.2]$$

and

$$\begin{aligned} \Omega_1 &= (I_3 - 1)^2 \\ \Omega_2 &= \left(\frac{I_1}{I_3^{1/3}} + \frac{I_2^3}{I_3^2} - 30 \right) \end{aligned} \quad [6.3]$$

The parameters Ω_1 and Ω_2 in Equation [4.8] represent the volumetric and isochoric components of the strain-energy density; c_1 and c_2 are constants which represent material properties; and I_1 , I_2 , and I_3 are the scalar invariants of the right Cauchy-Green deformation tensor, \mathbf{C} . The second Piola-Kirchhoff stress tensor is therefore [67]

$$\mathbf{S} = \frac{2}{3} \left[6c_1 I_3 (I_3 - 1) - c_2 \left(\frac{I_1}{I_3^{1/3}} + 6 \frac{I_2^3}{I_3^2} \right) \right] \mathbf{C}^{-1} + 2c_2 \left(\frac{1}{I_3^{1/3}} + 3 \frac{I_1 I_2^2}{I_3^2} \right) \mathbf{I} - 6c_2 \frac{I_2^2}{I_3^2} \mathbf{C} \quad [6.4]$$

where \mathbf{I} is the identity tensor.

Equation [6.4] contains material parameters c_1 and c_2 which were evaluated for each microstate by equating the equivalent-continuum strain energy and the molecular

potential energy for a set of identical deformation fields applied to the equivalent continuum and the molecular models [21, 67, 68, 70, 90]. For the molecular models, the strain-energy densities are computed from the force field using

$$\Psi_m = \frac{1}{V_0} (\Lambda_m - \Lambda_m^0) \quad [6.5]$$

where, Λ_m^0 and Λ_m are the molecular potential energies before and after application of the deformations, which are directly computed from the force field, and V_0 is the volume of the simulation box in the undeformed state.

Two sets of finite deformations were applied to each of the RVEs and the equivalent-continuum in incremental steps. For the volumetric deformation, volumetric strains ($E_{11} = E_{22} = E_{33}$ where \mathbf{E} is the Green strain tensor) of 0.1%, 0.2%, 0.3%, 0.4% and 0.5% were applied. For the isochoric deformations, three-dimensional shear strain levels of $\gamma_{23} = \gamma_{13} = \gamma_{12} = 0.1\%$, 0.2%, 0.3%, 0.4% and 0.5% ($\gamma_{ij} = 2E_{ij}$ when $i \neq j$) were applied. By equating the energies of deformation for the RVEs and the equivalent continuum for each of the two deformation types, the elastic properties were determined as described in detail elsewhere [67].

6.4 EFFECTIVE POLYMER PROPERTIES

The equivalent-continuum properties of each RVE obtained as described in the previous section was used to determine effective bulk properties of the polymer materials for each of the RVE sizes. The equivalent-continuum properties represent the deformation response of the particular chain arrangements associated with the RVEs. It is expected that the approach described in the previous section will generally yield different predicted properties for different RVEs (for a given RVE size). Each of the RVEs is of the order of a few nanometers in length. However, the bulk-polymer

response is an average mechanical response of a the large number of RVEs that are statistically probable for a given polymer system. Due to the computational time and cost associated with establishing every possible conformational microstate for a polymer system, the modeling procedure described herein approximates the bulk material behavior with only a finite number of RVEs obtained as described in Section 6.2. To this end, the bulk polymer elastic behavior of each polymer system was determined using a physically-motivated weighted-averaging scheme. The details of this scheme are discussed below in the context of the more simple and traditional Voigt modeling approach.

The Voigt model (rule-of-mixtures) assumes that the strains in all of the phases of a composite material are the same for a given bulk-level deformation. As a result, the predicted properties of a composite from the Voigt model corresponds to the upper bound of possible bulk elastic properties [36]. This approach provides a simple estimate of the expected properties for a material composed of phases or microstates of varying properties. The Voigt model prediction for a material with arbitrary number of constituents is given by,

$$\mathbf{L}^V = \sum_{r=0}^N c_r \mathbf{L}_r \quad [6.6]$$

where \mathbf{L}^V are the effective stiffness tensor associated with the Voigt estimate; \mathbf{L}_r is the stiffness tensor components of phase r ; N is the total number of microstates considered; and c_r is the volume fraction of phase r where

$$\sum_{r=0}^N c_r = 1 \quad [6.7]$$

Although better estimates for multi-phase materials have been established for composite materials [27], these generally assume a more specific geometry of the phases, such as fibrous or spherical reinforcements. Because the exact geometric shapes of the microstates considered herein are unknown, Equation [6.6] was utilized to estimate the bulk mechanical properties of the two polymer systems.

The evaluation of the properties based on the Voigt approach is dependent on the volume fractions of the constituent microstates, as indicated by Equation [6.6]. However, the distribution of microstates in a polymer material is generally unknown. A simple approach for selecting the relative volume fractions of the phases was recently proposed. For this approach, it is assumed that the volume fraction of a particular microstate is equal to the probability of its existence so that c_r in Equation [6.6] is replaced by the probability p_r . Because there are no well-established distribution functions that describe p_r for an amorphous polymer material, assumed forms of the function have been proposed.

For the research described herein, it was assumed that p_r is determined using a physically-intuitive distribution that is biased based on the equilibrium potential energy of a particular microstate. Many engineering polymers operate much below the glass transition temperature, and thus exist in a glassy state. Due to the statistical nature of the growth of polymer networks during polymerization of addition polymers [144], the networks do not crystallize due to hindered chain dynamics as a consequence of the formation of elaborate entangled networks. It is expected that the lower-energy microstates are thermodynamically favored, with a higher probability than high-energy microstates. This approach has been shown to provide accurate estimates for the mechanical properties of polymers [162, 176]. Motivated by this argument, a probability distribution function that satisfies this requirement is

$$p_r = \frac{\Lambda_r^{-1}}{\sum_{s=1}^N (\Lambda_s)^{-1}} \quad [6.8]$$

where N is the total number of different microstates considered and Λ_r is the potential energy of microstate r calculated using Equations from Chapter 3. The definition in Equation [4.18] satisfies the requirement analogous to [6.7]

$$\sum_{r=1}^N p_r = 1 \quad [6.9]$$

More detail on this modeling approach can be found elsewhere.

6.5 RESULTS AND DISCUSSIONS

Table 6.1 – Microstate properties for the small RVE size of polycarbonate with AMBER

Microstate	Λ_r (kcal/mole)	Density (g/cc)	Young's modulus (GPa)	Shear modulus (GPa)	p_r
1	482.91	1.1379	26.6	9.75	0.805
2	3872..13	1.137	6.22	2.15	0.1
3	23001.84	1.137	20.1	7.25	0.016
4	25470.26	1.129	11.5	3.99	0.015
5	27832..29	1.142	4.9	1.68	0.013
6	30000.92	1.096	4.87	1.66	0.012
7	31939.19	1.111	1.29	0.43	0.012
8	33221.32	1.135	6.57	2.24	0.011
9	36176.15	1.131	-1.92	-0.64	0.01
Average	23555.67	1.126	8.9	3.17	-
Std. Dev.	12780.03	0.015	9.12	3.34	-

Table 6.2 – Microstate properties for the medium-sized RVE of polycarbonate with
AMBER

Microstate	Λ_r (kcal/mole)	Density (g/cc)	Young's modulus (GPa)	Shear modulus (GPa)	p_r
1	13,706.69	1.09	2.29	0.78	0.175
2	13,722.27	1.12	5.14	1.77	0.175
3	15,905.73	1.07	2.01	0.68	0.151
4	18,093.05	1.11	12.00	4.21	0.133
5	21,674.48	1.15	20.90	7.65	0.111
6	23,372.80	1.11	0.09	0.03	0.103
7	38,850.61	1.12	5.69	1.95	0.062
8	50,629.76	1.09	7.08	2.44	0.047
9	55,728.69	1.03	1.65	0.56	0.043
Average	27964.89	1.098	6.32	2.23	-
Std. Dev.	16250.79	0.033	6.55	2.39	-

Table 6.3 – Microstate properties for the large RVE size of polycarbonate with AMBER

Microstate	Λ_r (kcal/mole)	Density (g/cc)	Young's modulus (GPa)	Shear modulus (GPa)	p_r
1	16523.09	1.0234	0.97	0.32	0.237
2	32070.92	1.038	6.54	2.28	0.122
3	35512.99	1.05	2.31	0.78	0.11
4	36568.99	1.076	6.54	2.24	0.107
5	37445.09	1.111	9.33	3.25	0.104
6	37548.48	1.035	14.3	5.34	0.104
7	45790.31	1.103	3.44	1.17	0.085
8	56070.49	1.107	8.06	2.80	0.069
9	68552.23	1.115	1.9	0.64	0.057
Average	40675.84	1.073	5.92	2.09	-
Std. Dev.	14838.23	0.037	4.28	1.59	-

Table 6.4 Microstate properties for the small RVE size of polycarbonate with OPLS-AA

Microstate	Λ_r (kcal/mole)	Density (g/cc)	Young's modulus (GPa)	Shear modulus (GPa)	p_r
1	297.58	1.165	3.27	1.1	0.827
2	2123.78	1.156	1.55	0.528	0.115
3	21236.35	1.147	-0.12	-0.04	0.011
4	27204.39	1.149	11.5	3.98	0.009
5	30984.07	1.147	3.01	1.01	0.007
6	33364.17	1.149	1.08	0.36	0.007
7	33826.32	1.119	7.32	2.52	0.007
8	35127	1.142	4.2	1.42	0.007
9	39157.65	1.156	1.4	0.47	0.006
Average	24823.48	1.148	3.69	1.26	-
Std. Dev.	14310.28	0.012	3.64	1.26	-

Table 6.5 – Microstate properties for medium-sized RVE of polycarbonate with OPLS-AA

Microstate	Λ_r (kcal/mole)	Density (g/cc)	Young's modulus (GPa)	Shear modulus (GPa)	p_r
1	12398.52	1.153	3.8	1.28	0.197
2	12492.38	1.094	5.16	1.76	0.196
3	17059.73	1.107	3.81	1.3	0.143
4	19048.08	1.089	8.11	2.82	0.128
5	24761.87	1.12	3.91	1.28	0.099
6	25743.496	1.147	7.67	2.63	0.095
7	44663.33	1.125	0.06	0.02	0.054
8	56942.82	1.094	3.11	1.06	0.043
9	59766.92	1.038	0.624	0.2	0.041
Average	30319.68	1.107	4.03	1.38	-
Std. Dev.	18625.79	0.034	2.73	0.94	-

Table 6.6 – Microstate properties for the large RVE size of polycarbonate with OPLS-AA

Microstate	Λ_r (kcal/mole)	Density (g/cc)	Young's modulus (GPa)	Shear modulus (GPa)	p_r
1	13530.63	1.118	2.65	0.89	0.267
2	30914.25	1.112	0.7	0.23	0.117
3	31583.09	1.066	-0.22	-0.07	0.114
4	34535.6	1.136	3.63	1.23	0.104
5	36451.64	1.127	13.4	4.81	0.099
6	37015.12	1.133	2.97	1.01	0.097
7	45468.66	1.11	7.6	2.61	0.079
8	53327.23	1.131	8.24	2.83	0.067
9	71084.22	1.116	6.17	2.12	0.05
Average	38555.22	1.117	5.02	1.74	-
Std. Dev.	16105.17	0.021	4.29	1.53	-

Table 6.7 – Microstate properties for the small RVE size of polyimide with AMBER

Microstate	Λ_r (kcal/mole)	Density (g/cc)	Young's modulus (GPa)	Shear modulus (GPa)	p_r
1	15743.83	1.155	4.75	1.63	0.319
2	51174.15	1.042	17.6	6.93	0.098
3	53526.26	1.066	4.51	2.66	0.094
4	55058.21	1.056	-1.17	-0.38	0.091
5	55516.97	1.096	-0.15	-0.05	0.09
6	55557.35	1.096	1.83	0.61	0.09
7	60056.82	1.013	7.73	2.84	0.083
8	75161.14	1.051	7.67	2.76	0.066
9	78308.8	0.989	5.11	1.81	0.064
Average	55567.06	1.063	5.32	2.09	-
Std. Dev.	17786.53	0.049	5.56	2.18	-

Table 6.8 – Microstate properties for the medium-sized RVE of polyimide with
AMBER

Microstate	Λ_r (kcal/mole)	Density (g/cc)	Young's modulus (GPa)	Shear modulus (GPa)	p_r
1	42,788.42	1.16	0.02	0.01	0.233
2	52,780.01	1.16	0.24	0.08	0.189
3	79,859.22	1.14	4.71	1.64	0.125
4	84,264.01	1.12	11.10	4.14	0.118
5	84,682.77	1.11	3.82	1.31	0.118
6	85,469.25	1.11	10.20	3.66	0.116
7	97,465.05	1.14	16.70	6.44	0.102
Average					-
Std. Dev.					-

Table 6.9 – Microstate properties for the large RVE size of polyimide with AMBER

Microstate	Λ_r (kcal/mole)	Density (g/cc)	Young's modulus (GPa)	Shear modulus (GPa)	p_r
1	15452.11	1.177	7.15	2.49	0.403
2	71639.58	1.146	3.88	1.33	0.086
3	75685.3	1.118	1.88	0.636	0.082
4	76987.37	1.139	2.8	0.95	0.08
5	81381.59	1.14	0.97	0.32	0.076
6	84809.88	1.143	7.87	2.79	0.073
7	88712.45	1.089	0.74	0.25	0.07
8	95048.65	1.124	0.98	0.33	0.065
9	101785.9	1.115	6.47	2.27	0.061
Average	76833.65	1.132	3.5	1.22	-
Std. Dev.	24939.49	0.024	3.02	1.06	-

Table 6.10 – Microstate properties for the small RVE size of polyimide with OPLS-AA

Microstate	Λ_r (kcal/mole)	Density (g/cc)	Young's modulus (GPa)	Shear modulus (GPa)	p_r
1	31463.94	1.2746	3.07	1.04	0.17
2	34374.37	1.245	13.4	4.68	0.156
3	50756.19	1.25	1.32	0.44	0.105
4	50985.01	1.228	10.1	3.52	0.105
5	51413.68	1.233	-2.87	-0.94	0.104
6	54828.14	1.251	7.93	2.73	0.097
7	59784.71	1.242	10.5	3.72	0.089
8	60652.94	1.221	3.51	1.19	0.088
9	66368.38	1.174	24.6	10.5	0.08
Average	51180.82	1.235	7.95	2.98	-
Std. Dev.	11614.63	0.027	8.08	3.33	-

Table 6.11 – Microstate properties for the medium-sized RVE of polyimide with OPLS-AA

Microstate	Λ_r (kcal/mole)	Density (g/cc)	Young's modulus (GPa)	Shear modulus (GPa)	p_r
1	32600.76	1.25	12.5	4.36	0.203
2	42839.15	1.256	6.97	2.39	0.154
3	48154.57	1.228	1.18	0.39	0.137
4	62307.69	1.253	6.64	2.27	0.106
5	75285.48	1.212	18.5	6.79	0.088
6	77523.24	1.208	10.4	3.62	0.085
7	78490.9	1.218	0.82	0.29	0.084
8	93697.66	1.202	3.92	1.33	0.07
9	97849.8	1.225	-0.48	-0.16	0.067
Average	67638.81	1.228	6.73	2.36	-
Std. Dev.	22683.84	0.02	6.24	2.26	-

Table 6.12 – Microstate properties for the large RVE size of polyimide with OPLS-AA

Microstate	Λ_r (kcal/mole)	Density (g/cc)	Young's modulus (GPa)	Shear modulus (GPa)	p_r
1	13746.45	1.263	5.1	1.73	0.458
2	58721.58	1.223	-0.17	-0.06	0.107
3	74433.07	1.229	8.59	2.97	0.084
4	79589.23	1.224	1.52	0.51	0.079
5	81744.56	1.2	6.72	2.34	0.077
6	86585.92	1.239	2.74	0.92	0.072
7	93289.68	1.237	1.25	0.42	0.067
8	121395.4	1.206	7.76	2.68	0.051
Average	76188.24	1.228	4.19	1.44	-
Std. Dev.	30923.51	0.019	3.3	1.15	-

Tables 6.1-6.12 summarize the results obtained for each microstate for the two different polymers for OPLS-AA and AMBER force fields. For each microstate, the methodology outlined in Section 6.3 was utilized for homogenization to predict the equivalent-continuum properties. It was found that there was a significant variation in the predicted properties for the various microstates. The deformation response for an entangled polymer system is a consequence of the elaborate molecular chain network. As these microstates sample different conformational space in the molecular models, it is expected that they exhibit a wide range of properties. A previous study also indicated a large variation in the local mechanical properties of amorphous polymers [175]. It was also reported that there was a strong correlation between the size of the simulated model

and the variation in the predicted properties with a wider distribution in properties observed at smaller RVE sizes.

Some predicted microstate mechanical properties for the two polymers in Tables 6.1-6.12 show negative stiffnesses. In general, negative stiffness materials are considered unstable, and assumed not to exist at the bulk level under normal conditions. The current methodology relies on the change in energy of the RVE under applied deformations for evaluation of the equivalent-continuum properties. The energy of the RVE is governed by the force field which is a function of the atomic positions of the constituent atoms and empirical constants. This dependence of the energy of a glassy polymer on atomic coordinates can be understood in terms of the *energy landscape* concept. The energy landscape is a conceptual representation of the potential energy of the molecular system as a function of its constituent atomic coordinates. The energy of the system is altered when any or all of the atomic coordinates are changed. This landscape is sampled during MD simulation and driven by kinetic energy. A molecular structure (microstate) at a local minimum of this landscape represents an equilibrated structure that is energetically stable. When the polymer network is mechanically deformed, the energy landscape of the polymer is altered [179] and a microstate can potentially relax to an adjacent local minimum with energy lower than the pre-deformed state leading to an overall negative change in energy, resulting in an apparent negative stiffness per Equation [6.5]. This is a likely even if a particular microstate is in a rather “shallow” minimum energy valley. Deformation energy can provide an impetus for such a microstate to move to an adjacent local minimum with lower energy.

Recent studies have shown that a large inhomogeneity in amorphous materials can result in localized regions of negative stiffness [175]. It is hypothesized that the interface between the negative and the positive stiffness can be responsible for localized events in amorphous materials [175], such as shear bands in metallic glasses and crazing in polymers. Also, it has been shown that isotropic material with negative stiffness can be

a stable phase in a composite [180]. It has also been reported that composites with negative-stiffness phases can result in extremely high composite stiffnesses [181].

The issue of negative microstate stiffnesses can be handled in two ways: with and without ignoring the microstates that resulted in negative stiffnesses. The results of this study have been analyzed with respect to these two approaches and discussed below.

A. Ignoring Negative Stiffness Microstates

The two methods described in Section 4 were used to estimate the bulk-level properties of the two polymers systems based on the data presented in Tables 6.1-6.12 while disregarding the microstates with negative stiffness. The Young's moduli of the bulk materials calculated as a simple average of the Young's moduli all the simulated microstates is plotted in Figure 6.2. With the exception of polycarbonate with OPLS-AA force field, all the other simulations resulted in decreasing moduli with increasing RVE size. The polycarbonate model with AMBER force field exhibited an asymptotic-like limit as the size of the RVE increased.

Figure 6.3 is a plot of standard deviation (SD) of the Young's modulus as a function of the RVE size. Again, the polycarbonate simulated with the AMBER force field resulted in a decreasing SD with increasing RVE size, indicating a strong trend of convergence to a limit. However, the polycarbonate simulated with the OPLS-AA force field and the polyimide with AMBER exhibited non-monotonic trends in SD with the RVE size. It is expected that increasing the number of microstates further will result in better trends in these cases [175, 178]. However, due to the computational expense, the current study had been restricted to a maximum of nine microstates for each polymer and RVE size.

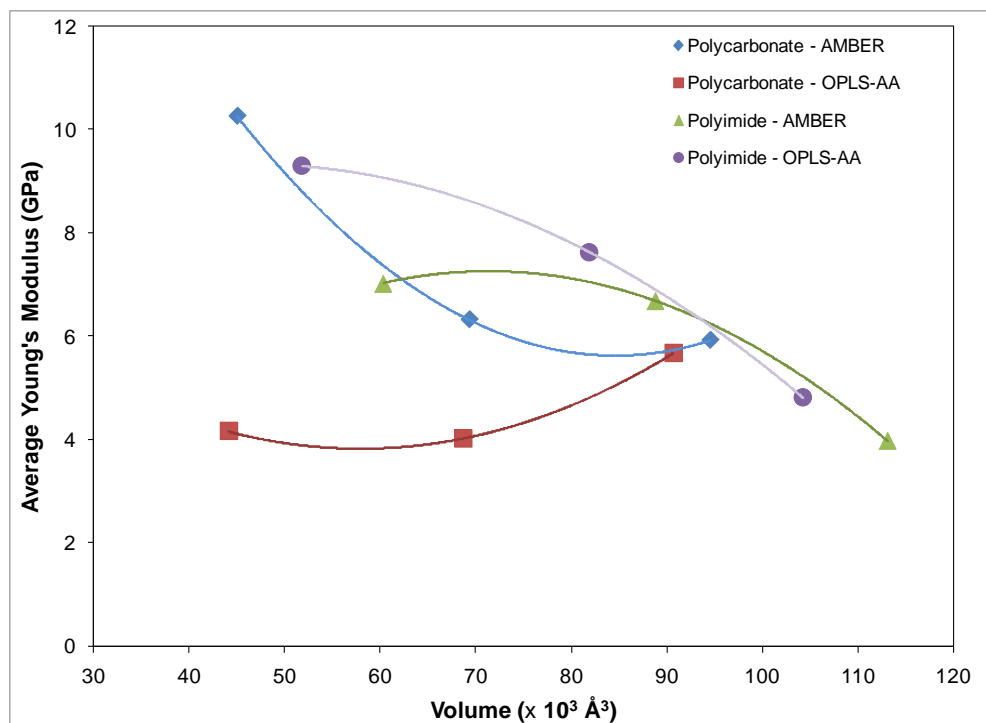


Figure 6.2. Average predicted Young's moduli versus RVE size excluding negative microstate values

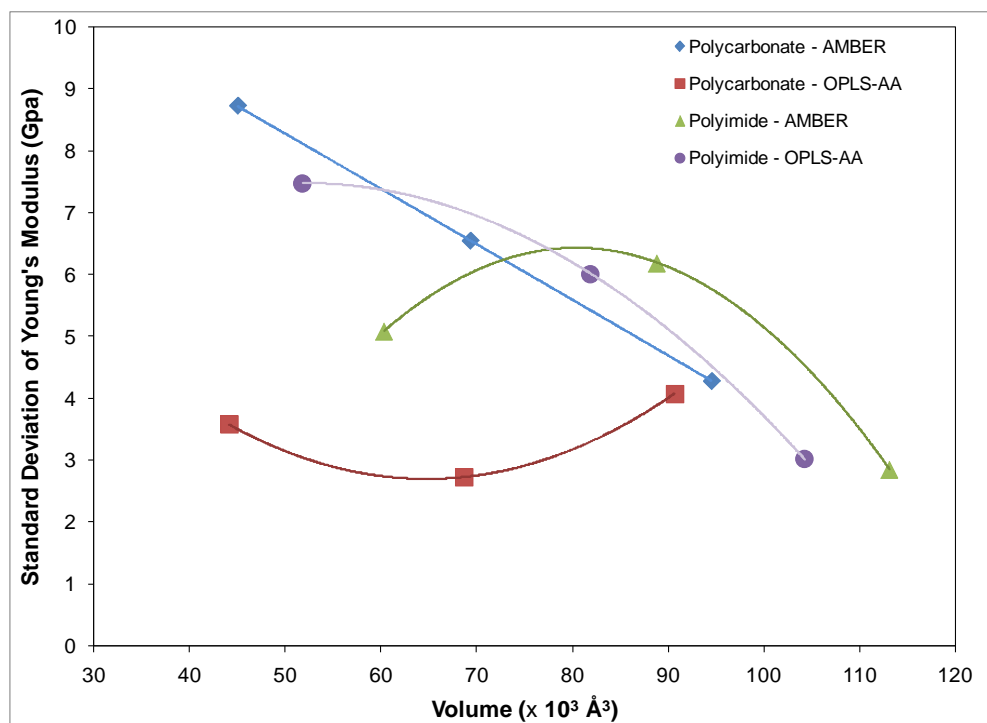


Figure 6.3. Standard deviation of predicted Young's modulus as a function of the RVE size excluding negative microstate values

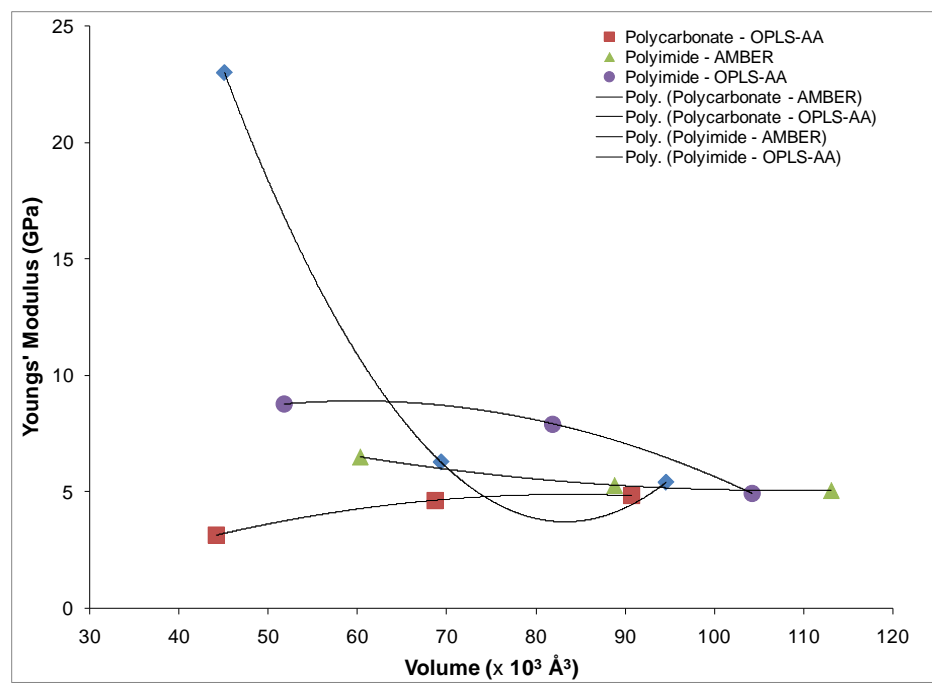


Figure 6.4. Energy-biased weighted average of Young's Modulus versus RVE size excluding negative microstate values

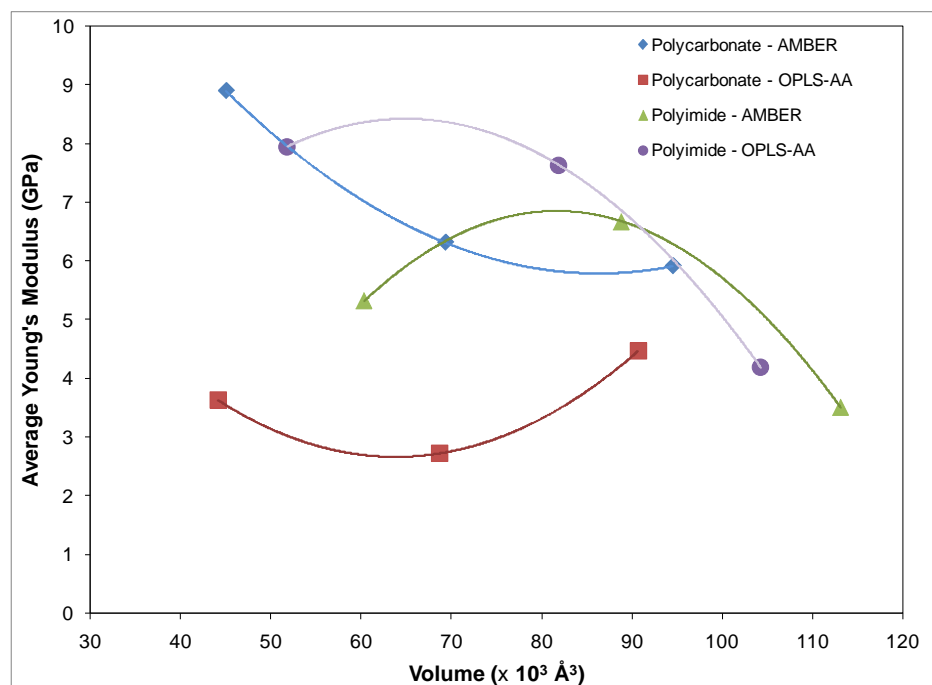


Figure 6.5 Average predicted Young's moduli versus RVE size including negative microstate values

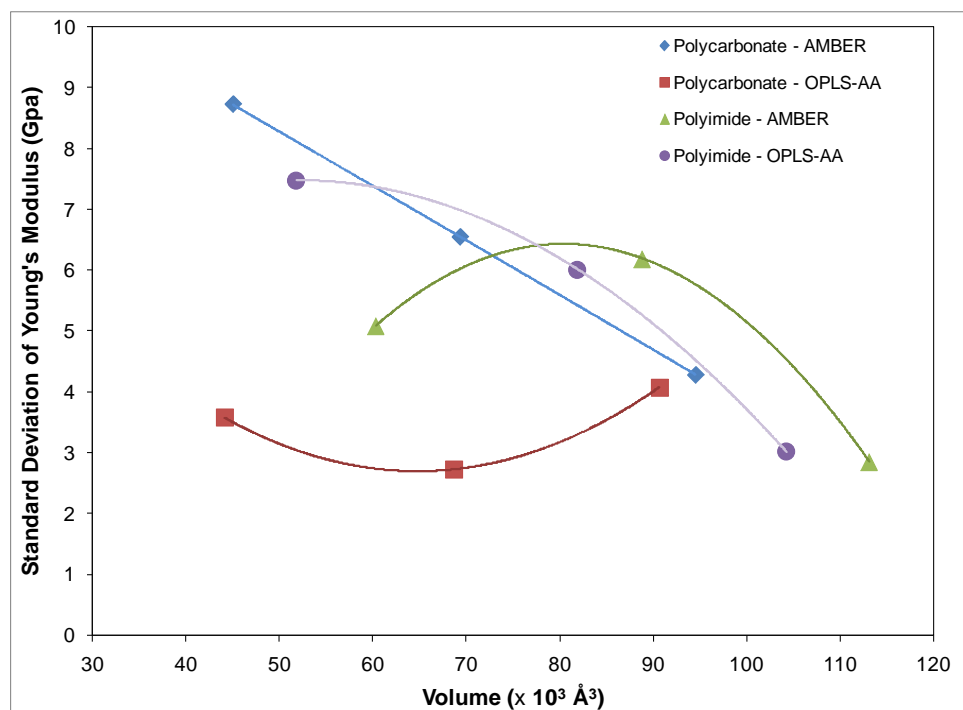


Figure 6.6. Standard deviation of predicted Young's modulus as a function of the RVE size including negative microstate values

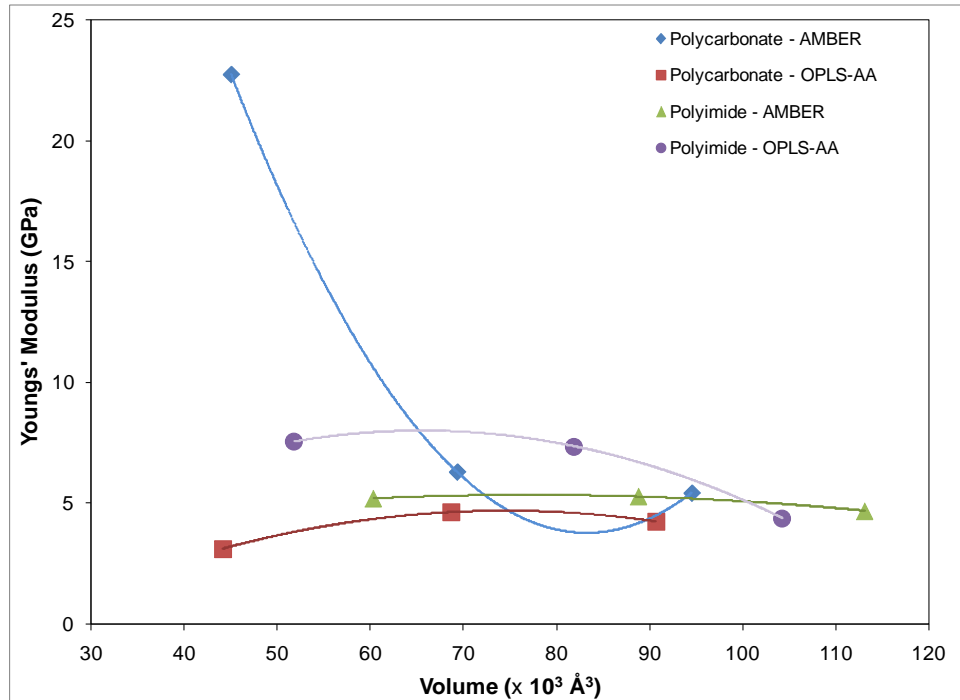


Figure 6.7. Energy-biased weighted average of Young's Modulus versus RVE size excluding negative microstate values

Figure 6.4 shows a plot of the bulk Young's modulus determined with the weighted averages of the microstates. The weighted averages showed a decrease in predicted Young's modulus with increasing RVE size with the exception of polycarbonate with simulated with OPLS-AA. Three of the cases, polycarbonate and polyimide with AMBER and polycarbonate with OPLS-AA, show a strong convergence trend to an asymptotic limit with increase in RVE size. Although an asymptotic trend is not seen in case of polyimide with OPLS-AA, there is a decrease in properties that is approaching the experimental value. It has been experimentally observed [178] that with smaller RVE sizes an increasing variation in the measured strains is observed in response to applied loads. Therefore, it is expected that more conclusive patterns would emerge with the inclusion of more samples.

B. Including Negative Stiffness Microstates

A similar analysis was conducted with the inclusion of the negative-stiffness microstates. Figure 6.5 shows a plot of the average Young's modulus as a function of the RVE size. In the figure, the polycarbonate material simulated with AMBER and polyimide with OPLS-AA show a decrease in the predicted moduli as opposed to the other two cases that exhibit a non-monotonic change. The average modulus values are lower as compared to the corresponding data in Figure 6.2 due to the inclusion of negative stiffness microstates. Figure 6.6 shows the SD in the different cases as a function of the RVE size. The SD of the Young's modulus also follows a similar trend as the averages shown in Figure 6.5, as was observed with the SDs in Figure 6.3 with respect to Figure 6.2. Figure 6.7 shows the energy-biased weighted averages as a function of RVE size. It is found that three of the cases show a strong asymptotic convergence to a limiting value. In case of polyimide with OPLS-AA, there is a decrease in the predicted values with increasing size, however, there is no clear indication of the convergence.

6.6 SUMMARY

MD simulations and micromechanical modeling were used to predict the bulk-level Young's modulus of polycarbonate and polyimide polymer systems as a function of RVE size and force field type. For each of the Young's modulus predictions, the estimate associated with simple averages of the microstate Young's moduli (with SDs) and an energy-biased weighted averaging approach were performed. Additionally, all of these calculations were performed including and excluding negative microstate Young's modulus values for comparative purposes.

The data generally indicate that as the RVE sizes increase, the predicted values of Young's modulus approach the experimental value for both polymer systems and force fields. Also, the SD generally decreases as the RVE size increases for the simple averaging approach. These results are expected since larger RVEs sample a larger portion of the conformational energy space for polymer chain configurations, thus resulting in predicted values that are in more agreement with bulk-level measurements of Young's modulus. Also, the predicted Young's moduli using the energy-biased approach generally show better agreement with experiment than the corresponding values determined by simple averages of microstate properties. This observation is consistent with those previously reported.

The inclusion of negatively-valued microstate Young's moduli in the bulk-level Young's modulus predictions yielded results that are closer to experiment. This conclusion makes physical sense because of the expected presence of such microstates in polymer materials. By including these microstate samples in the bulk-level predictions, more realistic values of bulk Young's modulus are determined. There is no clear influence of force field type (AMBER versus OPLS-AA) on the predicted bulk Young's moduli values for the polymer systems.

This data indicates that accurate predictions of bulk elastic properties of polymers using multiscale modeling approaches require relatively large RVEs for more accurate properties. Although it is unclear how large molecular RVEs need to be for accurate predictions, it is clear that multiple microstates need to be considered for the molecular RVEs of practical size (given normal computational resource limits), and that energy-biased micromechanical predictions provide improved predicted properties over simple microstate property averages.

Chapter 7

Effect of Water

In this chapter, we have applied the multiscale modeling technique developed in the previous chapters to study the effect of water on predicted mechanical properties. Molecular models have not been extensively applied for studying the effect of these parameters. The effect of water was studied through introducing three different weight percentages of moisture in polycarbonate models. It is found that the increase in the water content in the polymer suggests possible expansion of the material. It is also found that the water lowers the mechanical properties of the material when compared to “dry” polymer. This reduction in properties is caused from creation of additional free volume in the material due to expansion that reduces the interaction between adjacent chains leading to a more compliant material.

7.1 INTRODUCTION

Polymers are used in a wide variety of applications and their operating conditions can vary from normal to extremely harsh environment. Most structural polymers are subjected to daylight, moisture and thermal effects that can potentially influence their properties. A number of experimental studies have been reported to study the influence of effects of water on the physical behavior of polymers [182-189]. Many polymer swell in presence of water, along with temperature has been found to cause hygrothermal aging in epoxy based polymers [182, 183]. Phase separation in epoxy networks because of hydrothermal loading was reported [184]. The loss of strength due to hydrolysis of bonds was identified as the main reason for causing the polymer to fail in presence of water [184, 185]. In case of polymer composites, loss of interfacial forces

at the interface is a consequence of swelling in water [184]. An epoxy system of diglycidyl ether of bisphenol F cured with 2-ethyl-4-methyl-imidazole with borosilicate glass adherends and these were treated with different adhesion promoters to generate different interfaces. Adhesive strengths were measured as functions of time in dry and 85% relative humidity conditions and they observed a drop in the strain-energy release rate due to loss of interfacial forces and hydrolysis of siloxane bonds [184]. Another epoxy-based anisotropic conductive film joints was found to be susceptible to moisture absorption when exposed to hygrothermal conditions [183]. Hygrothermal aging was found to increase the polymer's susceptibility to hydrolysis and oxidation which could lead to irreparable damages of the conductive film [183]. Thermoporometry studies on cellophane films by differential scanning calorimetry (DSC) showed a low temperature peak caused by melting of water and this phenomenon is due to Gibbs-Thomson effect (effect of surface energy on melting temperature) [187]. A depression in melting point due to Gibbs-Thomson effect can be used to evaluate the pore size distributions [187].

Hydrogels are network polymers which have three-dimensional structures and generally swell in water. Superporous hydrogels (SPHs) of poly (acrylamide-co-acrylic acid)/polyethylenimine (P (AM-co-AA)/PEI) were used to study the influence of water on their compressive strength [190]. It was found that increasing AA or PEI concentrations decreased the water sorption rate due to the interaction between the PAA and PEI molecules resulting in decrease in pore sizes of SPHs [190]. The maximum swelling ratios were found were observed at 0.4 weight fraction of PAA and with increasing concentration of PEI, mechanical strength of water swollen SPHs increased [190]. A similar study investigated swelling behavior of copolymers varying in composition of their copolymerized monomers (N-isopropylacrylamide and methacrylic acid) as a function of composition, pH and temperature [188].

Molecular dynamics (MD) can help to simulate the presence of water to understand its effects on mechanical properties. Atomistic simulations on the effects of temperature and hydration level of two different polymers- sulfonated poly (thioether sulfone) and Nafion-117 has been reported [189]. It was showed that the polymer system density decreased with increasing hydration level and there was a drop in the glass transition temperature from 320K to 300K over a range of hydration level [189]. This behavior is attributed to the plasticization induced by the water molecules. An increase in the coefficient of thermal expansion with increasing hydration above the glass transition temperature was reported but this was not observed below the glass transition [189]. Multiscale modeling techniques have not been extensively applied for studying the effect of water on elastic properties of polymers. The effect water was studied through introducing different weight percentages of moisture in polycarbonate models. It is found that the increase in the water content in the polymer suggests possible expansion of the material. It is also found that the water lowers the mechanical properties of the material when compared to “dry” polymer. This reduction in properties is caused from creation of additional free volume in the material due to expansion that reduces the interaction between adjacent chains leading to a more compliant material.

7.2 MOLECULAR MODEL

Force fields define interactions in atomistic simulations to relate a specific molecular morphology to the potential energy of the material system. Force fields are generally semi-empirical and allow specific degrees of freedom for a given atomic structure. The total energy of the RVE of a molecular system is obtained as the summation over the energies associated with each degree of freedom. One of the most widely-used force fields, AMBER, implemented as AMBER99 in the Tinker software package[106] was utilized for this study. A total of seven RVEs were prepared for the four different molecular models, 0 wt. %, 3.6 wt. %, 7.2 wt. % and 14.4 wt. % of moisture respectively. All RVE structures for 0 wt. % were prepared initially in a gas-like phase

with extremely low densities. Energy minimization simulations with periodic boundary conditions were conducted at gradually-increasing densities. The MINIMIZE [119] and NEWTON [141] subroutines of the TINKER [106, 142] modeling package were used for the energy minimization, which correspond to a quasi-Newton L-BFGS method and a truncated Newton energy minimization methods, respectively. The minimizations were performed to RMS gradients of 1×10^{-2} and 1×10^{-5} kcal/mole/Å, respectively. After obtaining the seven “dry” polymer structures predetermined number of water molecules were randomly added to the “dry” RVE to obtain the different “wet” RVEs with three distinct weight percentage of water. The potential parameters for the water molecules were chosen from the TIP3 model as implemented in TINKER.

Once the RVEs were established with the approximately solid-like density, a series of MD simulations were used to establish thermally-equilibrated solid structures in the following order at 300 K: (1) a 50 ps simulation with the NVT (constant number of atoms, volume, and temperature) ensemble to prepare the structure for further equilibration, (2) a 100 ps simulation with the NPT (constant number of atoms, pressure, and temperature) ensemble at 100 atm to evolve the system to higher densities as the structure was prepared from a low density structure, (3) a 100 ps NPT simulation at 1atm to reduce the effects of high-pressure simulations and to let the system evolve to a state of minimal residual stresses, and (4) a 100 ps NVT simulation to allow the system to equilibrate at the simulated temperature and density for a specific microstate. The DYANAMIC subroutine of the TINKER modeling package was used for the MD simulations with periodic boundary conditions. Periodic boundary conditions were employed.

7.3 EQUIVALENT CONTINUUM PROPERTIES

To relate the molecular structure of the microstates of the polymer systems to their corresponding bulk mechanical properties, an equivalent-continuum modeling approach

was used as described in Chapter 3 that effectively represents the mechanical behavior of the molecular RVEs. Because the molecular structures of the polymers were completely amorphous, it was assumed that the equivalent-continuum constitutive equation for the microstates exhibited isotropic symmetry. Based on this material symmetry for the equivalent continuum, a hyperelastic continuum constitutive relation [67] was used to model the deformation characteristics of the discrete molecular models. The elastic properties for each microstate were determined as described in detail elsewhere [67].

The operational temperature of most engineering polymers is much below the glass transition temperature, and thus many polymers are in a glassy state. It is expected that the approach described in the previous chapters will generally yield different predicted properties for different RVEs (for a given RVE size) [162, 176]. The bulk polymer elastic behavior of the polymer system is assumed to be cumulative response of the various microstates and is determined using two different methods: simple averaging and a physically-motivated weighted-averaging scheme. The details of this method are described in detail elsewhere [162, 176].

7.4 RESULTS AND DISCUSSIONS

Tables 7.1-7.4 summarize the results for the polycarbonate with different water weight percentage. The average potential energy of the molecular models decreases from 29,519 kcal/mol for “dry” polymer to 29,051 kcal/mol for ~14 % water model. However, the number of atoms increased from 5958 atoms to 7062 atoms. It should also be noted that although the average density for the polymer from Tables 7.1-7.3 ~ 1.1 g/cc, the standard deviation continually decrease for these polycarbonate models. From Table 7.4 we can see that there is a definite decrease in the density, it can be concluded that the density of the polycarbonate is decreasing with increase in water content leading to swelling of polymer chains. This not very evident from Tables 7.1-7.3 as the

density fluctuations are a consequence of the finite size of the molecular models and have overlapping density range that makes it difficult to discern a clear trend until ~7% water model. Also, the data presented in Tables 7.1-7.4 represent a snapshot of the trajectory of the simulated system. Upon, further increase of the water content the density drop is more than the fluctuation in density that it exhibits distinguishable decrease. The decrease in density can be indirectly confirmed from the potential energy of the system. The potential energy of the polymer models were compared for each degree of freedom as the water was added to these models, the intermolecular interaction energy monotonically decreases with increase of water content which is a consequence of increased free volume in the material caused by swelling of the polymer chain due to hydration.

The elastic properties are calculated using the procedure described in the previous sections. It is known that a amorphous material system comprised of polymer chains has a complex potential “energy landscape” [191]. The choice of the local minimum of the potential energy surface influences the calculated mechanical properties. MD evolves the system under the influence of the interaction forces to sample the “phase space” accessible to the material system. The current procedure relies on the static minimum energy morphology to calculate the mechanical properties. The kinetic energy provides the impetus to sample this localized “phase space” accessible to the material that governs the predicted properties which leads to the fluctuation in properties [175], also in each model the presence of water molecules can influence the predicted moduli due to the swelling induced by them. The negative moduli predicted in the current study are expected and have been shown in previous studies [175, 180, 181, 192]. The addition of water has a stark effect on the elastic properties. It can be seen from Tables 7.1-7.4 that there is a sudden drop in the average predicted modulus of the polymeric material. However, the influence of increase in the water content beyond ~3.6 % of water by weight does not show profound changes in the properties. There is an apparent increase in predicted modulus from 3.6 % to 7.2 % of water weight. This increase is within the

scatter of the properties from the two cases and is expected to show better trend with increase in the number of microstates considered in the modeling methodology. MD simulations are computationally exhaustive; the choice of the limited number of “microstates” used in the current study is intended for efficiency. It has been shown that a limited number of microstates are capable of capturing the salient features of polymer physical behavior [67, 162, 176, 192]. It can be inferred from the data that there is a sudden drop in the properties of the polymer with the addition of water and its effect on mechanical properties is saturated at ~3.6 % of water by weight. However, the swelling of polycarbonate is observed with increase in water content within the range studied.

7.5 SUMMARY

In summary, we applied a multiscale modeling technique to study the influence of water on polymer materials. The influence of water on the mechanical properties of a hydrophobic polycarbonate material was studied. It can be concluded that the addition of water results in swelling of the polymer and leads to lowering of the interaction forces within the material. This mechanism can explain the reduction in the mechanical properties with introduction of water.

Table 7.1 Properties of Polycarbonate without water

Microstate	Λ_r (kcal/mole)	Density (g/cc)	Young's modulus (GPa)	Shear modulus (GPa)	p_r
1	13706.69	1.09	2.29	0.78	0.22
2	13722.27	1.12	5.14	1.77	0.22
3	15905.74	1.07	2.01	0.68	0.19
4	18093.05	1.11	12.0	4.21	0.16
5	38850.61	1.12	5.69	1.95	0.08
6	50629.76	1.09	7.08	2.44	0.06
7	55728.7	1.03	1.65	0.56	0.05
Average	29519.54	1.1	5.12	1.77	-
Std. Dev.	18417.06954	0.03	3.68	1.3	-

Table 7.2 Properties of Polycarbonate with ~ 3.6 % water by weight

Microstate	Λ_r (kcal/mole)	Density (g/cc)	Young's modulus (GPa)	Shear modulus (GPa)	p_r
1	13568.68	1.13	0.3	0.1	0.22
2	13577.01	1.1	1.52	0.51	0.22
3	15724.98	1.09	1.61	0.54	0.19
4	17925.99	1.12	1.82	0.61	0.17
5	38626.05	1.13	1.76	0.6	0.08
6	50422.53	1.12	5.18	1.77	0.06
7	55471.52	1.04	5.56	1.91	0.05
Average	29330.97	1.1	2.54	0.86	-
Std. Dev.	17014.34	0.02	2.01	0.68	-

Table 7.3 Properties of Polycarbonate with ~ 7.2 % water by weight

Microstate	Λ_r (kcal/mole)	Density (g/cc)	Young's modulus (GPa)	Shear modulus (GPa)	p_r
1	13451.5	1.09	8.47	2.94	0.22
2	13463.56	1.08	4.14	1.41	0.22
3	15603.45	1.08	-0.13	-0.04	0.19
4	17814.85	1.11	-0.24	-0.08	0.17
5	38523.96	1.1	-0.26	-0.08	0.08
6	50331.92	1.09	3.83	1.3	0.06
7	55318.93	1.06	11.2	4.00	0.05
Average	29215.46	1.09	3.86	1.35	-
Std. Dev.	17011.88	0.015	4.56	1.61	-

Table 7.4 Properties of Polycarbonate with ~ 14.5 % water by weight

Microstate	Λ_r (kcal/mole)	Density (g/cc)	Young's modulus (GPa)	Shear modulus (GPa)	p_r
1	13268.04	0.96	0.19	0.06	0.22
2	13290.19	0.97	1.58	0.53	0.22
3	15492.62	0.95	2.45	0.83	0.19
4	17655.37	0.95	5.19	1.81	0.17
5	38384.58	0.94	3.19	1.12	0.08
6	50133.55	0.97	-0.44	-0.14	0.06
7	55138.09	0.93	7.01	2.61	0.05
Average	29051.77	0.95	2.74	0.97	-
Std. Dev.	17001.35	0.01	2.66	0.9	-

Chapter 8

Summary and Conclusions

Materials are inherently multi-scale in nature consisting of distinct characteristics at various length scales from atoms to bulk material. There are no widely accepted predictive multi-scale modeling techniques that span from atomic level to bulk relating the effects of the structure at the nanometer (10^{-9} meter) on macro-scale properties. Traditional engineering deals with treating matter as continuous with no internal structure. In contrast to engineers, physicists have dealt with matter in its discrete structure at small length scales to understand fundamental behavior of materials. Multiscale modeling is of great scientific and technical importance as it can aid in designing novel materials that will enable us to tailor properties specific to an application like multi-functional materials.

Polymer nanocomposite materials have the potential to provide significant increases in specific strength-to-weight and stiffness-to-weight ratios relative to current polymers used for engineering applications. The nanoscale reinforcements have the potential to increase the effective interface between the reinforcement and the matrix by orders of magnitude for a given reinforcement volume fraction as relative to micro- or macro-scale reinforcements. To facilitate the development of polymer nanocomposite materials, predictive constitutive relationships must be established for bulk mechanical properties of the materials as a function of the molecular structure. A computational hierarchical multiscale modeling technique is developed to study the bulk-level constitutive behavior of polymeric materials as a function of its molecular chemistry. Various parameters and modeling techniques from molecular dynamics to continuum mechanics were utilized for the current modeling method. The cause and effect relationship of the parameters are studied to establish an efficient modeling framework.

The proposed methodology is applied to three different polymers and validated using experimental data available in literature.

8.1 HYPERELASTIC CONTINUUM MODELING

In this study, a combined atomistic-hyperelastic multiscale modeling technique, based on the Equivalent-Continuum Model, was developed and used to predict elastic properties of thermoplastic polymers. A continuum hyperelastic model was formulated with a strain-energy potential function that had a functional form based on molecular simulation predictions. This method was applied to polycarbonate, and polyimide polymer systems. A set of widely used fully atomistic force fields namely AMBER, OPLS-AA, and MM3 were used for molecular simulations. Both static and dynamic molecular simulations were performed using Molecular Mechanics and Molecular Dynamics simulation techniques, respectively. The predicted bulk properties of the polymers using the three force fields were compared to experimentally-measured values.

A. Static versus Dynamic Simulation

The predicted values of Young's and shear moduli for the two polymers indicates that the static simulations predicted mechanical properties that are lower than those predicted by the dynamic simulations, with the properties from static simulations closer to the experimental properties than the properties from the dynamic simulations.

The results also indicate that the scatter in the data from the dynamic simulations is much greater than that from the static simulations and therefore there is a greater chance of the dynamic simulations yielding predicted mechanical properties that are less accurate than those from the static simulations (when comparing to the experiment). It

is expected that with dynamic simulations of larger molecular systems when run for longer simulation times, the scatter would generally decrease.

The mechanical relaxation of the polymer chains that occurs in the experiments and in the static simulations is not expected to be accurately accounted for in the dynamic simulations. Polymers generally behave in a viscoelastic manner when subjected to applied deformations because of the time-dependent response of polymer-chain sliding and chain-torsional motions. It is speculated that the strain rates were small enough that relaxation time for the constituent chains are of the same order at which the specimens were deformed, thus reducing the resultant stress on the specimen. In the static simulations, energy minimizations are performed that mimic the relaxation mechanisms of a deformed polymer; conversely, in the dynamic simulations, the time scale is on the order of picoseconds, which is not long enough to allow for significant mechanical relaxation [193]. Therefore, the strain-energy density is much higher for a given deformation in the dynamic simulations relative to the static simulations, and the corresponding constitutive equations will predict higher stresses for a given applied deformation. As a result, the predicted elastic material properties from the dynamic simulations are greater than those from the static simulations and the experiments.

B. Force Field Comparisons

The predicted moduli from the static simulations are larger than those from experiment for the AMBER force field, and are smaller than the experimental values for the OPLS-AA and MM3 force fields. The relatively low predicted elastic properties from the OPLS-AA force field are likely a direct result of the lower simulated polymer densities because it is expected that higher elastic constants would result from simulations of denser materials. The functional forms of the AMBER and OPLS-AA force fields, from Equations (A.1) to (A.10), are nearly identical. The differences in the two force fields (as used in this study) are the presence of electrostatic interactions in the OPLS-

AA force field and the differences in the force constant parameters, particularly for the torsions. These differences result in the significantly different predicted densities for both polymer systems. The lower predicted properties of the MM3 static simulations cannot be attributed to the same effect because the simulated material densities were close to the expected values. The functional form of the MM3 force field from Equations (A.11) - (A.18) attempts to account for a wider range of behavior than those of the AMBER and OPLS-AA force fields. However, because the predicted properties using the MM3 force field in static simulations are farther from the experimental properties than those predicted with the AMBER and OPLS-AA force fields, the more complex functional form does not predict properties as accurately as the more simple functional forms of AMBER and OPLS-AA for the polymer systems used in this study.

The relatively high predicted mechanical properties from the static simulations with the AMBER force field follow a trend that has been observed in the literature. Previous studies [92, 125] have pointed out that the predicted mechanical properties from molecular simulations are expected to be 50 - 100% larger than those obtained from experiments. In the current study, the predicted properties from the AMBER force field were 70 - 115% higher than experiment. Most likely, this difference can be attributed to the fact that the RVEs in molecular modeling simulations represent a nearly perfect molecular structure, whereas, in the actual experimental test specimens, the material contains low volume fractions of air pockets, inclusions, and unreacted monomers. Therefore, it is expected that simulated mechanical properties should be larger than experimentally-obtained properties if the polymer system imperfections are not included in the molecular modeling. It is also expected that the computational modeling of these imperfections in these polymer systems would yield predicted properties that are closer to the experiment than those predicted in the current study. From this perspective, for the polymer systems investigated in this study, the AMBER force field appears to be more accurate than the OPLS-AA and MM3 force fields for predicting elastic properties.

8.2 STATISTICS-BASED MICROMECHANICS APPROACH

Unlike crystalline materials, amorphous polymer materials contain an elaborate network of molecular chains with highly-complex and irregular conformations that dictate the bulk mechanical properties. Many combinations of the conformations of multiple polymer chains are possible for a particular representative volume element (RVE) in an equilibrated or non-equilibrated state because of the finite entropy of the material for any temperature above 0 K owing to the dynamics of the constituent chains. As a result, the molecular structure, and thus density, of a polymer material varies substantially on the nanometer length-scale. The large number of possible conformations for a specific volume of a polymer material constitutes a conformation space. Each combination of chain conformations in a RVE has an associated potential energy which can be interpreted as an energy landscape that depends on the conformational state of the polymer network. The conformational space does not necessarily have a one-to-one correspondence to the energy landscape. Therefore, the energy landscape generally consists of multiple local minima. As a result, for a RVE consisting of a finite number of polymer chains, there can exist multiple locally-equilibrated states.

A majority of high performance polymer-based materials operate at temperatures much below their glass transition temperatures. An amorphous polymeric material in a glassy state can be envisioned as a super-cooled liquid that is “frozen” in a local potential energy equilibrium state, which is not necessarily a globally-minimized potential energy state. The different microstates that are not at the global-minimum energy state are essentially “frozen” states with exceptionally long relaxation times as the energy barriers to cross over to the global minimum energy state in are generally very high. Therefore, the bulk material behavior can be imagined to be an average response from all the available conformational microstates. In order to accurately predict the bulk-level

behavior of polymer-based systems based on molecular structure, a range of conformational microstates of a polymeric network must be included in multiscale constitutive modeling approaches. In this study, a multiscale modeling technique is used to predict the bulk elastic moduli of a polyimide and a polycarbonate material system using multiple conformational states. and establish statistical bounds of the predicted moduli are subsequently established. Physically-motivated statistically weighting of properties obtained from individual microstates for each polymer was incorporated into the modeling approach. It was found that the established bounds included experimentally-measured values of moduli for these materials. The framework of modeling presented here is very adaptable and can be extended to include any bulk physical property for an amorphous polymer material.

The bulk elastic properties of a polyimide system and a polycarbonate polymer have been predicted based on the molecular structure of several microstate representative volume elements whose cubic side dimensions are on the order of a few nanometers. A micromechanical approach has been used to predict the bulk properties based on the predicted mechanical response of each microstate for both polymer systems. The theoretical bounds of possible predicted properties have also been established. The results indicate that individual microstates can have a wide range of Young's moduli, differing by as much as 16.7 GPa for the polyimide and 21.8 GPa for the polycarbonate. These differences are a factor of 4 and 10, respectively, higher than the experimentally-obtained values of Young's modulus from the literature. On the other hand, using the proposed statistics-based modeling approach has yield predicted bulk Young's modulus values that are higher than the experimental values by a factor of 1 to 3, depending on the assumed probability distribution function. Therefore, the consideration of multiple microstates for a polymer is necessary for the multiscale prediction of elastic properties based on molecular structure.

Although the predicted Young's moduli of both polymers systems are higher than the experimental values for all three distribution functions proposed, an over-prediction of elastic properties is expected for two reasons. First, the molecular systems modeled in the current study represent polymer structures without any chain length distribution and unreacted monomer, both of which are expected to reduce the overall elastic properties of a polymer. Therefore, the predicted properties from these models are expected to be higher than those experimentally-observed in the laboratory. Second, the proposed micromechanics model functional form is a simple rule-of-mixtures formulation. The form of the model is identical with the upper-bound of possible elastic properties. Therefore, a more realistic, and possibly more complex, micromechanics model will likely predict bulk Young's modulus values that are closer to experiment than those presented herein.

8.3 EFFECTS OF TEMPERATURE

The effects of temperature on the predicted mechanical properties of an amorphous polyimide (LaRC-CP2) have been investigated. A multiscale constitutive modeling approach was used to evaluate the equivalent-continuum properties of the modeled polyimide over a series of temperatures ranging from 73K to experimentally measured glass transition temperature. The resulting mechanical properties have been compared to experimentally-obtained properties. The predicted moduli did not show the expected temperature dependence and the sudden change at the glass transition temperature. The lack of expected trends in the results is discussed in the context of the mechanism proposed by three widely accepted theories of glass transition phenomenon and energy landscape interpretation of MD simulation.

The lack of definite trends in predicted properties of LaRC-CP2 when compared to the experimental values of mechanical properties. The temperature dependence of physical

properties can be explained using different theories. Although most of these theories were initially proposed for explaining the glass transition phenomenon in polymers, they are also well-suited to explain the trends in other physical properties. These theories can be broadly classified into free volume theories, kinetic theories, and thermodynamic theories. Free volume theory assumes that a small fraction of the polymer is empty (not occupied by polymer molecules) which plays a large role in the temperature-dependent behavior of polymers. The glassy state of a polymer is governed by very limited molecular mobility a consequence of an iso-free volume state. The kinetic theories propose that the temperature-dependent behavior is entirely governed by the polymer chain kinetics and its response time when compared to the experimental time scales.

Thermodynamic theories have been established to explain the entropy “Kauzmann” paradox. The Kauzmann paradox states that for a supercooled liquid below a critical temperature, the liquid has lower entropy than the corresponding solid at the same temperature. This gives rise to the Gibbs-DiMarzio theory which states that there is a phase transition that occurs above that critical temperature at which the configurational entropy of a polymer network goes to zero leading to a glassy phase. From these three different theories, it is clear that there is no general agreement on the physical basis of the glass transition behavior of polymers. Furthermore, the applicability of these theories to molecular modeling has not been fully explored. Thermodynamic theories are not easily usable with molecular simulations as they require complete knowledge of entropy of the system, which involved extensive sampling of the energy landscape making it computationally cumbersome. The kinetic theory mechanism in the context of classical MD relies on the time scale of the simulation which poses a severe restriction on its application with the current methodology. Therefore, there is currently no definite physics-based approach to modeling the glass transition effects of polymer materials using molecular simulations. However, what is clear from these theories is that as the temperature of a polymer increases, the mobility of the molecular chains also increases,

which results in a rapid change in the properties at the glass transition temperature. These effects are not properly accounted for in currently-used force fields (e.g. AMBER). Thus, a definite trend between properties and temperatures is not expected, and not observed, in Table 5.1.

An efficient and accurate approach to modeling the effect of temperature on the mechanical response of a molecular RVE using molecular simulations is needed. This approach must account for the increased mobility of polymer molecules near the glass transition temperature. The increase in polymer chain mobility, or the increase in the RVE size as a function of temperature, is not accounted for in simple state-of-the-art force fields that are used to predict the properties of large polymer systems.

8.4 INFLUENCE OF REPRESENTATIVE VOLUME ELEMENT (RVE) SIZE

RVEs have been extensively used in the constitutive modeling of both crystalline and amorphous materials. However, central to this methodology is the choice of the RVE that can accurately capture the material's bulk-scale mechanical behavior. The optimal choice of an RVE for an amorphous nanostructured material remains a challenge. Although traditional methodologies have been applied to continuous materials, selection of nanometer-sized RVEs for discrete polymer structures has not been rigorously addressed. A multiscale modeling approach has been recently developed to account for a range of conformational microstates of a polymeric network must be accounted for.

The mechanical response of polymers is a consequence of the entanglement of the constituent molecular chains. The entangled network of a finite number of chains can only sample a small portion of the conformational space of the bulk polymer. As a result, the physical properties of a polymer can vary substantially on the nanometer length-scale. Similarly, the RVE size can influence the predicted mechanical properties

of a polymer using multiscale modeling techniques. Increasing the RVE size of a modeled polymer establishes predicted physical properties over a larger conformational space. The effect of the molecular RVE size on predicted polymer properties in multiscale models of polymers has been investigated.

MD simulations and micromechanical modeling were used to predict the bulk-level Young's modulus of polycarbonate and polyimide polymer systems as a function of RVE size and force field type. For each of the Young's modulus predictions, the estimate associated with simple averages of the microstate Young's moduli (with SDs) and an energy-biased weighted averaging approach were performed. Additionally, all of these calculations were performed including and excluding negative microstate Young's modulus values for comparative purposes.

The data generally indicate that as the RVE sizes increase, the predicted values of Young's modulus approach the experimental value for both polymer systems with AMBER force fields. Also, the SD generally decreases as the RVE size increases for the simple averaging approach. These results are expected since larger RVEs sample a larger portion of the conformational energy space for polymer chain configurations, thus resulting in predicted values that are in more agreement with bulk-level measurements of Young's modulus. Also, the predicted Young's moduli using the energy-biased approach generally show better agreement with experiment than the corresponding values determined by simple averages of microstate properties. This observation is consistent with those reported in Chapter 4.

The inclusion of negatively-valued microstate Young's moduli in the bulk-level Young's modulus predictions yielded results that are closer to experiment. This conclusion makes physical sense because of the expected presence of such microstates in polymer materials. By including these microstate samples in the bulk-level predictions, more realistic values of bulk Young's modulus are determined.

This data indicates that accurate predictions of bulk elastic properties of polymers using multiscale modeling approaches require relatively large RVEs for more accurate properties. Although it is unclear how large molecular RVEs need to be for accurate predictions, it is clear that multiple microstates need to be considered for the molecular RVEs of practical size (given normal computational resource limits), and that energy-biased micromechanical predictions provide improved predicted properties over simple microstate property averages.

8.5 EFFECTS OF WATER

We have applied the multiscale modeling technique developed in the previous chapters to study the effect of water on predicted mechanical properties. Molecular models have not been extensively applied for studying the effect of these parameters. The effect of water was studied through introducing three different weight percentages of moisture in polycarbonate models. It is found that the increase in the water content in the polymer suggests possible expansion of the material. It is also found that the water lowers the mechanical properties of the material when compared to “dry” polymer. This reduction in properties is caused from creation of additional free volume in the material due to expansion that reduces the interaction between adjacent chains leading to a more compliant material.

8.6 CONCLUDING REMARKS

A computational framework was developed to predict mechanical constitutive behavior of polymeric materials. The effects of the modeling parameters, including; force fields, simulation methods (MD & MM), conformational sampling, RVE size and temperature were studied. An efficient modeling routine was developed and applied to predict mechanical properties of a simple material system (pure polymer) as a function of their

molecular structure. This methodology was also validated using experimental data available in the literature on the modeled materials.

Chapter 9

Recommendations

The current research has developed a basic predictive model for constitutive response of a nanostructured polymer based material. Also, the current framework lends itself conducive for application to reinforced composite and the influence of the interface in the ultimate properties of the composite material. The influence of the interface modification and its effect on the composite properties can be studied for various situations such as chemical and non-chemical interaction between the constituent phases. This method can also be extended to predicting other physical properties beyond deformation response.

9.1 HIGHER ORDER AND NON-LOCAL CONTINUUM THEORIES

Classical continuum mechanics was used for constitutive modeling of the mechanical behavior of polymers. The scale of interactions of the constituent phases in nanocomposites is of the order of a few nanometers and highly non-linear at the lengths involved. The current study has shown that a hierarchical multiscale modeling approach involving computational chemistry and continuum mechanics can help predict constitutive behavior of polymer nanocomposites without the need for assumption of continuum. However, classical continuum theories provide only translational degrees of freedom; the use of higher order theories can alleviate the problems associated with reduced degrees of freedom compared to atomistic models. The homogenization can be applied in the confines of certain approximations.

Microcontinuum theories generally allow for a more complex description of material than allowed under the construct of classical continuum theory. Micromorphic theory

allows for the possibility of an internal structure within material and non-local continuum theory allows accounting for long-range interactions that are generally implemented through pair interactions in atomistic simulations.

9.2 IMPROVED ALGORITHMS

Molecular dynamics is a very computationally intensive technique which restricts the size of the model and the length of simulations time. New algorithms and methods have been proposed recently that provide gains over the traditionally algorithms. These methods employ various techniques to speed up the MD simulation process; conventional truncation methods, cutoff, advanced integration schemes and multiple time stepping, multipole methods, well as the grid and Ewald summation methods.

9.3 COARSE-GRAINED MODELS

Atomistic models such as the ones used in the current study account for interactions between the constituent chemical species in extreme detail. However, such a detail has a definite computational overhead that restricts the size and length of time for which the system can be simulated. This obstacle can be overcome by the use of coarse-grained models that lump a group of atoms to a pseudo-atom creating a reduced representation where possible, thereby reducing the number of degrees of freedom compared to the fully atomistic description. These pseudo-atoms are then treated similar to atoms in a fully atomistic simulation and can possess similar degrees of freedom as an atom. This method also has an advantage of larger time increments while simulating the system dynamically. It is not fully understood if coarse-grained models are capable of predicting the constitutive response as efficiently as fully atomistic models.

9.4 POLYMER MODELING

Real polymers are comprised of an elaborate complex network that is critical to their mechanical behavior. Polymer molecular models can be prepared from in a number of ways. Most of the methods assume the existence of polymer chains and focus on the assembling of these chains to form a network of chains that resemble a real polymer entanglement. These methods do not do on the kinetics of an actual polymerization process or the growth mechanism of the chains. A stochastic process that can emulate the reaction kinetics and information on the yield of a particular process is capable of producing thermodynamically sound models.

9.5 TEMPERATURE EFFECTS

Polymers exhibit interesting changes properties with temperature with marked changes occurring around a characteristic temperature known as the glass transition temperature. However, due to their glassy behavior characterized by a rough “energy landscape”, such transitions are difficult to simulate. During an MD simulation the system samples the portions of the energy landscape that are accessible due to the kinetic energy of the system. In the presence of high energy barriers in glasses a system is trapped in a potential energy minimum that hinders it from undergoing a transition. Some methods such as “mode-coupling theory” employ study of correlation in time that is indicative of transition in a molecular system. Other methods include techniques analogous to “transition path sampling” that rely on a stochastic process to move to different areas of the “energy landscape” where the transition are likely.

References

1. Feynman, R.P., *There's Plenty of Room at the Bottom - An Invitation to Enter a New Field of Physics in Engineering & Science*, 1960, California Institute of Technology
2. (NMAB), N.M.A.B. and E.a.P.S. (DEPS), *Materials Research to Meet 21st Century Defense Needs*. 2003.
3. Kroto, H.W., et al., *C-60 - Buckminsterfullerene*. Nature, 1985. **318**(6042): p. 162-163.
4. Iijima, S., *Helical Microtubules of Graphitic Carbon*. Nature, 1991. **354**(6348): p. 56-58.
5. Treacy, M.M.J., T.W. Ebbesen, and J.M. Gibson, *Exceptionally high Young's modulus observed for individual carbon nanotubes*. Nature, 1996. **381**(6584): p. 678-680.
6. Qian, D., et al., *Load transfer and deformation mechanisms in carbon nanotube-polystyrene composites*. Applied Physics Letters, 2000. **76**(20): p. 2868-2870.
7. Chou, T.-W., *Microstructural Design of Fiber Composites*. 1992: Cambridge University Press.
8. Spaepen, F. and D. Turnbull, *A Mechanism for the Flow and Fracture of Metallic Glasses*. Scripta Metallurgica, 1974. **8**: p. 563.
9. Ahn, S.H., et al., *Mechanical properties of silica nanoparticle reinforced poly(ethylene 2, 6-naphthalate)*. Macromolecular Research, 2004. **12**(3): p. 293-302.
10. Kojima, Y., et al., *Mechanical-Properties of Nylon 6-Clay Hybrid*. Journal of Materials Research, 1993. **8**(5): p. 1185-1189.
11. Usuki, A., et al., *Synthesis of Nylon 6-Clay Hybrid*. Journal of Materials Research, 1993. **8**(5): p. 1179-1184.

12. Huang, W., et al., *Attaching Proteins to Carbon Nanotubes via Diimide-Activated Amidation*. Nano Lett., 2002. **2**(4): p. 311-314.
13. Velasco-Santos, C., et al., *Chemical functionalization of carbon nanotubes through an organosilane*. Nanotechnology, 2002. **13**(4): p. 495-498.
14. Banerjee, S. and S.S. Wong, *Structural Characterization, Optical Properties, and Improved Solubility of Carbon Nanotubes Functionalized with Wilkinson's Catalyst*. Journal of American Chemical Society, 2002. **124**(30): p. 8940-8948.
15. Sinnott, S.B., *Chemical functionalization of carbon nanotubes*. Journal of Nanoscience and Nanotechnology, 2002. **2**(2): p. 113-123.
16. Frankland, S.J.V., et al., *Molecular Simulation of the Influence of Chemical Cross-Links on the Shear Strength of Carbon Nanotube-Polymer Interfaces*. Journal of Physical Chemistry B, 2002. **106**(12): p. 3046-3048.
17. Hu, Y., I. Jang, and S.B. Sinnott, *Modification of Carbon Nanotube-Polystyrene Matrix Composites Through Polyatomic-Ion Beam Deposition: Prediction from Molecular Dynamics Simulations*. Composites Science and Technology, 2003. **63**(11): p. 1663-1669.
18. Hu, Y.H. and S.B. Sinnott, *Molecular Dynamics Simulations of Polyatomic-Ion Beam Deposition-Induced Chemical Modification of Carbon Nanotube/Polymer Composites*. Journal of Materials Chemistry, 2004. **14**(4): p. 719-729.
19. Chen, X.L. and Y.J. Liu, *Square representative volume elements for evaluating the effective material properties of carbon nanotube-based composites*. Computational Materials Science, 2004. **29**(1): p. 1-11.
20. Liu, Y.J. and X.L. Chen, *Evaluations of the effective material properties of carbon nanotube-based composites using a nanoscale representative volume element*. Mechanics of Materials, 2003. **35**(1-2): p. 69-81.
21. Van Workum, K. and J.J. de Pablo, *Computer Simulation of the Mechanical Properties of Amorphous Polymer Nanostructures*. Nano Letters, 2003. **3**(10): p. 1405-1410.

22. Sheng, N., et al., *Multiscale Micromechanical Modeling of Polymer/Clay Nanocomposites and the Effective Clay Particle*. Polymer, 2004. **45**(2): p. 487-506.
23. Ospina, S.A., M. Hess, and B.L. Lopez, *Room temperature Monte Carlo study of the mechanical properties of thermoplastic polymers*. E-Polymers, 2004: p. -.
24. Ospina, S.A., J. Restrepo, and B.L. Lopez, *Deformation of polyethylene: Monte Carlo simulation*. Materials Research Innovations, 2003. **7**(1): p. 27-30.
25. Gates, T.S. and J. Hinkley, *Computational Materials: Modeling and Simulation of Nanostructured Materials and Systems*. 2003.
26. Odegard, G.M., et al., *Constitutive Modeling of Nanotube-Reinforced Polymer Composites* 2002, NASA CR-2002-211760
27. Hashin, Z. and S. Shtrikman, *A variational approach to the elastic behaviour of multiphase materials*. Journal of the Mechanics and Physics of Solids, 1962. **11**: p. 127-140.
28. Hill, R., *Theory of mechanical properties of fibre-strengthened materials: I. Elastic behaviour*. Journal of the Mechanics and Physics of Solids, 1964. **12**(4): p. 199-212.
29. Hill, R., *Theory of mechanical properties of fibre-strengthened materials: II. Inelastic behaviour*. Journal of the Mechanics and Physics of Solids, 1964. **12**(4): p. 213-218.
30. Hill, R., *Theory of mechanical properties of fibre-strengthened materials—III. self-consistent model*. Journal of the Mechanics and Physics of Solids, 1965. **13**(4): p. 189-198.
31. Hill, R., *A self-consistent mechanics of composite materials*. Journal of the Mechanics and Physics of Solids, 1965. **13**(4): p. 213-222.
32. Hill, R., *Continuum micro-mechanics of elastoplastic polycrystals*. Journal of the Mechanics and Physics of Solids, 1965. **13**(2): p. 89-101.
33. Hashin, Z., *The elastic moduli of heterogeneous materials*. Journal of Applied Mechanics, 1962. **29**: p. 143–150.

34. Hashin, Z. and S. Strikman, *A variational approach to the theory of the elastic behavior of multiphase systems*. Journal of the Mechanics and Physics of Solids, 1963. **11**.
35. Hashin, Z. and B.W. Rosen *The elastic moduli of fiber-reinforced materials*. Journal of Applied Mechanics, 1965. **32**: p. 630.
36. Qu, J. and M. Cherkaoui, *Fundamentals of Micromechanics of Solids* 2006: Wiley
37. Eshelby, J.D., *The Determination of the Elastic Field of an Ellipsoidal Inclusion, and Related Problems*. Proceedings of the Royal Society of London, Series A, 1957. **241**: p. 376-396.
38. Mori, T. and K. Tanaka, *Average Stress in Matrix and Average Elastic Energy of Materials with Misfitting Inclusions*. Acta Metallurgica, 1973. **21**(5): p. 571-574.
39. Benveniste, Y., *A New Approach to the Application of Mori-Tanaka's Theory in Composite Materials*. Mechanics of Materials, 1987. **6**(2): p. 147-157.
40. Budiansky, B., *On the elastic moduli of heterogeneous materials*. Journal of the Mechanics and Physics of Solids, 1965. **13**: p. 223–227.
41. Halpin, J.C. and S.W. Tsai, *Environmental Factors in Composite Materials Design*. 1967, Air Force Materials Laboratory -TR-67-423.
42. Hashin, Z., *Theory of mechanical properties of fibre-strengthened materials: II. Inelastic behaviour*, 1972, NASA CR-1974
43. Pipes, R.B. and P. Hubert, *Helical Carbon nanotube Arrays: Mechanical Properties*. Composites Science and Technology, 2002. **62**: p. 419-428.
44. Pipes, R.B. and P. Hubert, *Helical Carbon Nanotube Arrays: Thermal Expansion*. Composites Science and Technology, 2003. **62**: p. 1571-1579.
45. Pipes, R.B. and P. Hubert, *Scale Effects in Carbon nanostructures: Self-Similar Analysis*. Nano Letters, 2003. **3**(2): p. 239-243.
46. Odegard, G.M., et al., *Constitutive Modeling of Nanotube-Reinforced Polymer Composites*. Composites Science and Technology, 2003. **63**(11): p. 1671-1687.

47. Thostenson, E.T. and T.W. Chou, *On the elastic properties of carbon nanotube-based composites: modelling and characterization*. Journal of Physics D-Applied Physics, 2003. **36**(5): p. 573-582.
48. LAGOUDAS, D. and G. SEIDEL. *Effective Elastic Properties of Carbon Nanotubes and Carbon Nanotube Reinforced Composites*. in *45th AIAA/ASME/ASCE/AHS/ASC Structures, Structural Dynamics & Materials Conference*. 2004. Palm Springs, CA.
49. Adams, D.F., *Inelastic Analysis of a Unidirectional Composite Subjected to Transverse Normal Loading* Journal of Composite Materials, 1970. **4**(3): p. 310-328.
50. Lin, T.H., D. Salinas, and Y.M. Ito, *Elastic-Plastic Analysis of Unidirectional Composites* Journal of Composite Materials, 1972. **6**(1): p. 48-60.
51. Dvorak, G.J., M.S.M. Rao, and J.Q. Tarn, *Yielding in Unidirectional Composites Under External Loads and Temperature Changes* Journal of Composite Materials, 1973. **7**(2): p. 194-216.
52. Li, C.Y. and T.W. Chou, *Multiscale Modeling of Carbon Nanotube Reinforced Polymer Composites*. Journal of Nanoscience and Nanotechnology, 2003. **3**(5): p. 423-430.
53. Bradshaw, R.D., F.T. Fisher, and L.C. Brinson, *Fiber Waviness in Nanotube-Reinforced Polymer Composites-II: Modeling Via Numerical Approximation of the Dilute Strain Concentration Tensor*. Composites Science and Technology, 2003. **63**(11): p. 1705-1722.
54. Fisher, F.T., R.D. Bradshaw, and L.C. Brinson, *Fiber Waviness in Nanotube-Reinforced Polymer Composites-I: Modulus Prediction Using Effective Nanotube Properties*. Composites Science and Technology, 2003. **63**(11): p. 1689-1703.
55. Banerjee, P.K., *The Boundary Element Methods in Engineering*. 1994: McGraw-Hill College.

56. Liu, Y.J., et al., *A Fast Boundary Element Method for the Analysis of Fiber-Reinforced Composites Based on a Rigid-Inclusion Model*. Journal of Applied Mechanics 2005. **Volume 72**(1): p. 115-128
57. Ingber, M.S. and T.D. Papathanasiou, *A parallel-supercomputing investigation of the stiffness of aligned, short-fiber-reinforced composites using the boundary element method*. International Journal for Numerical Methods in Engineering, 1997. **40**(18): p. 3477-3491.
58. Huang, Y., K.X. Hu, and A. Chandra, *Stiffness evaluation for solids containing dilute inclusions and microcracks*. Stiffness evaluation for solids containing dilute inclusions and microcracks, 1995. **62**: p. 71-77.
59. Haile, J.M., *Molecular Dynamics Simulations: Elementary Methods*. 1992, New York: John Wiley & Sons, Inc.
60. Rappe, A.K. and C.J. Casewit, *Molecular Mechanics Across Chemistry*. 1997, Sausalito, CA: University Science Books.
61. Brenner, D.W., *Empirical Potential for Hydrocarbons for use in Simulating the Chemical Vapor Deposition of Diamond Films*. Physical Review B, 1990. **42**: p. 9458-9471.
62. Brenner, D.W., *Relationship between the Embedded-Atom Method and Tersoff Potentials*. Physical Review Letters, 1989. **63**(9): p. 1022-1022.
63. Cornell, W.D., et al., *A Second Generation Force Field for the Simulation of Proteins, Nucleic Acids, and Organic Molecules*. Journal of the American Chemical Society, 1995. **117**: p. 5179-5197.
64. Allinger, N.L., Y.H. Yuh, and J.H. Lii, *Molecular Mechanics. The MM3 Force Field for Hydrocarbons*. Journal of the American Chemical Society, 1989. **111**: p. 8551-8566.
65. Kaminski, G., et al., *Free-Energies of Hydration and Pure Liquid Properties of Hydrocarbons from the Opls All-Atom Model*. Journal of Physical Chemistry, 1994. **98**(49): p. 13077-13082.

66. Odegard, G.M., T.C. Clancy, and T.S. Gates. *Constitutive Modeling of Nanoparticle-Reinforced Polyimides*. in *ASME International Mechanical Engineering Congress and Exposition*. 2003. Washington, DC.
67. Valavala, P.K., et al., *Nonlinear Multiscale Modeling of Polymer Materials*. International Journal of Solids and Structures, 2007. **44**(3-4): p. 1161-1179.
68. Odegard, G.M., et al., *Equivalent-Continuum Modeling of Nano-Structured Materials*. Composites Science and Technology, 2002. **62**(14): p. 1869-1880.
69. Odegard, G.M., S.J.V. Frankland, and T.S. Gates. *The Effect of Chemical Functionalization on Mechanical Properties of Nanotube/Polymer Composites*. in *44th AIAA/ASME/ASCE/AHS Structures, Structural Dynamics, and Materials Conference*. 2003. Norfolk, VA.
70. Frankland, S.J.V., et al., *The Stress-Strain Behavior of Polymer-Nanotube Composites from Molecular Dynamics Simulation*. Composites Science and Technology, 2003. **63**(11): p. 1655-1661.
71. Odegard, G.M., et al. *Constitutive Modeling of Crosslinked Nanotube Materials*. in *45th AIAA/ASME/ASCE/AHS/ASC Structures, Structural Dynamics, and Materials Conference*. 2004. Palm Springs, CA.
72. Wei, C.Y., D. Srivastava, and K.J. Cho, *Thermal Expansion and Diffusion Coefficients of Carbon Nanotube-Polymer Composites*. Nano Letters, 2002. **2**(6): p. 647-650.
73. Lordi, V. and N. Yao, *Molecular Mechanics of Binding in Carbon-Nanotube-Polymer Composites*. Journal of Materials Research, 2000. **15**: p. 2770-2779.
74. Liang, Z., et al., *Investigation of Molecular Interactions Between (10,10) Single-Walled Nanotube and Epon 862 Resin/DETDA Curing Agent Molecules*. Materials Science and Engineering A, 2004. **356**: p. 228-234.
75. Frankland, S.J.V. and V.M. Harik, *Analysis of carbon nanotube pull-out from a polymer matrix*. Surface Science, 2003. **525**(1-3): p. L103-L108.
76. Fishman, G.S., *Monte Carlo: Concepts, Algorithms, and Applications*. 1995: Springer Verlag.

77. Ford, M.H., S.M. Auerbach, and P.A. Monson, *On the mechanical properties and phase behavior of silica: A simple model based on low coordination and strong association*. Journal of Chemical Physics, 2004. **121**(17): p. 8415-8422.
78. Chui, C. and M.C. Boyce, *Monte Carlo modeling of amorphous polymer deformation: Evolution of stress with strain*. Macromolecules, 1999. **32**(11): p. 3795-3808.
79. Levine, I.N., *Quantum Chemistry*. 1991: Prentice Hall.
80. Kohanoff, J., *Electronic Structure Calculations for Solids and Molecules: Theory and Computational Methods* 2006: Cambridge University Press.
81. Mylvaganam, K. and L.C. Zhang, *Nanotube functionalization and polymer grafting: An ab initio study*. Journal of Physical Chemistry B, 2004. **108**(39): p. 15009-15012.
82. Mylvaganam, K. and L.C. Zhang, *Important issues in a molecular dynamics simulation for characterising the mechanical properties of carbon nanotubes*. Carbon, 2004. **42**(10): p. 2025-2032.
83. Mylvaganam, K. and L.C. Zhang, *Chemical bonding in polyethylene-nanotube composites: A quantum mechanics prediction*. Journal of Physical Chemistry B, 2004. **108**(17): p. 5217-5220.
84. Bauschlicher, C.W., *Hydrogen and fluorine binding to the sidewalls of a (10,0) carbon nanotube*. Chemical Physics Letters, 2000. **322**(3-4): p. 237-241.
85. Griebel, M. and J. Hamaekers, *Molecular Dynamics Simulations of the Elastic Moduli of Polymer-Carbon Nanotube Composites*. Computer Methods in Applied Mechanics and Engineering, 2004. **193**: p. 1773-1788.
86. Zhu, L.J. and K.A. Narh, *Numerical simulation of the effect of nanotube orientation on tensile modulus of carbon-nanotube-reinforced polymer composites*. Polymer International, 2004. **53**(10): p. 1461-1466.
87. Zhu, L.J. and K.A. Narh, *Numerical simulation of the tensile modulus of nanoclay-filled polymer composites*. Journal of Polymer Science Part B-Polymer Physics, 2004. **42**(12): p. 2391-2406.

88. Gou, J., et al., *Computational and experimental study of interfacial bonding of single-walled nanotube reinforced composites*. Computational Materials Science 2004. **31**(3-4): p. 225-236.
89. Odegard, G.M., T.C. Clancy, and T.S. Gates, *Modeling the Mechanical Properties of nanoparticle/polymer composites*. Polymer, 2005. **46**(2): p. 553-562.
90. Theodorou, D.N. and U.W. Suter, *Atomistic Modeling of Mechanical Properties of Polymeric Glasses*. Macromolecules, 1986. **19**(1): p. 139-154.
91. Sane, S.B., et al., *Molecular Dynamics Simulations to Compute the Bulk Response of Amorphous PMMA*. Journal of Computer-Aided Materials Design, 2002. **8**(2-3): p. 87-106.
92. Fan, C.F., et al., *Molecular Modeling of Polycarbonate. 1. Force Field, Static Structure, and Mechanical Properties*. Macromolecules, 1994. **27**: p. 2383-2391.
93. Shenogin, S. and R. Ozisik, *Simulation of Plastic Deformation in Glassy Polymers: Atomistic and Mesoscale Approaches*. Journal of Polymer Science Part B: Polymer Physics, 2005. **43**: p. 994-1004.
94. Ogden, R.W., *Non-Linear Elastic Deformations*. 1997, Mineola, NY: Dover Publications, Inc.
95. Holzapfel, G.A., *Nonlinear Solid Mechanics: A Continuum Approach for Engineering*. 2000, West Sussex, England: John Wiley & Sons, Ltd.
96. Brooks, F.P., et al., *CHARMM: A Program for Macomolecular Energy, Minimization, and Dynamics Calculations*. Journal of Computational Chemistry, 1983. **4**: p. 187-217.
97. Clark, M., R.D. Crammer, and N. Van Opdenhosch, *Validation of the General Purpose Tripose 5.2 Force Field*. Journal of Computational Chemistry, 1989. **10**: p. 982-1012.

98. Ott, K.H. and B. Meyer, *Parametrization of GROMOS Force Field for Oligosaccharides and Assessment of Efficiency of Molecular Dynamics Simulations*. Journal of Computational Chemistry, 1996. **17**: p. 1068-1084.
99. Sun, H., *COMPASS: An ab Initio Force-Field Optimized for Condensed-Phase Applications - Overview with Details on Alkane and Benzene Compounds*. Journal of Physical Chemistry B, 1998. **102**: p. 7338-7364.
100. Jorgensen, W.L., D.S. Maxwell, and J. Tirado-Rives, *Development and Testing of the OPLS All-Atom Force Field on Conformational Energetics and Properties of Organic Liquids*. Journal of the American Chemical Society, 1996. **117**: p. 11225-11236.
101. Hergenrother, P.M., et al., *Polyimides from 2,3,3',4'-Biphenyltetracarboxylic Dianhydride and Aromatic Diamines*. Polymer, 2002. **43**(19): p. 5077-5093.
102. Srinivas, S., et al., *Semicrystalline Polyimides Based on Controlled Molecular Weight Phthalimide End-Capped 1,3-Bis(4-Aminophenoxy)Benzene and 3,3',4,4'-Biphenyltetracarboxylic Dianhydride: Synthesis, Crystallization, Melting, and Thermal Stability*. Macromolecules, 1997. **30**(4): p. 1012-1022.
103. Kaminsky, G.A., et al., *Evaluation and Reparametrization of the OPLS-AA Force Field for Proteins via Comparison with Accurate Quantum Chemical Calculations on Peptides*. Journal of Physical Chemistry B, 2001. **105**: p. 6474-6487.
104. Tersoff, J., *New Empirical Approach for the structure and energy of covalent systems*. Physical Review B, 1988. **37**(12): p. 6991-7000.
105. Tersoff, J., *Empirical Interatomic Potential for Carbon, with Applications to Amorphous Carbon*. Physical Review Letters, 1988. **61**(25): p. 2879-2882.
106. Ponder, J.W., *TINKER - Software Tools for Molecular Design*. 2004, Washington University School of Medicine: St. Louis, MO.
107. Odegard, G.M., S.J.V. Frankland, and T.S. Gates, *Effect of Nanotube Functionalization on the Elastic Properties of Polyethylene Nanotube Composites*. AIAA Journal, 2005. **43**(8): p. 1828-1835.

108. Dauber-Osguthorpe, P., et al., *Structure and Energetics of Ligand Binding to Proteins*. Proteins: Structure, Function and Genetics, 1988. **4**: p. 31-47.
109. Clancy, T.C., *Multi-Scale Modeling of Polyimides*. Polymer, 2004. **45**: p. 7001-7010.
110. Leach, A.R., *Molecular Modelling: Principles and Applications*. 2001, New York: Prentice Hall.
111. Ashby, M.F. and D.R.H. Jones, *Engineering Materials 1: An Introduction to Their Properties & Applications*. 1996, Oxford, UK: Butterworth-Heinemann.
112. Truesdell, C. and W. Noll, *The Non-Linear Field Theories of Mechanics*. Third ed. 2004, New York: Springer-Verlag.
113. Flory, P.J., *Principles of Polymer Chemistry*. 1953, Ithaca, NY: Cornell University Press.
114. Drozdov, A.D., *Finite Elasticity and Viscoelasticity: A Course in the Nonlinear Mechanics of Solids*. 1996, Singapore: World Scientific.
115. Ball, J.M., *Convexity Conditions and Existence Theorems in Nonlinear Elasticity*. Archive for Rational Mechanics and Analysis, 1977. **63**: p. 337-403.
116. Marsden, J.E. and T.J.R. Hughes, *Mathematical Foundations of Elasticity*. 1994, Mineola, NY: Dover Publications, Inc.
117. Ciarlet, P.G., *Mathematical Elasticity*. 1988, Amsterdam: Elsevier Science Publishers B.V.
118. Schroder, J. and P. Neff, *Invariant Formulation of Hyperelastic Transverse Isotropy Based on Polyconvex Free Energy Functions*. International Journal of Solids and Structures, 2003. **40**: p. 401-445.
119. Nocedal, J. and S.J. Wright, *Numerical Optimization*. 1999, New York: Springer-Verlag.
120. Berendsen, H.J.C., et al., *Molecular Dynamics with Coupling to an External Bath*. Journal of Chemical Physics, 1984. **81**(8): p. 3684-3690.

121. Sun, C.T. and R.S. Vaidya, *Prediction of Composite Properties from a Representative Volume Element*. Composites Science and Technology, 1996. **56**: p. 171-179.
122. Jiang, M., I. Jasiuk, and M. Ostoja-Starzewski, *Apparent Elastic and Elastoplastic Behavior of Periodic Composites*. International Journal of Solids and Structures, 2002. **39**: p. 199-212.
123. Malvern, L.E., *Introduction to the Mechanics of a Continuous Medium*. 1969, Upper Saddle River, NJ: Prentice-Hall, Inc.
124. Christopher, W.F. and D.W. Fox, *Polycarbonates*. 1962, New York: Reinhold Publishing Corporation.
125. Fan, C.F. and S.L. Hsu, *Application of the Molecular Simulation Technique to Characterize the Structure and Properties of an Aromatic Polysulfone System. 2. Mechanical and Thermal Properties*. Macromolecules, 1992. **25**: p. 266-270.
126. Dokholyan, N.V., et al., *Glassy behavior of a homopolymer from molecular dynamics simulations*. Physical Review E, 2002. **65**(3): p. -.
127. Lyulin, A.V. and M.A.J. Michels, *Molecular dynamics simulation of bulk atactic polystyrene in the vicinity of T-g*. Macromolecules, 2002. **35**(4): p. 1463-1472.
128. Capaldi, F.M., M.C. Boyce, and G.C. Rutledge, *Molecular response of a glassy polymer to active deformation*. Polymer, 2004. **45**(4): p. 1391-1399.
129. Laot, C.M., et al., *Effects of cooling rate and physical aging on the gas transport properties in polycarbonate*. Macromolecules, 2003. **36**(23): p. 8673-8684.
130. Stachurski, Z.H., *Strength and deformation of rigid polymers: structure and topology in amorphous polymers*. Polymer, 2003. **44**(19): p. 6059-6066.
131. Rutledge, G.C. and U.W. Suter, *Calculation of Mechanical-Properties of Poly(P-Phenylene Terephthalamide) by Atomistic Modeling*. Polymer, 1991. **32**(12): p. 2179-2189.
132. Cohen, M.H. and D. Turnbull, *On the Free-volume Model of Liquid-Glass Transition*. Journal of Chemical Physics, 1970. **52**: p. 3038.

133. Rigby, D. and R.J. Roe, *Molecular-Dynamics Simulation Of Polymer Liquid And Glass .4. Free-Volume Distribution*. Macromolecules, 1990. **23**(26): p. 5312-5319.
134. Roe, R.J. and D. Rigby, *Free-Volume Distribution And Local Chain Motion In Polymer Liquid And Glass Studied By Md-Simulation*. Abstracts Of Papers Of The American Chemical Society, 1990. **199**: p. 361-POLY.
135. Hinkley, J.A., et al., *Free-Volume in Glassy Poly(Arylene Ether Ketone)S*. Journal of Polymer Science Part B-Polymer Physics, 1992. **30**(11): p. 1195-1198.
136. Wilks, B.R., et al., *Structural and free-volume analysis for alkyl-substituted palladium-catalyzed poly(norbornene): A combined experimental and Monte Carlo investigation*. Journal of Polymer Science Part B-Polymer Physics, 2006. **44**(1): p. 215-233.
137. Dlubek, G., et al., *Free Volume of an Oligomeric Epoxy Resin and Its Relation to Structural Relaxation: Evidence from Positron Lifetime and Pressure-Volume-Temperature Experiments*. Physical Review E, 2007.
138. Roe, R.J. and J.J. Curro, *Small-Angle X-Ray-Scattering Study of Density Fluctuation in Polystyrene Annealed Below the Glass-Transition Temperature*. Macromolecules, 1983. **16**(3): p. 428-434.
139. Weiner, P.K., and Kollman, P. A., *AMBER: Assisted Model Building with Energy Refinement. A General Program for Modeling Molecules and Their Interactions*. Journal of Computational Chemistry, 1981. **2**: p. 287-303.
140. Clancy, T.C. and J. Hinkley, *Coarse-Grained and Atomistic Modeling of Polyimides*. 2004, National Aeronautics and Space Administration.
141. Ponder, J.W. and F.M. Richards, *An Efficient Newton-Like Methods for Molecular Mechanics Energy Minimization of Large Molecules*. Journal of Computational Chemistry, 1987. **8**: p. 1016-1024.
142. Ponder, J.W., *TINKER: Software Tools for Molecular Design*. 1998, Washington University School of Medicine: St. Louis, MO.

143. Hill, T.L., *An Introduction to Statistical Thermodynamics* 1986: Dover Publications.
144. Odian, G., *Principles of Polymerization*. Third Edition ed. 1991: Wiley-Interscience.
145. Valavala, P.K. and G.M. Odegard, *Modeling Techniques for Determination of Mechanical Properties of Polymer Nanocomposites*. Reviews on Advanced Materials Science, 2005. **9**(1): p. 34-44.
146. Weiner, S.J., Kollman, P.A., Case, D.A., Singh, U.C., Ghio, C., Alagona, G., Profeta, S., Jr., Weiner, P.K., *A new force field for molecular mechanical simulation of nucleic acids and proteins*. Journal of American Chemical Society, 1984. **106**: p. 765-784.
147. Weiner, S.J., Kollman, P. A., Nguyen, D. T., and Case, D. A., *An All Atom Force Field for Simulations of Proteins and Nucleic Acids*. Journal of Computational Chemistry, 1986. **7**: p. 230-252.
148. Qi, D., J. Hinkley, and G. He, *Molecular Dynamics Simulation of Thermal and Mechanical Properties of Polyimide–Carbon-Nanotube Composites*. Modelling and Simulation in Materials Science and Engineering, 2005. **13**: p. 493-507
149. Soldera, A. and N. Metatla, *Glass Transition of Polymers: Atomistic Simulation Versus Experiments*. Physical Review E, 2006. **74**.
150. Bennemann, C., et al., *Molecular Dynamics Simulations of the Thermal Glass Transition in Polymer Melts: α -Relaxation Behavior*. Physical Review E, 1998. **57**: p. 843 - 851.
151. Paul, W., *Molecular Dynamics Simulations of the Glass Transition in Polymer Melts*. Polymer, 2004. **45**: p. 3901–3905.
152. Wei, C., D. Srivastava, and K. Cho, *Thermal Expansion and Diffusion Coefficients of Carbon Nanotube-Polymer Composites* Nano Letters, 2002. **2**(6): p. 647 -650.
153. Reichman, D.R. and P. Charbonneau, *Mode-Coupling Theory*. Journal of Statistical Mechanics: Theory and Experiment, 2005.

154. Gao, G., *Large Scale Molecular Simulations with Application to Polymers and Nano-scale Materials*, in *Physics*. 1998, California Institute of Technology: Pasadena. p. 315.
155. Jenkins, C.H.M., ed. *Gossamer Spacecraft: Membrane/Inflatable Structure Technology for Space Applications*. AIAA Progress in Astronautics and Aeronautics Series. 2001, American Institute of Aeronautics and Astronautics: Reston, VA.
156. Joseph G. Smith, J., Kent A. Watson, Donavon M. Delozier and John W. Connell. *Carbon Nanotube/Conductive Additive/Space Durable Polymer Nanocomposite Films for Electrostatic Charge Dissipation* in *35th International SAMPE Technical Conference*. September 28–October 2, 2003. Dayton, Ohio.
157. Ruggiero, E.J., et al., *A Literature Review of Ultra-Light and Inflated Toroidal Satellite Components*. The Shock and Vibration Digest, 2003. **35**: p. 171 - 181.
158. St. Clair, A.K., T.L. St. Clair, and W.S. Slemp, *Optically Transparent/Colorless Polyimides*, in *Recent Advances in Polyimide Science and Technology*, W. Weber and M. Gupta, Editors. 1987, Society of Plastics Engineers: Poughkeepsie, NY. p. 16-36.
159. Odegard, G.M., T.C. Clancy, and T.S. Gates. *Prediction of Mechanical Properties of Polymers with Various Force Fields*. in *46th AIAA/ASME/ASCE/AHS/ASC Structures, Structural Dynamics, and Materials Conference*. 2005. Austin, TX.
160. Odegard, G.M., R.B. Pipes, and P. Hubert, *Comparison of Two Models of SWCN Polymer Composites*. Composites Science and Technology, 2004. **64**: p. 1011-1020.
161. Valavala, P.K., et al., *Nonlinear Multiscale Modeling of Polymer Materials*. in preparation, 2005.
162. Valavala, P.K. and G.M. Odegard. *Multiscale Constitutive Modeling of Polymer Materials*. in *ASME International Mechanical Engineering Congress and Exposition* 2007. Seattle: ASME.

163. Herring, H.M., *Dynamic Mechanical Characterization of Thin Film Polymer Nanocomposites*, 2003, National Aeronautics and Space Administration.
164. Gedde, U.W., *Polymer Physics*. 1st edition ed. 1995: Springer.
165. Brown, D. and J.H.R. Clarke, *Molecular-Dynamics Simulation of an Amorphous Polymer under Tension .1. Phenomenology*. *Macromolecules*, 1991. **24**(8): p. 2075-2082.
166. Hoy, R.S. and M.O. Robbins, *Strain hardening of polymer glasses: Effect of entanglement density, temperature, and rate*. *Journal of Polymer Science Part B- Polymer Physics*, 2006. **44**(24): p. 3487-3500.
167. Lyulin, A.V., et al., *Atomistic simulation of bulk mechanics and local dynamics of amorphous polymers*. *Macromolecular Symposia*, 2006. **237**: p. 108-118.
168. Theodorou, D.N., *Understanding and predicting structure-property relations in polymeric materials through molecular simulations*. *Molecular Physics*, 2004. **102**(2): p. 147-166.
169. Hill, R., *Elastic Properties of Reinforced Solids: Some Theoretical Principles*. *Journal of the Mechanics and Physics of Solids*, 1963. **11**: p. 357-372.
170. Hill, R., *The Essential Structure of Constitutive Laws for Metal Composites and Polycrystals*. *Journal of the Mechanics and Physics of Solids*, 1967. **15**: p. 79-95.
171. Drugan, W.J. and J.R. Willis, *A Micromechanics-Based Nonlocal Constitutive Equation and Estimates of Representative Volume Element Size for Elastic Composites*. *Journal of the Mechanics and Physics of Solids*, 1996. **44**: p. 497-524.
172. Drugan, W.J., *Micromechanics-Based Variational Estimates for a Higher-Order Nonlocal Constitutive Equation and Optimal Choice of Effective Moduli for Elastic Composites*. *Journal of the Mechanics and Physics of Solids*, 2000. **48**: p. 1359-1387.

173. Ostoja-Starzewski, M., *Microstructural Randomness Versus Representative Volume Element in Thermomechanics*. ASME Journal of Applied Mechanics, 2002. **69**: p. 25-35.
174. Ostoja-Starzewski, M., *Towards Stochastic Continuum Thermodynamics*. Journal of Non-Equilibrium Thermodynamics, 2002. **27**(4): p. 335-348.
175. Yoshimoto, K., et al., *Mechanical Heterogeneities in Model Polymer Glasses at Small Length Scales*. Physical Review Letters, 2004. **93**.
176. Valavala, P.K., et al., *Multiscale Modeling of Polymer Materials Using a Statistics-Based Micromechanics Approach*. Acta Materialia (In Review), 2008.
177. Falk, M.L. and J.S. Langer, *Dynamics Of Viscoplastic Deformation In Amorphous Solids*. Physical Review E, 1998. **57**(6).
178. Liu, C., *On the Minimum Size of Representative Volume Element: An Experimental Investigation*. Experimental Mechanics, 2005. **45**(3): p. 238-243.
179. Keten, S. and M.J. Buehler, *Geometric confinement governs the rupture strength of H-bond assemblies at a critical length scale*. Nano Letters, 2008. **8**(2): p. 743-748.
180. Drugan, W.J., *Elastic composite materials having a negative stiffness phase can be stable*. Physical Review Letters, 2007. **98**(5): p. -.
181. Lakes, R.S. and W.J. Drugan, *Dramatically stiffer elastic composite materials due to a negative stiffness phase?* Journal of the Mechanics and Physics of Solids, 2002. **50**(5): p. 979-1009.
182. Khayankarn, O., et al., *Strength of Epoxy/Glass Interfaces after Hygrothermal Aging*. The Journal of Adhesion, 2005. **81**(9): p. 941-961.
183. Lin, Y.C., et al., *Effects of hygrothermal aging on epoxy-based anisotropic conductive film*. Materials Letters, 2006. **60**(24): p. 2958-2963.
184. Bockenheimer, C., D. Fata, and W. Possart, *New aspects of aging in epoxy networks. II. Hydrothermal aging*. Journal of Applied Polymer Science, 2004. **91**(1): p. 369-377.

185. Fata, D. and W. Possart, *Aging Behavior of a Hot-Cured Epoxy System*. Journal of Applied Polymer Science, 2006. **99**(5): p. 2726-2736.
186. Luo, H.L., et al., *Moisture absorption in VARTMed three-dimensional braided carbon-epoxy composites with different interface conditions*. Materials Science & Engineering A, 2006. **425**(1-2): p. 70-77.
187. Hay, J.N. and P.R. Laity, *Observations of water migration during thermoporometry studies of cellulose films*. Polymer, 2000. **41**(16): p. 6171-6180.
188. Díez-Pena, E., I. Quijada-Garrido, and J.M. Barrales-Rienda, *On the water swelling behaviour of poly (N-isopropylacrylamide)[P (N-iPAAm)], poly (methacrylic acid)[P (MAA)], their random copolymers and sequential interpenetrating polymer networks (IPNs)*. Polymer, 2002. **43**(16): p. 4341-4348.
189. Berry, R.M.J. and M. Schwartz. *Dynamics of Hydrated Polymers, Effects of Hydration Level and Temperature*. in *SAMPE Fall Technical Conference*. 2007. Cincinnati, Ohio.
190. Kim, D. and K. Park, *Swelling and mechanical properties of superporous hydrogels of poly (acrylamide-co-acrylic acid)/polyethylenimine interpenetrating polymer networks*. Polymer, 2004. **45**(1): p. 189-196.
191. Stillinger, F.H., *Exponential multiplicity of inherent structures*. Physical Review E, 1999. **59**(1): p. 48-51.
192. Valavala, P.K., G.M. Odegard, and E.C. Aifantis, *Influence of Representative Volume Element Size on Multiscale Modeling of Polymer Materials* Modelling and Simulation in Materials Science and Engineering, 2008. **In Review**.
193. Payne, M.C., et al., *Iterative minimization techniques for ab initio total-energy calculations: molecular dynamics and conjugate gradients*. Reviews of Modern Physics, 1992. **64**(4): p. 1045.

This page is left blank intentionally

APPENDIX A

The total potential energy of a simulated molecular system computed with the AMBER force field is based on the summation of the bond stretching, bending, torsion and nonbonded energies given by

$$\Lambda_{\text{total}}^A = \Lambda_{\text{stretch}}^A + \Lambda_{\text{bend}}^A + \Lambda_{\text{torsion}}^A + \Lambda_{\text{nb}}^A \quad (\text{A.1})$$

where superscript A indicates the AMBER force field and

$$\Lambda_{\text{stretch}}^A = \sum_{\text{stretch}} K_r^A (r - r_{eq}^A)^2 \quad (\text{A.2})$$

$$\Lambda_{\text{bend}}^A = \sum_{\text{bend}} K_{\theta}^A (\theta - \theta_{eq}^A)^2 \quad (\text{A.3})$$

$$\Lambda_{\text{torsion}}^A = \sum_{\text{torsion}} \left\{ \frac{V_1^A}{2} [1 + \cos(\phi + \zeta^A)] + \frac{V_2^A}{2} [1 - \cos(2\phi + \zeta^A)] + \frac{V_3^A}{2} [1 + \cos(3\phi + \zeta^A)] \right\} \quad (\text{A.4})$$

$$\Lambda_{\text{nb}}^A = \sum_{I < J} 4\epsilon_{IJ}^A \left[\frac{(\sigma_{IJ}^A)^{12}}{r_{IJ}^{12}} - \frac{(\sigma_{IJ}^A)^6}{r_{IJ}^6} \right] \quad (\text{A.5})$$

where the summations are taken over all of the corresponding interactions in the molecular model; K_r^A and K_{θ}^A are the bond-stretching and bond-angle bending force constants, respectively; r and r_{eq}^A are the bond length and equilibrium bond length, respectively; θ and θ_{eq}^A are the bond angle and equilibrium bond angle, respectively; $V_n^A/2$, ζ^A , and ϕ are the torsion magnitude ($n=1,2,3$), phase offset, and the torsion angle, respectively; and ϵ_{IJ}^A , r_{IJ} , and σ_{IJ}^A are van der Waals well depth, non-bonded

distance between atoms I and J , and the equilibrium distance between atoms I and J , respectively.

Similarly, the total potential energy of the molecular model computed with the OPLS-AA force field is generally represented by

$$\Lambda_{\text{total}}^O = \Lambda_{\text{stretch}}^O + \Lambda_{\text{bend}}^O + \Lambda_{\text{torsion}}^O + \Lambda_{\text{nb}}^O \quad (\text{A.6})$$

where the superscript O indicates the OPLS-AA force field and

$$\Lambda_{\text{stretch}}^O = \sum_{\text{stretch}} K_r^O (r - r_{eq}^O)^2 \quad (\text{A.7})$$

$$\Lambda_{\text{bend}}^O = \sum_{\text{bend}} K_{\theta}^O (\theta - \theta_{eq}^O)^2 \quad (\text{A.8})$$

$$\Lambda_{\text{torsion}}^O = \sum_{\text{torsion}} \left\{ \frac{V_1^O}{2} [1 + \cos(\phi + \zeta^O)] + \frac{V_2^O}{2} [1 - \cos(2\phi + \zeta^O)] + \frac{V_3^O}{2} [1 + \cos(3\phi + \zeta^O)] \right\} \quad (\text{A.9})$$

$$\Lambda_{\text{nb}}^O = \sum_{I < J} \left\{ \frac{q_I^O q_J^O e^2}{r_{IJ}} + 4\epsilon_{IJ}^O \left[\frac{(\sigma_{IJ}^O)^{12}}{r_{IJ}^{12}} - \frac{(\sigma_{IJ}^O)^6}{r_{IJ}^6} \right] \right\} \quad (\text{A.10})$$

where q_I is the partial charge of atom I , e is the elementary charge, and the remaining quantities are analogous to those already defined for the AMBER force field.

For the MM3 force field, the total potential energy includes the previously mentioned terms along with additional terms representing bond deformations given by stretch-bend, torsion-stretch, bend-bend, and the van-der-Waals and electrostatic interactions

$$\Lambda_{\text{total}}^M = \Lambda_{\text{stretch}}^M + \Lambda_{\text{bend}}^M + \Lambda_{\text{torsion}}^M + \Lambda_{\text{stretch-bend}}^M + \Lambda_{\text{torsion-stretch}}^M + \Lambda_{\text{bend-bend}}^M + \Lambda_{\text{vdw}}^M + \Lambda_{\text{electrostatic}}^M + \Lambda_{\text{nb}}^M \quad (\text{A.11})$$

where the superscript M indicates the MM3 force field and

$$\Lambda_{\text{stretch}}^M = \sum_{\text{stretch}} 71.94 K_r^M (r - r_{eq}^M)^2 \left[1 - 2.55(r - r_{eq}^M) + 1.49(r - r_{eq}^M)^2 \right] \quad (\text{A.12})$$

$$\Lambda_{\text{bend}}^M = \sum_{\text{bend}} \left\{ \begin{aligned} &0.021914 K_{\theta}^M (\theta - \theta_{eq}^M)^2 \times \\ &\left[1 - 0.014(\theta - \theta_{eq}^M) + 5.6(10^{-5})(\theta - \theta_{eq}^M)^2 \right. \\ &\left. - 7.0(10^{-7})(\theta - \theta_{eq}^M)^3 + 9.0(10^{-10})(\theta - \theta_{eq}^M)^4 \right] \end{aligned} \right\} \quad (\text{A.13})$$

$$\Lambda_{\text{torsion}}^M = \sum_{\text{torsion}} \left\{ \frac{V_1^M}{2} [1 + \cos(\phi)] + \frac{V_2^M}{2} [1 - \cos(2\phi)] + \frac{V_3^M}{2} [1 + \cos(3\phi)] \right\} \quad (\text{A.14})$$

$$\Lambda_{\text{stretch-bend}}^M = \sum_{\text{stretch-bend}} 2.51118 K_{r\theta}^M \left[(r - r_{eq}^M) + (r' - r_{eq}^{\prime M}) \right] (\theta - \theta_{eq}^M) \quad (\text{A.15})$$

$$\Lambda_{\text{torsion-stretch}}^M = \sum_{\text{torsion-stretch}} 11.995 \left(\frac{K_{\phi r}^M}{2} \right) (r - r_{eq}^M) [1 + \cos(3\phi)] \quad (\text{A.16})$$

$$\Lambda_{\text{bend-bend}}^M = \sum_{\text{bend-bend}} \left[-0.021914 K_{\theta\theta'}^M (\theta - \theta_{eq}^M) (\theta' - \theta_{eq}^{\prime M}) \right] \quad (\text{A.17})$$

$$\Lambda_{\text{vdw}}^M = \sum_{I < J} \mathcal{E}_{IJ}^M \left\{ -2.25 \left[\frac{(\sigma_{IJ}^M)^6}{r_{IJ}^6} \right] + 1.84(10^5) \exp \left[-12.00 \left(\frac{\sigma_{IJ}^M}{r_{IJ}} \right) \right] \right\} \quad (\text{A.18})$$

where $K_{r\theta}^M$, $K_{\phi r}^M$, and $K_{\theta\theta'}^M$ are force constants; r' and $r_{eq}^{\prime M}$ are the bond length and equilibrium bond length, respectively, of the adjacent covalent bond; and θ' and $\theta_{eq}^{\prime M}$ are the bond angle and equilibrium bond angle, respectively, of the adjacent bond angle. The energy contribution from electrostatic forces, $\Lambda_{\text{electrostatic}}^M$, is determined by either partial charges or dipole moments. The energies associated with all remaining non-

bonded interactions, such as hydrogen bonding, are incorporated in Λ_{nb}^M . The remaining quantities in Equations (A.12)-(A.18) are analogous to those of the AMBER and OPLS-AA force fields.

APPENDIX B

Polymer materials typically operate below their glass transition temperature, where they predominantly exhibit amorphous glassy characteristics. It is well known that the properties of amorphous can be significantly influenced by their morphology such as chain length, polydispersity index, impurities and voids. In particular, it is expected that below a certain chain critical length, “*entanglement limit*”, the material does reach its plateau modulus and exhibit solid-like behavior. As the chain length of the polymer is increased so does its stiffness and strength. The current study investigates the influence of the chain length on predicted stiffness from a multiscale modeling technique.

Table B.1 and B.2 show the results obtained for five and ten monomers per polymer chain of polycarbonate model. It can be seen from Table I that the average Young’s modulus is 3.94 GPa for five monomers per chain which increased to 5.79 GPa for ten monomers per chain. These results show that the chain length influences the predicted properties in multiscale modeling of polymer materials.

Table B.1 Predicted properties of polycarbonate with 5 monomers per polymer chain

Microstate	Λ_r (kcal/mole)	Density (g/cc)	Young's modulus (GPa)	Shear modulus (GPa)	p_r
1	10600.79	1.07	3.33	1.12	0.27
2	12062.25	1.13	6.59	2.25	0.24
3	17977.77	1.14	1.52	0.51	0.16
4	23160.77	1.11	1.44	0.48	0.13
5	35635.98	1.13	6.98	2.44	0.08
6	47428.17	1.14	0.13	0.04	0.06
7	55409.5	1.15	7.63	2.65	0.05
Average	28896.46	1.13	3.94	1.36	-
Std. Dev.	16309.61	0.02	3.08	1.07	-

Table B.2 Predicted properties of polycarbonate with 10 monomers per polymer chain

Microstate	Λ_r (kcal/mole)	Density (g/cc)	Young's modulus (GPa)	Shear modulus (GPa)	p_r
1	12157.46	1.14	1.64	0.55	0.25
2	12159.09	1.1	1.24	0.42	0.25
3	18026.54	1.12	9.77	3.5	0.17
4	23270.56	1.12	8.26	2.85	0.13
5	35694.22	1.13	7.81	2.68	0.09
6	47559.96	1.09	5.81	1.99	0.06
7	55529.83	1.05	5.98	2.07	0.05
Average	29199.67	1.11	5.79	2.01	-
Std. Dev.	17384.71	0.03	3.27	1.16	-

Appendix C

This page is left blank intentionally

The next 12 pages are the copyright permissions for Figure 2.5 (p. 187- 193) and Chapter 3 (p. 194-200) respectively.

ELSEVIER LICENSE
TERMS AND CONDITIONS

Jul 31, 2008

This is a License Agreement between Pavan K Valavala ("You") and Elsevier ("Elsevier"). The license consists of your order details, the terms and conditions provided by Elsevier, and the payment terms and conditions.

Supplier Elsevier Limited

The Boulevard, Langford Lane

Kidlington, Oxford, OX5 1GB, UK

Registered Company Number 1982084

Customer name Pavan K Valavala

Customer address 2010 C Woodmar Drive, Houghton, MI 49931

License Number 1999161149540

License date Jul 31, 2008

Licensed content publisher Elsevier

Licensed content publication Composites Science and Technology

Licensed content title Constitutive modeling of nanotube-reinforced polymer composites

Licensed content author G. M. Odegard, T. S. Gates, K. E. Wise, C. Park and E. J. Siochi

Licensed content date August 2003

Volume number 63

Issue number 11

Pages 17

Type of Use Thesis / Dissertation

Portion Figures/table/illustration/abstracts

Portion Quantity 1

Format Electronic

You are an author of the Elsevier article No

Are you translating? No

Purchase order number

Expected publication date Aug 2008

Elsevier VAT number GB 494 6272 12

Permissions price 0.00 USD

Value added tax 0.0% 0.00 USD

Total 0.00 USD

Terms and Conditions

INTRODUCTION

1. The publisher for this copyrighted material is Elsevier. By clicking "accept" in connection with completing this licensing transaction, you agree that the following terms and conditions apply to this transaction (along with the Billing and Payment terms and conditions established by Copyright Clearance Center, Inc. ("CCC"), at the time that you opened your Rightslink account and that are available at any time at <<http://myaccount.copyright.com>>).

GENERAL TERMS

2. Elsevier hereby grants you permission to reproduce the aforementioned material subject to the terms and conditions indicated.

3. Acknowledgement: If any part of the material to be used (for example, figures) has appeared in our publication with credit or acknowledgement to another source, permission must also be sought from that source. If such permission is not obtained then that material may not be included in your publication/copies. Suitable

acknowledgement to the source must be made, either as a footnote or in a reference list at the end of your publication, as follows: “Reprinted from Publication title, Vol /edition number, Author(s), Title of article / title of chapter, Pages No., Copyright (Year), with permission from Elsevier [OR APPLICABLE SOCIETY COPYRIGHT OWNER].” Also Lancet special credit - “Reprinted from The Lancet, Vol. number, Author(s), Title of article, Pages No., Copyright (Year), with permission from Elsevier.”

4. Reproduction of this material is confined to the purpose and/or media for which permission is hereby given.

5. Altering/Modifying Material: Not Permitted. However figures and illustrations may be altered/adapted minimally to serve your work. Any other abbreviations, additions, deletions and/or any other alterations shall be made only with prior written authorization of Elsevier Ltd. (Please contact Elsevier at permissions@elsevier.com)

6. If the permission fee for the requested use of our material is waived in this instance, please be advised that your future requests for Elsevier materials may attract a fee.

7. Reservation of Rights: Publisher reserves all rights not specifically granted in the combination of (i) the license details provided by you and accepted in the course of this licensing transaction, (ii) these terms and conditions and (iii) CCC's Billing and Payment terms and conditions.

8. License Contingent Upon Payment: While you may exercise the rights licensed immediately upon issuance of the license at the end of the licensing process for the transaction, provided that you have disclosed complete and accurate details of your proposed use, no license is finally effective unless and until full payment is received from you (either by publisher or by CCC) as provided in CCC's Billing and Payment terms and conditions. If full payment is not received on a timely basis, then any license preliminarily granted shall be deemed automatically revoked and shall be void as if never granted. Further, in the event that you breach any of these terms and conditions or any of CCC's Billing and Payment terms and conditions, the license is automatically revoked and shall be void as if never granted. Use of materials as described in a revoked

license, as well as any use of the materials beyond the scope of an unrevoked license, may constitute copyright infringement and publisher reserves the right to take any and all action to protect its copyright in the materials.

9. Warranties: Publisher makes no representations or warranties with respect to the licensed material.

10. Indemnity: You hereby indemnify and agree to hold harmless publisher and CCC, and their respective officers, directors, employees and agents, from and against any and all claims arising out of your use of the licensed material other than as specifically authorized pursuant to this license.

11. No Transfer of License: This license is personal to you and may not be sublicensed, assigned, or transferred by you to any other person without publisher's written permission.

12. No Amendment Except in Writing: This license may not be amended except in a writing signed by both parties (or, in the case of publisher, by CCC on publisher's behalf).

13. Objection to Contrary Terms: Publisher hereby objects to any terms contained in any purchase order, acknowledgment, check endorsement or other writing prepared by you, which terms are inconsistent with these terms and conditions or CCC's Billing and Payment terms and conditions. These terms and conditions, together with CCC's Billing and Payment terms and conditions (which are incorporated herein), comprise the entire agreement between you and publisher (and CCC) concerning this licensing transaction. In the event of any conflict between your obligations established by these terms and conditions and those established by CCC's Billing and Payment terms and conditions, these terms and conditions shall control.

14. Revocation: Elsevier or Copyright Clearance Center may deny the permissions described in this License at their sole discretion, for any reason or no reason, with a full refund payable to you. Notice of such denial will be made using the contact information provided by you. Failure to receive such notice will not alter or invalidate the denial. In no event will Elsevier or Copyright Clearance Center be responsible or liable for any

costs, expenses or damage incurred by you as a result of a denial of your permission request, other than a refund of the amount(s) paid by you to Elsevier and/or Copyright Clearance Center for denied permissions.

LIMITED LICENSE

The following terms and conditions apply to specific license types:

15. Translation: This permission is granted for non-exclusive world English rights only unless your license was granted for translation rights. If you licensed translation rights you may only translate this content into the languages you requested. A professional translator must perform all translations and reproduce the content word for word preserving the integrity of the article. If this license is to re-use 1 or 2 figures then permission is granted for non-exclusive world rights in all languages.

16. Website: The following terms and conditions apply to electronic reserve and author websites: Electronic reserve: If licensed material is to be posted to website, the web site is to be password-protected and made available only to bona fide students registered on a relevant course if:

This license was made in connection with a course, This permission is granted for 1 year only. You may obtain a license for future website posting, All content posted to the web site must maintain the copyright information line on the bottom of each image, A hyper-text must be included to the Homepage of the journal from which you are licensing at <http://www.sciencedirect.com/science/journal/xxxxx> or the Elsevier homepage for books at <http://www.elsevier.com> , and Central Storage: This license does not include permission for a scanned version of the material to be stored in a central repository such as that provided by Heron/XanEdu.

17. Author website for journals with the following additional clauses: This permission is granted for 1 year only. You may obtain a license for future website posting, All content posted to the web site must maintain the copyright information line on the bottom of each image, and The permission granted is limited to the personal version of your paper. You are not allowed to download and post the published electronic version

of your article (whether PDF or HTML, proof or final version), nor may you scan the printed edition to create an electronic version, A hyper-text must be included to the Homepage of the journal from which you are licensing at <http://www.sciencedirect.com/science/journal/xxxxx> , or the Elsevier homepage for books at <http://www.elsevier.com> and Central Storage: This license does not include permission for a scanned version of the material to be stored in a central repository such as that provided by Heron/XanEdu.

18. Author website for books with the following additional clauses:

Authors are permitted to place a brief summary of their work online only. A hyper-text must be included to the Elsevier homepage at <http://www.elsevier.com> This permission is granted for 1 year only. You may obtain a license for future website

posting, All content posted to the web site must maintain the copyright information line on the bottom of each image, and The permission granted is limited to the personal version of your paper. You are not allowed to download and post the published electronic version of your article (whether PDF or HTML, proof or final version), nor may you scan the printed edition to create an electronic version,

A hyper-text must be included to the Homepage of the journal from which you are licensing at <http://www.sciencedirect.com/science/journal/xxxxx> , or the Elsevier homepage for books at <http://www.elsevier.com> and Central Storage: This license does not include permission for a scanned version of the material to be stored in a central repository such as that provided by Heron/XanEdu.

19. Website (regular and for author): “A hyper-text must be included to the Homepage of the journal from which you are licensing at <http://www.sciencedirect.com/science/journal/xxxxx>.”

20. Thesis/Dissertation: If your license is for use in a thesis/dissertation your thesis may be submitted to your institution in either print or electronic form. Should your thesis be published commercially, please reapply for permission. These requirements include permission for the Library and Archives of Canada to supply single copies, on demand, of the complete thesis and include permission for UMI to supply single copies, on

demand, of the complete thesis. Should your thesis be published commercially, please reapply for permission. v1.2

21. Other conditions: None

ELSEVIER LIMITED LICENSE
TERMS AND CONDITIONS

Jun 06, 2008

This is a License Agreement between Pavan K Valavala ("You") and Elsevier Limited ("Elsevier Limited"). The license consists of your order details, the terms and conditions provided by Elsevier Limited, and the payment terms and conditions.

Supplier Elsevier Limited

The Boulevard, Langford Lane

Kidlington, Oxford, OX5

1GB, UK

Registered Company Number 1982084

Customer name Pavan K Valavala

Customer address 2010 C Woodmar Drive, Houghton, MI 49931

License Number 1963260738703

License date Jun 06, 2008

Licensed content publisher Elsevier Limited

Licensed content publication International Journal of Solids and Structures

Licensed content title Nonlinear multiscale modeling of polymer materials

Licensed content author P.K. Valavala, T.C. Clancy, G.M. Odegard and T.S. Gates

Licensed content date February 2007

Volume number 44

Issue number 3-4

Pages 19

Type of Use Thesis / Dissertation

Portion Full article

Format Electronic

You are an author of the Elsevier article Yes

Are you translating? No

Purchase order number

Expected publication date Aug 2008

Elsevier VAT number GB 494 6272 12

Permissions price 0.00 USD

Value added tax 0.0% 0.00 USD

Total 0.00 USD

Terms and Conditions

INTRODUCTION

1. The publisher for this copyrighted material is Elsevier. By clicking "accept" in connection with completing this licensing transaction, you agree that the following terms and conditions apply to this transaction (along with the Billing and Payment terms and conditions established by Copyright Clearance Center, Inc. ("CCC"), at the time that you opened your Rightslink account and that are available at any time at [<http://myaccount.copyright.com>](http://myaccount.copyright.com)).

GENERAL TERMS

2. Elsevier hereby grants you permission to reproduce the aforementioned material subject to the terms and conditions indicated.

3. Acknowledgement: If any part of the material to be used (for example, figures) has appeared in our publication with credit or acknowledgement to another source, permission must also be sought from that source. If such permission is not obtained then that material may not be included in your publication/copies. Suitable acknowledgement to the source must be made, either as a footnote or in a reference list at the end of your publication, as follows: "Reprinted from Publication title, Vol

/edition number, Author(s), Title of article / title of chapter, Pages No., Copyright (Year), with permission from Elsevier [OR APPLICABLE SOCIETY COPYRIGHT OWNER].” Also Lancet special credit - “Reprinted from The Lancet, Vol. number, Author(s), Title of article, Pages No., Copyright (Year), with permission from Elsevier.”

4. Reproduction of this material is confined to the purpose and/or media for which permission is hereby given.

5. Altering/Modifying Material: Not Permitted. However figures and illustrations may be altered/adapted minimally to serve your work. Any other abbreviations, additions, deletions and/or any other alterations shall be made only with prior written authorization of Elsevier Ltd. (Please contact Elsevier at permissions@elsevier.com)

6. If the permission fee for the requested use of our material is waived in this instance, please be advised that your future requests for Elsevier materials may attract a fee.

7. Reservation of Rights: Publisher reserves all rights not specifically granted in the combination of (i) the license details provided by you and accepted in the course of this licensing transaction, (ii) these terms and conditions and (iii) CCC's Billing and Payment terms and conditions.

8. License Contingent Upon Payment: While you may exercise the rights licensed immediately upon issuance of the license at the end of the licensing process for the transaction, provided that you have disclosed complete and accurate details of your proposed use, no license is finally effective unless and until full payment is received from you (either by publisher or by CCC) as provided in CCC's Billing and Payment terms and conditions. If full payment is not received on a timely basis, then any license preliminarily granted shall be deemed automatically revoked and shall be void as if never granted. Further, in the event that you breach any of these terms and conditions or any of CCC's Billing and Payment terms and conditions, the license is automatically revoked and shall be void as if never granted. Use of materials as described in a revoked license, as well as any use of the materials beyond the scope of an unrevoked license,

may constitute copyright infringement and publisher reserves the right to take any and all action to protect its copyright in the materials.

9. Warranties: Publisher makes no representations or warranties with respect to the licensed material.

10. Indemnity: You hereby indemnify and agree to hold harmless publisher and CCC, and their respective officers, directors, employees and agents, from and against any and all claims arising out of your use of the licensed material other than as specifically authorized pursuant to this license.

11. No Transfer of License: This license is personal to you and may not be sublicensed, assigned, or transferred by you to any other person without publisher's written permission.

12. No Amendment Except in Writing: This license may not be amended except in a writing signed by both parties (or, in the case of publisher, by CCC on publisher's behalf).

13. Objection to Contrary Terms: Publisher hereby objects to any terms contained in any purchase order, acknowledgment, check endorsement or other writing prepared by you, which terms are inconsistent with these terms and conditions or CCC's Billing and Payment terms and conditions. These terms and conditions, together with CCC's Billing and Payment terms and conditions (which are incorporated herein), comprise the entire agreement between you and publisher (and CCC) concerning this licensing transaction. In the event of any conflict between your obligations established by these terms and conditions and those established by CCC's Billing and Payment terms and conditions, these terms and conditions shall control.

14. Revocation: Elsevier or Copyright Clearance Center may deny the permissions described in this License at their sole discretion, for any reason or no reason, with a full refund payable to you. Notice of such denial will be made using the contact information provided by you. Failure to receive such notice will not alter or invalidate the denial. In no event will Elsevier or Copyright Clearance Center be responsible or liable for any costs, expenses or damage incurred by you as a result of a denial of your permission

request, other than a refund of the amount(s) paid by you to Elsevier and/or Copyright Clearance Center for denied permissions.

LIMITED LICENSE

The following terms and conditions apply to specific license types:

15. Translation: This permission is granted for non-exclusive world English rights only unless your license was granted for translation rights. If you licensed translation rights you may only translate this content into the languages you requested. A professional translator must perform all translations and reproduce the content word for word preserving the integrity of the article. If this license is to re-use 1 or 2 figures then permission is granted for non-exclusive world rights in all languages.

16. Website: The following terms and conditions apply to electronic reserve and author websites:

Electronic reserve: If licensed material is to be posted to website, the web site is to be password-protected and made available only to bona fide students registered on a relevant course if:

This license was made in connection with a course, This permission is granted for 1 year only. You may obtain a license for future website posting, All content posted to the web site must maintain the copyright information line on the bottom of each image, A hyper-text must be included to the Homepage of the journal from which you are licensing at <http://www.sciencedirect.com/science/journal/xxxxx> or the Elsevier homepage for books at <http://www.elsevier.com> , and Central Storage: This license does not include permission for a scanned version of the material to be stored in a central repository such as that provided by Heron/XanEdu.

17. Author website for journals with the following additional clauses:

This permission is granted for 1 year only. You may obtain a license for future website posting, All content posted to the web site must maintain the copyright information line on the bottom of each image, and The permission granted is limited to the personal

version of your paper. You are not allowed to download and post the published electronic version of your article (whether PDF or HTML, proof or final version), nor may you scan the printed edition to create an electronic version, A hyper-text must be included to the Homepage of the journal from which you are licensing at <http://www.sciencedirect.com/science/journal/xxxxx> , or the Elsevier homepage for books at <http://www.elsevier.com> and Central Storage: This license does not include permission for a scanned version of the material to be stored in a central repository such as that provided by Heron/XanEdu.

18. Author website for books with the following additional clauses:

Authors are permitted to place a brief summary of their work online only. A hyper-text must be included to the Elsevier homepage at <http://www.elsevier.com> This permission is granted for 1 year only. You may obtain a license for future website

posting, All content posted to the web site must maintain the copyright information line on the bottom of each image, and The permission granted is limited to the personal version of your paper. You are not allowed to download and post the published electronic version of your article (whether PDF or HTML, proof or final version), nor may you scan the printed edition to create an electronic version,

A hyper-text must be included to the Homepage of the journal from which you are licensing at <http://www.sciencedirect.com/science/journal/xxxxx> , or the Elsevier homepage for books at <http://www.elsevier.com> and Central Storage: This license does not include permission for a scanned version of the material to be stored in a central repository such as that provided by Heron/XanEdu.

19. Website (regular and for author): “A hyper-text must be included to the Homepage of the journal from which you are licensing at <http://www.sciencedirect.com/science/journal/xxxxx>.”

20. Thesis/Dissertation: If your license is for use in a thesis/dissertation your thesis may be submitted to your institution in either print or electronic form. Should your thesis be published commercially, please reapply for permission. These requirements include permission for the Library and Archives of Canada to supply single copies, on demand,

of the complete thesis and include permission for UMI to supply single copies, on demand, of the complete thesis. Should your thesis be published commercially, please reapply for permission. v1.2

21. Other conditions: None